Abstract

BELYEA, JENNIFER LEE. Spectroscopic Characterization of the Function and Mechanism of Dehaloperoxidase. (Under the direction of Stefan Franzen.)

The research presented in this dissertation focused on the effects of substrate binding on dehaloperoxidase, (DHP). Using Resonance Raman, (RR), UV-Visible spectroscopy, (UV-VIS), electron spin resonance, (ESR) and cyclic voltammetry, (CV) techniques we have shown that substrate indeed does bind to DHP and, in doing so, the spin state of the iron heme is affected. The binding of substrate by DHP is significant since DHP has a globin fold, and traditional globins do not have a substrate binding sites. In addition to DHP's globin function, DHP is a peroxidase; thus it is capable of converting halogenated phenols to less halogenated quinones. The change in spin state of the heme iron which is observed when substrate binds to DHP indicates that the substrate binding acts as a trigger to switch DHP from a globin to a peroxidase.

Using RR has shown that DHP has a spin state between those of horse heart myoglobin, (Mb) and horseradish peroxidase, (HRP) and it is this spin state which allows for the globin and peroxidase activities of DHP. ESR and X-band experiments were used to measure the zero field splitting parameters of DHP with and without bound substrate and from the X-band experiments it is clear that the binding of the substrate increases the population of the high-spin state of the iron in DHP. CV of the oxyDHP/deoxyDHP couple has a redox potential of +440 mV verses NHE. When substrate is bound to oxyDHP, the redox potential shifts to increasingly positive values as a function of substrate concentration. In spite of the aforementioned methods employed to measure the effects of substrate binding on DHP, no detectable difference in the Soret band is observed upon substrate binding.

SPECTROSCOPIC CHARACTERIZATION OF THE FUNCTION AND MECHANISM OF DEHALOPEROXIDASE

by
JENNIFER LEE BELYEA

A dissertation submitted to the Graduate Faculty of
North Carolina State University
in partial fulfillment of the requirements
for the Degree of
Doctor of Philosophy

CHEMISTRY

Raleigh, North Carolina

2006

APPROVED BY:

_____	_____
Dr. Edmond Bowden	Dr. Steven Lommel
_____	_____
Dr. Stefan Franzen Chair of Advisory Committee	Dr. Tatyana Smirnova

Dedication

This work is dedicated to my family. My parents have always been my cheerleaders encouraging me to do to my best and keeping my sprits up when thing did not work out as I desired. My sister has become much more than a source of spare parts; she is a driving force that pushes me to better myself as a person. My husband is my greatest source of support, if it were not for Curtis none of this work would have been possible. Curtis has helped me with each and every experiment, task, frustration and accomplishment. I am grateful to be part of such as supportive family.

Biography

Jennifer Lee Belyea was born in Singapore, to Charles and Lek Lek Browning. Jennifer grew up with a younger sister, Carol Sui, in West Plains, Missouri, where she attended West Plains High School. After High School, Jennifer attended the University of Missouri in Columbia, Missouri, where she received a B.S in Chemistry. Jennifer married Curtis Matthew Belyea in 2001.

Acknowledgements

First, I feel that it would be with utmost disrespect, to overlook the support Dr. Stefan Franzen has provided me. Though there has been no shortage of differing opinions, it is undeniable that our collaboration has had positive interactions. That is to say that our collaborative efforts have been more productive than the individuals would suggest. Enough kind words can not be said to thank you for all the doors which your experience has opened. Your insight, and approach have been invaluable. I specifically wish to acknowledge the opportunity at LANL, which has exceeded my expectations for Post-doctoral education, and, until now, I never dreamed that such an opportunity would be possible.

I would like to thank Dr. Craig Roberts on whom I blame my interest in spectroscopy. I offer my greatest thanks to Curtis Belyea for more support than any one can imagine.

A special thanks to Mary Candler. The lessons you teach are of my most valued.

Lauren Gilvey, and Mike Davis (DHP team leaders) thank you for your interest and willingness to continue all that has been started. I extend my thanks to everyone I have worked with and around the names are to numerous to list.

I must acknowledge my family. You have been very patient, understanding and supportive. Without you I would never have been able to accomplish my degree. Curtis Belyea I can not say thank you enough. Your help and understanding has kept me focused when I needed to be and separated from my work when I NEEDED to be. Thank you.

Table of Contents

List of Tables

List of Figures

CHAPTER 5

Chapter 1: Introduction and Background

Introduction

One of the fundamental paradigms in the biosciences is the relationship between the three dimensional structure and the function of proteins. This paradigm is at the heart of understanding the molecular mechanism of enzyme activation. Little is known about the molecular mechanisms of enzyme activation for dehaloperoxidase (DHP), a hemoglobin with peroxidase activity. Enzymes undergo fluctuations in structure which facilitate substrate binding; the changes in the active site result in a favorable electrostatic environment necessary for conversion of reactants to products.[1] The following chapters contain an initial spectroscopic characterization of the function and the mechanism of dehaloperoxidase. In addition to studying the basic properties of the heme iron in the active site we also function on the effect of substrate binding.

DHP lies in a unique junction within the structure function relationships of heme proteins since it has a globin fold and peroxidase activity. Much is known about myoglobin, Mb, and horseradish peroxidase, HRP, both of which were used as comparisons in the study of DHP. Mb is an oxygen storage protein with a globin fold. HRP is a peroxidase that oxidizes substrates in one-electron transfers at the heme edge. HRP is capable of a two-electron oxidation leading to the same products as DHP, however, this would occur by sequential one-electron oxidation reactions.[5] Although DHP and HRP both can carry out peroxidase chemistry, the structure of HRP differs significantly from that of DHP. On the other hand, Mb and DHP are structural homologs. Mb and DHP have eight alpha helixes arranged in the same 3D structure around an iron containing protoporphyrin IX; X-ray structures for both are available.[2-4] Both Mb and DHP function as oxygen carriers and reversibly bind diatomic molecules. Mb has been

the model globin protein used in the characterization of protein fluctuations due to diatomic ligand binding. DHP provides a unique opportunity to study fluctuation in enzyme structure as result of an actual enzymatic process as well as the fluctuation related to a carrier protein.

The novelty of DHP extends to the presence of a substrate-binding pocket[2], which is not present in Mb or HRP. Since DHP has two distinctly different functions, the study of how the molecular fluctuations occur to form an active enzyme has the potential to explain the structure function relationship in a dual-function enzyme. This has been accomplished using resonant Raman, electroparamagnetic resonance (EPR) and UV-vis binding assays. The spectroscopic characterization of recombinant dehaloperoxidase from *Amphitrite ornata* is the focus of the work that follows.

Background. Amphitrite ornata is a sedentary, surface deposit feeding polychaete worm in the family *Terelebridae*. *A. ornata* is common along the east coast of North America from Cape Cod, Massachusetts[6] to South Carolina.[7] *A. ornata* grows to lengths of 8-20 cm in intertidal sands or sandy muds where it forms U-shaped (flat bottomed U) tubes or burrows with an internal diameter of 0.5-1.0 cm.[8,9] Both ends of the burrows reach the surface of the water or air at low tide. The ends of the tubes are surrounded by sediment that results from tube formation and feeding.[8,10]

Elevated levels of biological activity around the burrows were attributed to *A. ornata's* ability to gather organic material via tentacles for feeding.[10] Studies by researchers in South Carolina have shown that *A. ornata* has the ability to dehalogenate phenols present in the environment.[7] The ability of *A. ornata* to survive in shallow mud flats is in part due to the removal of the toxic halogens.[2] The presence of the halogenated

phenols is both natural and a result of human contamination (agriculture, industry and urban runoff).[7] The United States Environmental Protection Agency, EPA, lists chlorinated phenol as a prevalent pollutant related to human, plant and environmental health concerns.[11] Removing chlorinated phenols by bioremediation is a potential use of DHP.

The peroxidase activity of DHP is a likely result of necessity since *A. ornata* inhabits an environment that contains halogenated phenols. *A. ornata* shares habitat with *Notomastus lobatus* a marine organism that biogenically produces halogenated metabolites.[12] Due to the structural similarities between Mb and DHP, a working hypothesis is that DHP was originally a globin that carried oxygen, and the peroxidase activity of DHP evolved in response to environmental pressures. The genes that code for DHP were sequenced and it was determined that DHP is coded by multiple alleles (DHP I is coded by *dhpa*, GenBank accession number AF284381 and DHP II is coded by *dhpb*, GenBank accession number AF285090).[12]

Literature Summary. Biological, biochemical and structural characterization of the oxygen carrying globin of *A. ornata* was performed by the laboratory of Dr. Joseph Bonaventura from the mid 1970's to the mid 1980's.[13-16] Respiratory hemoproteins of *A. ornata* are divided into two classes, coelomic hemoglobins and erythrocruorins. Coelomic hemoglobins are characterized as low molecular weight proteins that occur in the poorly circulated bodily fluid and erythrocruorins are the globins dissolved in vascular fluids.[13] The coelomic hemoglobin acts as a small oxygen reserve that could sustain life for approximately 10 minutes and is reported to have a P_{50} = 2.72 mm Hg at 15-20^{o}C. Despite the high oxygen affinity of the coelomic hemoglobin the low

concentration of the globin is responsible for the lack of oxygen reserve character of the coelomic fluid.[13]

The coelomic hemoglobin is described as a monomeric protein with a molecular weight reported to be in the range of 11,000 – 12,200 Da, as determined by SDS-PAGE.[14] The erythrocruorin was reported to have a molecular weight of ~15,000 Da with occasional upper molecular weight bands of varying concentrations.[14,15] The presence of two different proteins that serve as the oxygen carrying globins was later confirmed by genetic sequencing that resulted in two genes for DHP, *dhpa* and *dhpb*.[7] The molecular weight according to the DNA sequence of the protein that results from *dhpa* is 15,472 Da and the protein that results from *dhpb* is 15,379 Da.

Identification of the *A. ornata* erythrocruorin or coelomic hemoglobin as DHP is still speculative. The amino acid composition of *A. ornata* erythrocruorin was determined by an automatic sequencer that relied on the Edman degradation method.[16] The derived amino acid sequence similarities are comparable to the known sequence of DHP.[7,12] However, the exact sequence and amino acid composition are still unknown for *A. ornata* erythrocruorin and coelomic hemoglobin thus it is not possible to assign as either DHP I (dhpa) or DHP II (dhpb). Studies of *A. ornata* erythrocruorin is comparable to work on DHP (I). Carbon monoxide (CO) binding coefficients were independently determined for both *A. ornata* erythrocruorin[14] and DHP [17]. DHP and *A. ornata* erythrocruorin are reported to have CO binding coefficients of 9.8 x 10^5 $M^{-1}S^{-1}$, at pH 8.0[17] and 7.5 x 10^5 $M^{-1}S^{-1}$, at pH 7.0 respectively.[14] The oxygen affinity of *A. ornata* erythrocruorins was reported as P_{50} = 10.00 mm Hg.[13] An interesting observation has been made for both *A. ornata* erythrocruorin and DHP, both protein average one mole of

iron for two moles of protein subunit.[15,7] However, in spite these reports there is an x-ray crystal structure for the sequence corresponding to dhp (I) that shows two iron atoms per dimeric hemoglobin.

Both globins and peroxidases have a histidine residue as the proximal ligand. However, the nature of the hydrogen bonding is very different.[19] Proximal heme ligation was examined via FTIR and RR spectroscopy to conclude that DHP has a typical globin proximal ligand. The proximal ligand of DHP is His 89, and according to the RR spectra the $\nu_{Fe\text{-}His}$ for DHP is at 233 cm^{-1}.[18] DHP $\nu_{Fe\text{-}His}$ is higher than typical globins yet lower than the range for strongly polarized histidines in peroxidases.[18-20] The FTIR spectra of the CO ligated DHP shows a peak at 1951 cm^{-1}, the position of this CO peak is in the range found for heme proteins that have neutral His proximal ligands typical of globins.[18] In chapter two of this thesis I will present RR data that will further confirm that the proximal ligation in DHP is not typical for either globins or peroxidases, but rather it is in between the two.

Distal heme ligation is of central interest. The distal side of the heme is where the substrate binds. I would like to distinguish between the distal pocket itself, which is what surrounds the iron and the substrate-binding pocket. Admittedly, the two binding sits overlap. According to the crystal structures of DHP, the iron heme is 5-coordinate however UV-vis, RR, and X-band EPR data will be presented that indicate that a water molecule is at the sixth coordination site. Magnetic circular dichroism spectroscopy, MCD, experiments provided evidence that the crystal structure was missing a water molecule at the sixth coordination site of the heme.[21] The presence of a water molecule

as the sixth ligand was confirmed by UV-Vis experiments where the structure of the Q-bands showed the presence of a sixth ligand.[17]

The available data suggest that DHP is a coelomic hemoglobin rather than the erythrocruorin of *A. ornata*. [15,17,18] The isoelectric point, (pI), of *A. ornata* erythrocruorin is reported as 5.0 in the presence of 1 mM $CaCl_2$,[15] the pI of DHP is reported as 4.0[17] in the absence of additional calcium ions. The Soret peak for the deoxy species of DHP is observed at 432 nm, which corresponds to the coelomic hemoglobin. [18] The deoxy species of *A. ornata* erythrocruorin is observed at 430 nm.[15]

Enzymatic activity catalyzed by DHP to oxidatively dehalogenate halo-phenols may have bioremediation applications. DHP's ability to dehalogenate halogenated substrates has been the focus of recent literature.[2,3,5,7,21] DHP has been studied by X-ray crystallography, UV-Visible, magnetic circular dichroism, transient absorption (TA) pump-probe spectroscopy, Resonance Raman, and Fourier transform infrared spectroscopy. The following experimental techniques confirm that DHP is a globin *and* a peroxidase. Characterization of the DHP heme active site has led to unique observations. The isolation and crystallization of DHP revealed an α-helical protein with a protoprophyrin IX prosthetic group [2,3] consistent with the role of DHP as a hemoglobin of *A. ornata*. The presence of a substrate binding site was revealed in the second crystal structure, in which 4-iodiophenol was used as a substrate analog.[2] The presence of the substrate binding site causes the distal ligating residue, His 55, to move to a solvent-exposed position. This new position of the distal His is of central focus when studying the mechanism of activation for DHP will be discussed in detail in the following paragraphs and chapters. The nature of DHP's hydrophobic active site was probed by

multicolor transient absorption (TA) pump-probe spectroscopy.[22] The TA experiments concluded that the hydrophobic active of DHP resulted in a slower recombination rate of photolysis ligands similar to the viscosity effect seen in the myoglobin mutant H64V.[22] The H64V mutant of myoglobin has a hydrophobic active site similar to DHP. The hydrophobic active site allows for the binding of hydrophobic substrates. This tells us that the heme active site has been designed as a compromise between globin and peroxidase.

A. ornata's ability to dehalogenate phenols by oxidative dehalogenation is facilitated by the enzyme dehaloperoxidase, DHP. Products of enzymatic activity of DHP on 2,4,6-tribromophenol (TBP) and 2,4,6-trichlorophenol (TCP) were studied by mass spectrometry.[7] The products were identified as 2,6-dihalogenated quinones, thus indicating the removal of the para halogen and the addition of one oxygen.[2] The reaction is shown in Scheme 1.

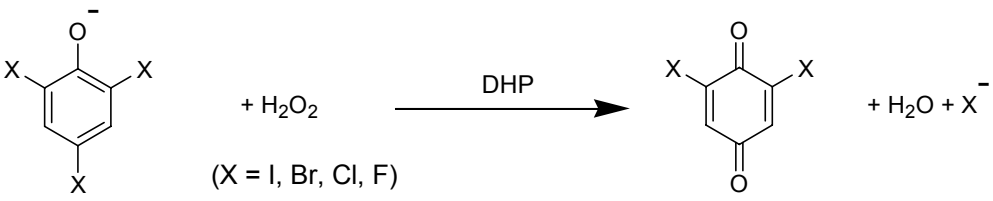

Note that the reaction shown is for the phenolate form of the substrate since this is the form of TBP and TCP present at pH 7.4, which is thought to be the physiologically relevant pH. The binding of substrate has been identified as a trigger for peroxidase activity in DHP. Stopped flow assays showed that greater peroxidase activity was achieved when substrate was introduced to the protein before activation with peroxide.[5] Substrate binding facilitates a spin state population shift from low spin (S = 1/2) to high spin (S = 5/2) and a redox potential shift.

Although DHP is classified as a peroxidase there are a number of features that suggest that DHP may represent a novel class of heme enzymes. One such characteristic is the substrate-binding site on the distal side of the heme iron. Substrate binding sites are known in the cytochrome P450 superfamily, but not in the peroxidase family of enzymes. Typical peroxidases react via an edge-binding mechanism. DHP is one of the smallest known heme enzymes. The order of activation for DHP is unique in comparison to known peroxidases. The triggering of DHP to switch from a globin to a peroxidase is unique. All the features of DHP point to DHP being a dual function protein globin and peroxidase.

The following chapters explore the mechanism of activation of DHP. Resonance Raman (RR), electron pair resonance (EPR), X-band EPR, UV-Visible spectroscopy and electrochemistry are employed to detail the heme active site in DHP. The aforementioned techniques lead to detailed spin state of the iron heme in DHP, effects of ligation of anionic ligands on the spin state, substrate binding effects on spin state and substrate binding effects on visible spectra, substrate binding effects on redox potential and the substrate binding effects on product formation.

Protein function as illustrated by oxygen-binding proteins: a review of myoglobin and hemoglobin.

The two x-ray crystal structures of DHP provide information about the static three-dimensional structure. From the crystal structures, His 55 is shown to occupy two conformations. An internal substrate-binding site adjacent to the distal pocket of the heme is defined by hydrophobic residues. The heme iron is ligated by the proximal His 89. The physical similarities to Mb include the eight α-helical structure, open and closed

confirmations assumed by the distal His and ligation of the proximal His to the iron. DHP diverges from Mb in structure by formation of the substrate-binding site.

There is a great deal of information contained in the three-dimensional structure of a protein. However, the static structure at any one time is a snapshot of the protein and does not reflect its dynamic nature. Proteins function by changing conformation. Specifically His 55 must swing out to the solvent to allow substrate to bind, neighboring residues must move to allow for the substrate and intermediates in the oxidation reactions must be accommodated this includes the one electron oxidation product that is a radical and the changes in the oxidation state of the iron. Thus, understanding the dynamics of protein structural changes is key to understanding how the protein facilitates its function.[23, 24]

What follows is a short exploration of protein function and its relationship to dynamic protein structure. The discussion will be developed using the oxygen-binding proteins myoglobin and hemoglobins as examples. Both myoglobin and hemoglobin are well-studied oxygen carrier proteins that have solved three-dimensional structures.

Since the focus of the research in the following chapters is centered on the substrate-binding site of DHP, it is necessary to define a few terms and concepts that will be used throughout the thesis. Protein function involves the binding of molecules called ligands. A ligand is bound at a certain site on the protein referred to as the binding site. Proteins are not solids they change in conformation and are said to breath or be dynamic This statement indicates that proteins assume different highly specific conformations that are critical to function.[24] When a protein catalyzes transformation of a molecule, the molecule is initially called a substrate and subsequent to the reaction it is called a

product. If the reaction with a substrate occurs in a localized location in the protein where the substrate is bound, the area is called a substrate-binding site or active site. A co-substrate is a second substrate that must be present to aid in the reaction between the enzyme and substrate.

Oxygen is a highly reactive molecule that serves as a ligand for ferrous heme proteins, and specifically for myoglobins and hemoglobins. There are no amino acids that can reversible bind oxygen. Therefore, nature has developed prosthetic groups called hemes that utilize iron or other centers that use transition metals such as iron and copper to bind oxygen.[23] Heme is a protoporphyrin IX ring bound to an iron. Four nitrogen atoms of the porphyrin ring bind the iron forming the porphyrin plane. Two additional coordination sites are available on the iron, both are perpendicular to the plane of the heme. [23] Heme is the prosthetic group of myoglobins, hemoglobin, DHP and HRP and is pictured in figure 1.

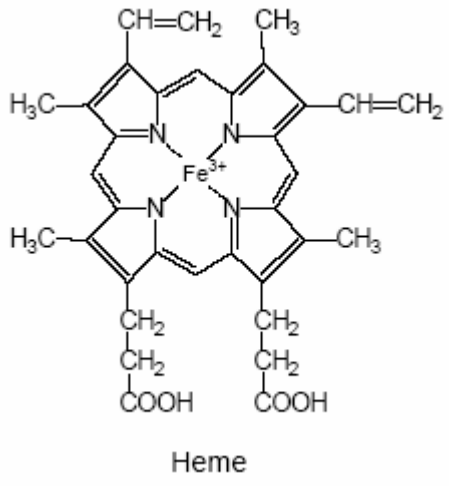

Figure 1. Heme

Oxygen binding occurs at one of the two coordination sites perpendicular to the plane of the heme. The second of the two sites is bound by a His residue (93 for Mb and 89 for DHP). Each oxygen-binding site is a separate iron containing heme, since Mb is a monomer Mb has one oxygen-binding group DHP has two and Hb has four. Oxygen binding is a key function for all three proteins.[25]

Human myoglobin is a single polypeptide chain of 153 amino acid residues folded into eight α helical segments labeled A-H. Approximately 78% of the amino acid residues are in α helices. Human hemoglobin is a tetrameric protein, containing four heme prosthetic groups comprised of two α and two β subunits each with 141 and 146 residues, respectively. The structure of Hb is similar to Mb however, adult human α subunit of Hb lacks the short D helix.[26]

Ligand binding.

The function of a globin is to reversibly bind oxygen in the ferrous form. However, both myoglobin and hemoglobin can bind a variety of other ligands such as NO, CO in the ferrous form and CN-, N_3-, Br-, Cl-, F- etc. in the ferric form. For the general case we write the following equation:

$$P + L \leftrightarrow PL \qquad (1)$$

where P represents protein, L is a ligand and PL is the ligand bound protein complex. An association constant of K_a can be expressed as:

$$K_a = [PL]/[P][L] \qquad (2).$$

Equation 2 can be rearranged to indicate that the ratio bound to free protein should be directly proportional to the concentration of free ligand:

$$K_a[L] = [PL]/[P] \qquad (3).$$

Binding equilibria are simplified when the concentration of the ligand is much greater than the concentration of ligand-binding sites, because the binding of the ligand by the protein does not appreciable change the concentration of free ligand.

Experimental data are often plotted as the fraction bound θ as shown in equation 4.

$$\theta = [PL] / [PL] + [P] \qquad (4)$$

Substituting from equation 3 into equation 4 generates equation 5.

$$\theta = K_a[L]/(K_a[L] +1) \qquad (5)$$

K_a can be determined form a plot of θ vs. the concentration of free ligand. In the case of Mb, the graph is a hyperbola and $1/K_a$ (or the dissociation coefficient K_d) is found a θ = 0.5.

For proteins with more than one binding site, we must start with the following equation 6:

$$P + nL \leftrightarrow PL_n \qquad (6)$$

where *n* is the number of binding sites. The expression for θ is:

$$\theta = [L]^n / [L]^n + K_d \qquad (7)$$

now rearrange to:

$$\theta / (1 - \theta) = [L]^n / (K_d) \qquad (8)$$

Take the log of both sides yields the Hill equation:

$$\log (\theta / (1 - \theta)) = n \log [L] – \log K_d. \qquad (9)$$

The plot of log (θ / (1 - θ)) versus log [L] is called a Hill plot. The slope from a Hill plot is called the Hill coefficient, n_H. The degree of cooperativity can be determined from the Hill coefficient. When n_H is greater than 1 there is positive cooperatively in ligand

binding. Positive cooperativity means that the binding of one ligand molecule facilitates the binding of additional ligand molecules. When $n = n_H$ the theoretical limit has been met, thus binding would be completely cooperative thus all binding sites on the protein are occupied simultaneously. When n_H is less than 1, there is negative cooperatively thus, the binding of one ligand inhibits additional binding other ligands.[27]

Cooperative binding models.

The first model proposed to explain cooperative binding was the symmetry model. The symmetry model assumes that the subunits of an allosteric protein are functionally identical and each can exist in the bound and unbound states. The two conformations are in equilibrium.[28] The second model is the sequential model. The sequential model assumes that ligand binding can induce a change of conformation in an individual subunit.[29] The conformational change in one subunit makes a similar change in another subunit more likely, thus binding of one ligand lowers the energy barrier for the binding of a second ligand. The symmetry model is viewed as the lower and upper limit of the sequential model.[29]

When the pH of the solution effects the binding of a ligand this is termed the Bohr effect.[30] The binding of Hb to oxygen is more complicated than:

$$Hb + O_2 \leftrightarrow HbO_2 \qquad (10).$$

The true equation is proton dependent thus should be written as:

$$HHb^+ + O_2 \leftrightarrow HbO_2 + H^+ \qquad (11).$$

When determining the K_d or K_a for a protein and ligand the effects of pH must be considered.[30]

Peroxidase: ***general overview of catalytic cycle***

The heme peroxidase superfamily has members from many different sources. While a diverse superfamily, similarities exist and most notably the activation or formation of compound I. Compound I is formed by oxidation of the native ferric, Fe(III), by hydrogen peroxide forming a water molecule as shown in scheme 2.[4]

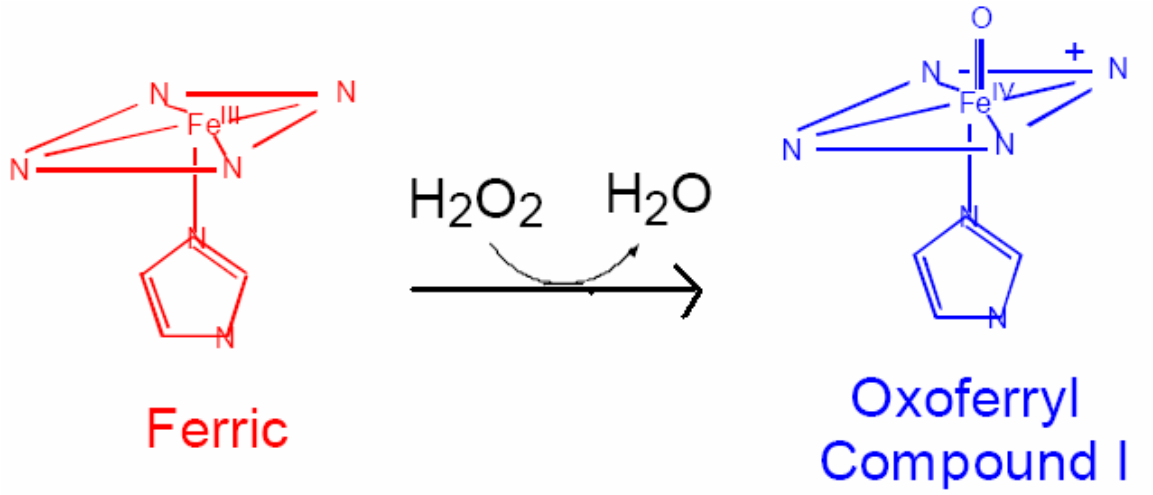

Scheme 2. The formation of Compound I from ferric protein and hydrogen peroxide.

Compound I is an oxoferryl species and the oxygen atom originates from the hydrogen peroxide. Compound I reacts with a wide array of substrates by 1-electron oxidation producing a radical product and elimination of the ferryl porphyrin π – cation radical to generate compound II as shown in scheme 3.[4] Compound II then reacts with substrate to regenerate the resting ferric protein and an additional radical product, as shown in scheme 4. The radicals can polymerize or become substrates in reactions with compounds I or II.[4]

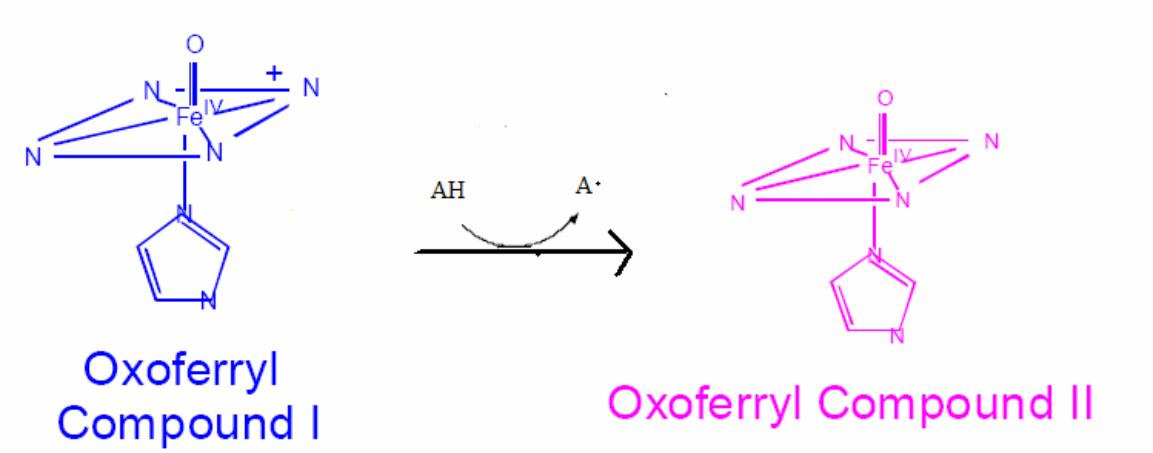

Scheme 3. One-electron oxidation of substrate (AH) by compound I resulting in compound II and a radical product (A•).

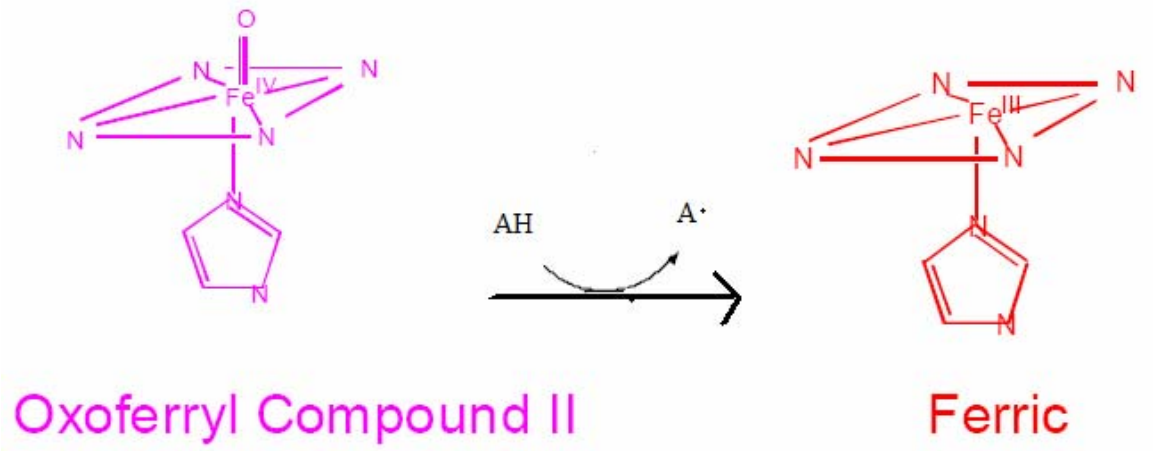

Scheme 4 compound II catalyzes the second 1-electron oxidation of substrate to generate a second radical product and returns the protein to the resting ferric state.

Resonance Raman Spectroscopy

C. V. Raman and K. S. Krishnan observed that a small portion of light scattered by a sample is changed in wavelength. [31] This process has become known as Raman scattering. Raman scattered light is observed when a light is passed through a sample producing an inelastic scattering event between the molecules of the sample and photons. Inelastic scattering results when the photon absorbs or releases energy from or to the sample that it collides with. Most of the light experiences elastic scattering and is referred to as Rayleigh scattering.

Inelastic scattering offers a means of probing the Raman active modes of a sample since energy is conserved, the energy gained or lost by the photon must equal the energy lost or gained by the sample. A resonance Raman spectrum is obtained when the excitation source has the same wavelength as an electronic absorption band of a chromophore. When this condition is met, an intensity enhancement of certain Raman bands occur that are related to the electronic absorption band. The intensity increase of the Raman bands can be several orders of magnitude. In biological samples resonance Raman is particularly useful for the study of visible chromophores, such as heme. Since the scattering of visible light by chromophores is many orders of magnitude greater than the scattering due to amino acids of the protein. For heme, which has an extinction coefficient of 9.3 mM^{-1} cm^{-1} in the ferric form, adequate Raman scattering can be obtained at concentrations of 50 μM or greater. Thus, Raman activity of the sample can be probed under physiological conditions.[32]

The structure and vibrations of the heme chromophore

Figure 1 shows iron protoporphyrin IX, or heme. In this example ferric heme has Fe^{3+} bound in the center of the heme by four pyrrole nitrogens that define the porphine cavity. The most studied Raman active vibrations of the heme group are the axial vibrations such as the Fe-His stretching mode (deoxy), Fe-C stretching mode and C-O stretching (carbonmonoxy), vinyl stretching modes, the core size marker modes, and the electron density marker mode. In fact, there is information from other vibrational modes and the complete assignments are available.[32]

Core size determination of DHP adducts using Resonance Raman.

This experiment was conducted in order to determine the spin state of the heme iron. The size of the metal cation causes reorganization of the macrocycle, for instance a large metal ion will be forced out of the heme plane in what is known as a domed structure. When a small ion is at the center of the macrocycle the bond between the nitrogens and the metal are longer and thus weaker and the metal will be in the heme plane. The spin state of the iron dictates the size of the atom, ferrous is larger than ferric which is larger than ferryl. The following empirical relationship exists between the vibrational frequency of a porphyrin mode and the size of the cavity:[33]

$$\tilde{\nu} = A - Kd \qquad (12)$$

where K (cm^{-1}/Å) and A (cm^{-1}) are empirical constants that vary for different porphyrins, and d is the average metal nitrogen bond distance in Å. There are several core size marker modes each with a different K value. The larger the K value, the more sensitive the mode is to changes on the core size. [33]

Electron Spin Resonance (ESR)

The iron in protoporphyrin IX is bound by four pyrrole nitrogens in a square planar arrangement that has 4-fold symmetry. The protoporphyrin IX embedded in a protein acts as scaffolding, enforcing geometry constraints on the heme. Interactions of the protein by perturbations of the π-electron distribution of the heme or by π-electron binding of ligands to the iron at the fifth and/or sixth coordination sites of the protoporphyrin IX. The departure from tetragonal symmetry are measurements of the protein or ligand interactions with the protoporphyrin IX and are measured by differences in the EPR spectra. Moreover, the different geometries of the ferric protoporphyrin IX in dehaloperoxidase with and without the substrate 2,4,6-tribromophenol bound can be studied by X-band EPR to determine the effect of bound substrate on the heme iron spin state.

The zero-field splitting as the name implies is present in the environment of the heme iron even the absence of an external magnetic field. The zero-field states are separated by the energy splittings of a few wave numbers, and when expressed in terms of the axial zero-field splitting parameter D the energy differences are 2D, and 4D between the lowest, middle and highest Kramers doublets. Using X-band EPR we can measure the contributions from low spin and high spin heme iron. Using the temperature dependence of the high spin component we can determine the zero-field splitting parameter, D, in ferric and ferric substrate bound DHP.

The energy separation between the three Kramers doublets in the high-spin ferric and singlets in the high-spin ferrous heme is small enough for all sublevels to be populated at room temperature. The splitting of the ground term of the high-spin ferric

and ferrous heme can be approximated by the zero-field parameters D and E of the spin Hamiltonian.[2] The parameters D and E describe axial and rhombic distortion from the tetragonal symmetry, respectively. The ratio E/D for high-spin ferric heme can be determined from splitting of the EPR signal at g = 6.0.[33-36]

The characteristics of the EPR spectrum were used to describe the symmetry of the heme. Transitions from the ground state to the lowest Kramers doublets results in absorptions extending from g ≅ 6, g ≅ 4, and g ≅ 2. The EPR spectrum arises from absorption between energy levels with an effective spin of S = ½, thus the unpaired electrons are sensitive toward axial and rhombic symmetry elements. The axial symmetry element is tetragonal due to the 4-fold symmetry of the pyrrole nitrogens. The spread of the absorption between g = 6 and g = 2 is credited to the large value of the tetragonal field. The decrease of distortion from tetragonal to rhombic symmetry is quantitatively expressed by the zero field splitting parameters D and E, which are defined by the spin Hamiltonian equation 13.[37]

$$\mathcal{H} = \beta H \cdot g \cdot S + D[S_z^2 - S(S+1)/3] + E(S_x^2 - S_y^2) \qquad (13)$$

The zero-field splitting of the heme in DHP and DHP-TBP were determined by measuring the integrated intensity of the heme iron g_x EPR transition as the function of temperature. Only the $|5/2, -1/2\rangle \leftrightarrow |5/2, +1/2\rangle$ transition is observed thus populations in the Ms = ±3/2, ±5/2 doublets reduce the signal intensity of the observed, transitions. Data collected as a function of temperature was fit by equation 14. [38]

$$S(T) = \frac{N(1 - e^{-\theta/T})}{1 + e^{-\theta/T} + e^{-(2D-\theta)/T} + e^{-2(D+\theta)/T} + e^{-2(3D-\theta)/T} + e^{-3(2D+\theta)/T}}. \qquad (14)$$

where S(T) is the integrated EPR signal intensity, θ is the Zeeman splitting $h\upsilon/k_B$ = 0.44 K, D is the zero-field splitting parameter, and N is an overall scale factor. When D is positive, the doublet $|5/2, \pm 3/2\rangle$ lies 2D above the ground state doublet $|5/2, \pm 5/2\rangle$ is 4D above the $|5/2, \pm 3/2\rangle$ doublet in the absence of an external magnetic field.

Anionic ligands bind to DHP

Anionic ligand binding to ferric DHP is characterized by the formation of a charge transfer band or a shift in the Soret band for fluoride and cyanide binding respectively. The binding of fluoride does not show cooperativities. The binding of fluoride to ferric DHP results in the displacement of a weakly bound water molecule for a weakly bound fluoride. Both forms of DHP are high spin thus the displacement of one weak ligand for another weak ligand does not result in a shift in the Soret band. Binding of cyanide to ferric DHP results in the displacement of water for a strong ligand thus DHP becomes low spin. The binding of the cyanide is cooperative and similar to the transition of Hb when O_2 binds.

References

1. Eisenmesser, E. Z.; Millet, O.; Labeikovsky, W.; Korzhnev, D. M.; Wolf-Watz, M.; Bosco, D. A.; Skalicky, J. J.; Kay, L. E.; Kern, D. **Intrinsic dynamics of an enzyme underlies catalysis.** Nature (London, United Kingdom) (2005), 438(7064), 117-121.

2. LaCount, Michael W.; Zhang, Erli; Chen, Yung Pin; Han, Kaiping; Whitton, Margaret M.; Lincoln, David E.; Woodin, Sarah A.; Lebioda, Lukasz. **The crystal structure and amino acid sequence of dehaloperoxidase from Amphitrite ornata indicate common ancestry with globins.** Journal of Biological Chemistry (2000), 275(25), 18712-18716.

3. Zhang, E.; Chen, Y-P.; Roach, M. P.; Lincoln, D. E.; Lovell, C. R.; Woodin, S. A.; Dawson, J. H.; Lebioda, L. **Crystallization and initial spectroscopic characterization of the heme-containing dehaloperoxidase from the marine polychaete Amphitrite ornata.** Acta Crystallographica, Section D: Biological Crystallography (1996), D52(6), 1191-1193.

4. Dunford, H. B. **Heme Peroxidases**, Wiley-VCH, New York, 1993

5. Belyea, J.; Gilvey, L. B.; Davis, M. F.; Godek, M.; Sit, T. L.; Lommel, S. A.; Franzen, S. **Enzyme function of the globin dehaloperoxidase from *amphitrite ornata* Is activated by substrate binding.** Biochemistry (2005), 44(48), 15637-15644.

6. Pettibone, N. H**. Marine polychaete worms of the New England region. 1. *Aphroditidae* through *Trochaetidae*.** U.S. National. Museum Bulletion (1963), 227, 1-356.

7. Chen, Y-P.; Woodin, S. A.; Lincoln, D. E.; Lovell, C. R. **An unusual dehalogenating peroxidase from the marine terebellid polychaete Amphitrite ornata.** Journal of Biological Chemistry (1996), 271(9), 4609-12.

8. Linville, H. R. **The natural history of some tube-forming annelids (*Amphitrite ornata, Diopatra cuprea*)**, Holt, New York, 1903, 227-235.

9. Scott, J. W. **Some egg-laying habits of Amphitrite ornata**. Verrill. Biological Bulletin (1909), 17, 327-340.

10. Rhoads, D. C. **Biogenic graded bedding**. Journal of Sediment Pet (1967), 35, 956-963.

11. http://www.epa.gov/owow/oceans/regulatory/sec301tech/table2.html

12. Franzen, S.; Roach, M. P.; Chen, Y-P.; Dyer, R. B.; Woodruff, W. H.; Dawson, J. H. **The Unusual Reactivities of Amphitrite ornata Dehaloperoxidase and Notomastus lobatus Chloroperoxidase Do Not Arise from a Histidine Imidazolate Proximal Heme Iron Ligand.** Journal of the American Chemical Society (1998), 120(19), 4658-4661.

13. Mangum, C. P.; Woodin, B. R.; Bonaventura, C.; Sullivan, B.; Bonaventura, J. **Celomic and vascular hemoglobin in the annelid family Terebellidae.** Comparative Biochemistry and Physiology, Part A: Molecular & Integrative Physiology (1975), 51(2A), 281-94.

14. Weber, R. E.; Magnum, C.; Steinman, H.; Bonaventura, C.; Sullivan, B.; Bonaventura, J. **Hemoglobins of two terebellid polychetes: Enoplobranchus sanguineus and Amphitrite ornata.** Comparative Biochemistry and Physiology, Part A: Molecular & Integrative Physiology (1977), 56(2A), 179-87.

15. Chiancone, E.; Brenowitz, M.; Ascoli, F.; Bonaventura, C.; Bonaventura, J. **Amphitrite ornata erythrocruorin. I. Structural properties and characterization of subunit interactions.** Biochimica et Biophysica Acta, Protein Structure (1980), 623(1), 146-62.

16. Fushitani, K.; Bonaventura, J.; Bonaventura, C. **Isolation of polypeptide chains with heme from the extracellular hemoglobin of Amphitrite ornata (Polychaeta, Annelida).** Comparative Biochemistry and Physiology, Part B: Biochemistry & Molecular Biology (1986), 84B(1), 137-41.

17. Nienhaus, K.; Deng, P.; Belyea, J.; Franzen, S.; Nienhaus, G. U. **Spectroscopic Study of Substrate Binding to the Carbonmonoxy Form of Dehaloperoxidase from Amphitrite ornata.** Journal of Physical Chemistry B (2006), 110(26), 13264-13276.

18. Han, K.; Woodin, S. A.; Lincoln, D. E.; Fielman, K. T.; Ely, B. **Amphitrite ornata , a marine worm, contains two dehaloperoxidase genes.** Marine Biotechnology (2001), 3(3), 287-292.

19. Spiro, T. G.; Smulevich, G.; Su, C. **Probing protein structure and dynamics with resonance Raman spectroscopy: cytochrome c peroxidase and hemoglobin.** Biochemistry (1990), 29(19), 4497-508.

20. Shelnutt, J. A.; Alden, R. G.; Ondrias, M. R. **Heme-linked ionizations in horseradish peroxidase detected by Raman difference spectroscopy.** Journal of Biological Chemistry (1986), 261(4), 1720-3

21. Osborne, R. L.; Sumithran, S.; Coggins, M. K.; Chen, Y-P.; Lincoln, D. E.; Dawson, J. H. **Spectroscopic characterization of the ferric states of Amphitrite ornata dehaloperoxidase and Notomastus lobatus chloroperoxidase: His-ligated peroxidases with globin-like proximal and distal properties.** Journal of Inorganic Biochemistry (2006), 100(5-6), 1100-1108.

22. Franzen, S.; Jasaitis, A.; Belyea, J.; Brewer, S. H.; Casey, R.; MacFarlane, A. W., IV; Stanley, R. J.; Vos, Marten H.; M, J-L. **Hydrophobic Distal Pocket Affects NO-Heme Geminate Recombination Dynamics in Dehaloperoxidase and H64V Myoglobin.** Journal of Physical Chemistry B (2006), 110(29), 14483-14493.

23. Case, D.A., Karplus, M. **Dynamics of ligand binding to heme proteins**. *J. Mol. Biol*. (1979) 132, 343-368.

24. Koshland, D.E., Jr. (1973) **Protein shape and biological control**. *Sci. Am*. 229 (Oct.), 52-64.

25. Dickerson, R.E., Geis, I. (1982) **Hemoglobin: Structure, Function, Evolution, and Pathology**. The Benjamin Publishing Company, Redwood City, CA.

26. Perutz, M.F. (1989) **Myoglobin and heamoglobin: role of distal residues in reactions with haem ligands**. *Trends Biochem. Sci*. 14, 42-44.

27. Di Prisco, G., Condo, S.G., Tamburrini, M., Giardina, B. (1991) **Oxygen transport in extreme environments**. Trends Biochem. Sci. 16, 471-474.

28. Mondo, J., Wyman, J., Changeux, J.P. (1965) **On the nature of allosteric transitions: a plausible model**. *J. Mol. Biol*. 12, 88-118.

29. Koshland, D.E., Jr., Nemethy, G., Filmer, D. (1966) **Comparison of experimental binding data and theoretical models in proteins containing subunits**. *Biochemistry* 5, 365-385.

30. Ho, C., Russu, I.M. (1987) **How much do we know about the Bohr effect of hemoglobin?** *Biochemistry* 26, 6299-6305.

31. Raman, C. V., Krishnam, K. S. **A new type of Secondary Radiation**. (1928). *Nature* (*London*) **121**, 501.

32. Spiro, T. G., **Resonace Raman Spectra of Heme Matalloproteins**. Wiley, New York, 1988.

33. Carey, P. R., **Biochemical Applications of Raman and Resonace Raman Spectroscopies**. Academic Press, New York, 1982.

33. Peisach, J.; Blumberg, W. E.; Ogawa, S.; Rachmilewitz, E. A.; Oltzik, R.. **Effects of protein conformation on the heme symmetry in high spin ferric heme proteins as studied by electron paramagnetic resonance.** Journal of Biological Chemistry (1971), 246(10), 3342-55.

34. Yonetani, T.; Drott, H. R.; Leigh, J. S., Jr.; Reed, G. H.; Waterman, M. R.; Asakura, T. **Electromagnetic properties of hemoproteins. III. Electron paramagnetic resonance characteristics of iron(III) and manganese(II) protoporphyrins IX and their apohemoprotein complexes in high spin states.** Journal of Biological Chemistry (1970), 245(11), 2998-3003.

35. Blumberg, W. E.; Peisach, J.; Wittenberg, B. A.; Wittenberg, J. B. **Electronic structure of protoheme proteins. I. Electron paramagnetic resonance and optical study of horseradish peroxidase and its derivatives.** Journal of Biological Chemistry (1968), 243(8), 1854-62.

36. Bleaney, B.; Stevens, K. W. H.. **Paramagnetic Resonace.** Reports on progeress in physics (1953), 16(1), 108-159.

37. Wittenberg, B. A.; Kampa, L.; Wittenberg, J. B.; Blumberg, W. E.; Peisach, J. **Electronic structure of protoheme proteins. II. Electron paramagnetic resonance and optical study of cyctochrome c peroxidase and its derivatives.** Journal of Biological Chemistry (1968), 243(8), 1863-70.

38. Galli, C.; MacArthur, R.; Abu-Soud, H. M.; Clark, P.; Stuehr, D. J.; Brudvig, G. W. **EPR Spectroscopic Characterization of Neuronal NO Synthase.** Biochemistry (1996), 35(8), 2804-2810.

Resonant Raman Study of Ferric Heme Adducts of Dehaloperoxidase from *Amphitrite ornata*

Abstract

The study of axial ligation by anionic ligands to ferric heme iron by resonant Raman spectroscopy provides a basis for comparison of the intrinsic electron donor ability of the proximal histidine in horse heart myoglobin (HHMb), dehaloperoxidase (DHP) and horseradish peroxidase (HRP). DHP is a dimeric hemoglobin (Hb) originally isolated from the terebellid polychaete *Amphitrite ornata*. The monomers are structurally related to Mb and yet DHP has a peroxidase function. The core size marker modes, ν_2 and ν_3, were observed using Soret excitation and DHP-X was compared to HHMb-X for the ligand series, X = F, Cl, Br, SCN, OH, N_3, CN. Special attention was paid to the hydroxide adduct, which is also formed during the catalytic cycle of peroxidases. The Fe-OH stretching frequency was observed and confirmed by deuteration and is higher in DHP than in HHMb. The population of high spin states of the heme iron in DHP was determined to be intermediate between HHMb and HRP. The data provide the first direct measurement of the effect of axial ligation on the heme iron in DHP. The Raman data support a modified charge relay in DHP, in which a strongly hydrogen-bonded backbone carbonyl (>C=O) polarizes the proximal histidine. The charge relay mechanism by backbone carbonyl >C=O-His-Fe is the analog of the Asp-His-Fe of peroxidases and Glu-His-Fe of flavohemoglobins.

Dehaloperoxidase, DHP, is an enzyme native to the terebellid polychaete *Amphitrite ornata* that has peroxidase activity and a globin fold.[1,2] DHP is a dimeric Hb consisting of eight α–helices (a-h) and a protoporphyrin IX prosthetic group[3,4] with a central metal atom that reversibly binds diatomic ligands such as molecular oxygen (O_2), carbon monoxide (CO), and nitric oxide (NO).[5-8] DHP bears a resemblance to dimeric Hbs such as *Ascaris scarpharca* Hb[9] and cytoglobin.[10] However, the dual function of DHP appears unique in the known evolution of globins.[4, 11, 12] The peroxidase activities of typical globins have been characterized and are known to have turnover numbers that are more than one hundred times smaller than horseradish peroxidase (HRP).[13-16] Recently DHP has been expressed and purified in a recombinant form in *E. coli*[5] and the enzymatic rate for conversion of trihalogenated phenols to dihalogenated quinone by DHP is 12 times slower than that of HRP and 13 times faster than that of Horse Heart myoglobin (HHMb). In spite of the low structural homology with peroxidases, DHP clearly has a peroxidase function. However, the fact that DHP apparently binds the substrate in an internal binding site suggests that a two-electron oxidation mechanism is an important pathway for oxidation of the substrate.[3,4]

Comparison of the proximal histidine structures of HHMb, DHP, and HRP poses a question regarding the catalytic mechanism of DHP. DHP resembles a Hb much more than it does a peroxidase in the hydrogen bonding of the proximal histidine. Specifically, peroxidases are known to have strong hydrogen bonding to a negatively charged aspartate.[17-22] The recently discovered class of bacterial flavohemoglobins also has a strong hydrogen bond of the proximal histidine to glutamate.[23] This strong hydrogen bonding leads to a greater negative charge on the imidazole ring ligated to the heme iron.

The charge relay comprised by the Asp-His-Fe catalytic triad permits higher oxidation states of iron to be formed consistent with the requirement for the formation of compound I. DHP lacks this feature, [24] although the proximal histidine of DHP does form a strong hydrogen bond with the carbonyl group of Leu83.[25, 26] This hydrogen bonding does not, at first, appear significantly different from the bifurcated hydrogen bond in myoglobin that involves a weak interaction with the lone pair of Ser92 and an interaction with carbonyl group of Ile89. Attempts to engineer myoglobin by means of the Ser92Asp mutation that would introduce a charge relay do not produce a significant increase in peroxidase activity.[27, 28] DHP may have evolved a different more subtle charge relay that permits it to function both as a globin and as a peroxidase. In DHP, the Leu93-C=O…Nδ-His89 hydrogen bond length is 2.9 Å, which is significantly shorter than the corresponding hydrogen bond in myoglobin.[3, 4] It is still not understood how the >C=O-His-Fe catalytic triad facilitates peroxide activation in DHP that is analogous to the Asp-His-Fe charge relay in peroxidases.

The ligation strength of the proximal histidine should be directly correlated with the charge supported on the heme iron and inversely correlated with the spin state of the iron. The spin states of ferric heme proteins are S=1/2, S=3/2 and S=5/2, which will be referred to as LS, MS and HS, respectively. The greater the basicity of the axial ligand, the higher the energy of the d_{z2} and d_{π} (d_{xz}, d_{yz}) orbitals, due to σ- and π- bonding interactions, respectively. The charge density in the ligand field causes these d-orbitals to increase in energy and consequently lowers the spin state.[29] In addition to effects of axial ligation on spin state, the axial ligands (F^-, Cl^-, Br^-, OH^-, SCN^-, N_3^-, and CN^-) can have differential effects on the Soret band spectrum depending on the mixing of the π-system

of the ligand. While one can compare the native ferric state, this is complicated by the fact that water is ligated in ferric HHMb, but not ferric HRP.[18, 19, 30] The situation is still under investigation for DHP since the x-ray crystal structure shows the heme to be five-coordinate,[3, 4] but magnetic circular dichroism[31] and UV-vis titrations[6] suggest that water may be bound in the ferric form. This type of comparison is complicated in part by distal interactions hydrogen bonding interactions.[32-35]

On the distal side peroxidases and globins both have a prominent histidine, known as the distal histidine. However, peroxidases also have a highly conserved arginine that is thought to stabilize proton transfer essential to rapid activation of bound peroxide to form compound.[13, 18, 19, 30, 36-38] However, bound hydroxide presents an especially interesting situation since there are both hydrogen bond donor and acceptor interactions. Depending upon the nature of the hydrogen bonding groups in the distal pocket, the Fe-OH bond can either be strengthened or weakened by interactions in the distal pocket. A hydrogen bond donor interaction with a σ-bonding distal ligand acts as a charge relay in reverse and reduces the ligation strength of the bound ligand. The situation for π-bonding ligands such as CO is more complex due to the competition between σ-donation and π-backbonding.[39] The proximal and distal charge relays are illustrated in scheme 1.

The distal and proximal differences between globins and peroxidases can be related to their functional differences. In peroxidases, the greater negative charge on the proximal histidine Nε, that arises due to the interaction of Nδ with a hydrogen bonding aspartate[17, 24] results in a greater tendency for low spin iron, which reduces the core size of the iron. The greater ligation strength leads to a "push" at the heme iron that is thought to be necessary for peroxidase activation.[40] Specifically, compound I formation

is facilitated by the strong proximal histidine ligation, which stabilizes LS iron and the Fe(IV) oxidation state of the iron required for compounds I and II. Globins have a weaker ligation between the proximal histidine and the iron, resulting in a greater population of the HS state.[41] A structural displacement of the heme iron out of the heme plane in the high spin state gives rise to the domed conformation in globins. DHP is predicted to have spin states and iron charge values that are between globins and peroxidases based on axial ligation discussed above and based on the observed reactivity, which is intermediate between HRP and HHMb. Commensurate with this expectation, the $\upsilon_{Fe\text{-}His}$ frequency in ferrous deoxy DHP is observed at 233 cm^{-1},[8] which is intermediate between HHMb $\upsilon_{Fe\text{-}His}$ = 221 cm^{-1} [42] and HRP $\upsilon_{Fe\text{-}His}$ = 243 cm^{-1}.[17] One of the goals of the present study is to test whether the trends in the spin states of ferric heme of the three proteins, HHMb, DHP and HRP, are analogous to the ligation strength for ferrous heme.

The distal pocket structure of DHP has important differences with respect to both globins and peroxidases. The Nε-H of distal histidine in peroxidase is 1.5 Å farther away from the iron heme than in that of globins,[18, 20-22] which affects both function and spectroscopy.[33] In peroxidases, the greater distance allows the histidine to provide a "pull" to activate the cosubstrate, hydrogen peroxide.[43] Formation of compound I in peroxidases is accomplished by the distal histidine with the aid of an arginine residue that is absent in DHP.[13, 36-38] In globins, the distal histidine hydrogen bonds with the diatomic ligand to stabilize the bound ligand, but does not have any auxiliary hydrogen bonding partners.[39, 44, 45] The distal histidine in DHP, His55, is positioned 1.5 Å further from the heme iron and therefore has spatial similarity with the peroxidase geometry,[3, 4] but is

apparently not capable of strong hydrogen bonding to bound CO.[6, 8] His55 has two conformations in the DHP X-ray crystal structures.[3, 4] The terms "open" and "closed" conformations correspond to a solvent-exposed and internal conformation, respectively, for the distal histidine in Mb.[46] The "open" or solvent-exposed conformation of H64 is observed at pH ~4.5 in Mb.[47] While there is an analogy with DHP, the open conformation in DHP is observed at much higher pH. According to the crystallization conditions the open form is in equilibrium with the closed form at pH 6.5.[3, 4] Moreover, when substrate is present, the histidine is in the open confirmation.[3, 4] The functional consequence of the two conformations of the distal histidine is not known, but it is clear that His55 in DHP would need to be in the closed conformation to participate in hydrogen bonding with a ligand bound to the heme iron as well as for catalysis of Fe-H_2O_2 to form compound I since it is located more than 9 Å from the heme iron in the open conformation. Mutants in the His55 position result in severely reduced enzymatic acdtivity in DHP.[48] The ferric liganded heme species studied here are probes of the distal pocket polarity as shown in Scheme 1. The interactions of the amino acid residues in the distal pocket with bound ligands can affect the core size marker modes by modulating the ligation strength. The effect of hydrogen bonding by residues in the distal pocket is particularly noticeable for the weak ligand field of fluoride.[49]

Resonant Raman spectroscopy provides information on the axial ligand vibrations and the effect of axial ligation on heme structure. The interplay of axial ligation and heme geometry can be monitored by observation of three Raman bands known as the core size marker bands, ν_3, ν_2 and ν_{10} in the 1470-1510, 1560-1580, and 1610-1640 cm^{-1} regions, respectively, of the resonant Raman spectrum. These vibrations arise from motions on the

heme periphery, but their frequencies are sensitive to strain induced by the iron that depends upon the distribution of d-electrons.[50, 51] Since the axial ligand field has a strong effect on the iron spin state, the core size modes report on the strength of axial ligation. The ν_2 and ν_3 modes are of A_{1g} symmetry in a simplified D_{4h} model of the heme. These modes are Frank-Condon active and most intense for Soret band excitation. The ν_{10} mode has B_{1g} symmetry and is most intense for Q-band excitation. In ferric heme each core size marker appears as a pair of bands that correspond to two populations of spin states in equilibrium. We have found that the core size marker band ν_3 is the most reliable indicator of the relative population of each spin state because it is an isolated region of the Raman spectrum. At wavenumbers greater than 1600 cm^{-1} where ν_{10} is observed the spectrum is complicated by the presence the heme vinyl modes $\nu_{c=c}$.[49, 52] The ν_2 band is also in a spectrally congested region together with bands ν_{11}, ν_{19}, and ν_{35}.[52]

Although both globins and peroxidases have the same protoporphyrin IX prosthetic group, the heme geometries differ due to restrictions enforced by protein structure.[53] Globins have been shown to have both a planar and domed heme conformation.[25] Ferrous 6-coordinate hemes have a planar conformation consistent with an iron spin of S=0. A domed conformation has a 5-coordinate heme iron consistent with a spin of S=2. The transition from low to high spin of the ferrous heme in globins can be monitored by Raman spectroscopy.[54-56] Saddling of the heme is observed in peroxidases. The changes in heme structure for various ligation states are less pronounced in peroxidases than in globins. In 6-coordinate adducts both LS and HS forms are possible depending on the strength of the axial ligand field. The 5-coordinate heme in peroxidase may be a mixed or intermediate spin state, IS, or HS. The spin state is an important

observable for understanding the strength of axial ligation and the role it plays in supporting the Fe(IV) oxidation state of iron required for formation of compounds I and II. Moreover, the spin state is a crucial for understanding enzymatic activity observable because it is the consequence of the charge relay discussed above. The presence of a mixed spin state in peroxidases is likely a functional consequence of the strong axial ligation since 5-coordinate adducts would normally be expected to be high spin. Since DHP is a globin peroxidase the present study focuses on the role of ferric spin states in a domed heme that structurally resembles myoglobin rather than a typical peroxidase. We will address the spectroscopic similarities as a probe of the active site bonding and electronic structure.

Materials and Methods

Absorption spectroscopy

DHP samples were purified from *E. coli* according to published methods.[5] Protein was dialyzed against water to remove all salts and concentrated using Millipore Ultra-4 centrifugal filters, WMCO 10,000. Concentrated samples were flash frozen using liquid nitrogen or dry ice then lyophilized using a Labconco Freezer Dryer 4.5. DHP samples were prepared by dissolving lyophilized DHP in water at a final concentration of 6 μM. Excess potassium ferricyanide was added to the protein solution to oxidize the iron heme to the ferric state. Excess oxidant was removed by size exclusion chromatograpy using a Sephadex G-25 column (Sigma-Aldrich G2580-10G). Protein was collected and concentrated in Millipore Amicon Ultra-4 MWCO 10,000. A buffer exchange was preformed in the Amicon Ultra-4 so the resulting protein solutions were buffered in 100 mM citrate pH 6.0 and 100 mM carbonate pH 10.5. Lyophilized horseradish peroxidase

was purchased from Fluka (EC. 1.11.1.7), and lyophilized horse heart myoglobin was purchased from Sigma (CAS # M1882). Both horseradish peroxidase and horse heart myoglobin were used without further purification. Lyophilized HHMb and HRP proteins were dissolved in 100 mM citrate buffer pH 6.0 or 100 mM borate buffer pH 10.5.

Absorption spectra were recorded using a Hewlett Packard 8453 multi-wavelength spectrometer. The ferric DHP in 100 mM citrate buffer pH 6.0 had a Soret band max at 406 nm and a broad Q band from 550-575 nm, as shown in Figure 1. In order to produce ligated protein samples, aliquots of concentrated ligand solutions were added and the Soret and Q-band shifts were measured. Addition of ligand was done quantitatively up to concentrations of 500 mM to assure that spectroscopic changes associated with the binding of each ligand were observed. It was determined the 50 mM of each of the ligands F^-, Cl^- Br^-, SCN^-, N_3^- and CN^- was sufficient to produce a six-coordinate adduct and this concentration was used for the data reported in Table 1.

Protein Samples for Resonance Raman Experiments

Lyophilized proteins were dissolved in 0.5 M ligand and 100 mM citrate pH 6.0 with the final concentration of protein 120 μM. Ligands used were obtained from the dissolved salts of KF, NaCl, KBr, KSCN, KCN, and NaN_3 at concentrations of 100 mM. Carbonate buffer (100 mM) with a pH of 10.5 was used to obtain the hydroxide ligand. 200μL of each protein/ligand combination were placed into separate 5 mm diameter glass NMR tubes. Samples were stored on ice until used.

Resonance Raman Spectroscopy

Resonance Raman spectra were obtained by excitation at the edge of the Soret band 410 or 424 nm using Coherent verdi-low (N10-A1654) generating 10W of 532 nm

light which was used to power a Coherent Mira 900 to generate a 820 and 840 nm. The resulting beam was sent through a Coherent 5-050 doubler (01088) to generate 410-430 nm light as the excitation source for the Resonance Raman experiments. The laser output was calibrated using Rayleigh scattering, toluene and cyclohexane standards, and lines from Kr and Ar lamps. The excitation source was collimated and cylindrically focused to a vertical line of ~0.5 mm and typically 45-60 mW at the sample. Raman scattered light passed through a Spex 1877 Triplemate monochromator and was detected by a liquid N_2-cooled CCD camera (ISA Spex, model CCD-3000). Samples were placed in 5 mm NMR tubes and spun with an air piston spinning sample holder (Princeton Photonics, model Raman 101). Spectra were measured at room temperature for three acquisitions with exposure times of 180 s, alternating between samples to minimize sample degradation. Each sample scan was repeated four to eight times to improve the signal-to-noise ratio.

Fits of the resonance Raman spectra to a Gaussian fitting model were performed using Igor Pro 5.0. The results of the fits are represented in Tables 2-5. Each Gaussian is:

$$G(\omega) = \frac{A}{\sqrt{2\pi}\sigma}\exp\left\{-\frac{(\omega-\omega_0)^2}{2\sigma}\right\} \qquad (1)$$

The parameters in Tables 2-5 correspond to A, ω and σ for both of the modes ν_2, and ν_3. The percentage of high spin, HS, was determined for ν_3 and ν_{10} using Eqn. 2.

$$\frac{\left(\frac{A}{\sigma}\right)_{HS}}{\left(\frac{A}{\sigma}\right)_{LS}+\left(\frac{A}{\sigma}\right)_{HS}} \qquad (2)$$

Density Functional Theory Calculations. The model system used in this study consisted of a 5-coordinate iron-porphine-imidazole. The optimized ground state geometries at three spin states were obtained using the GGA functional[57] as implemented in DMol3

(Accelrys Inc.).[58, 59] All calculations were carried out on a PQS QuantumCube computer. Geometry optimizations were carried out without constraints until the energy difference was less than 10^{-6} a.u. on subsequent iterations. Numerically tabulated basis sets of double-ζ plus extra polarization (DNPP) quality were employed as described in the Supporting Information. For the DNPP basis there are four basis functions for H (1s, 2s, 2p, 3d), seven basis functions for C, N and O (1s, 2s(2), 2p(2), 3d, 4f). The potential energy surfaces were calculated using the Thermal option (grand canonical ensemble) treatments of the density functional[60] as reported elsewhere.[39, 61-63] The grand canonical (Thermal) option always converged to a lower overall energy. The grand canonical calculation was carried out at an electronic temperature of k_BT = 0.02 eV. Once a calculation was complete it was extrapolated to zero temperature by subtraction of the thermal electron occupation according to the grand canonical partition function.

Results

The absorption and resonance Raman spectra are presented for the ferric adducts of DHP. Experiments were performed on both HHMb and HRP for comparison. The ferric hydroxyl adduct was studied in particular detail to establish the nature of acid-alkaline transition.

Absorption spectroscopy

Absorption spectra were obtained for the entire series of ferric adducts ranging from no ligand (DHP) to the strongest ligand, cyanide (DHP-CN). Figure 1 shows the absorption spectra for ferric DHP with and without bound fluoride ligand. The Soret band and Q band are shown in Figures 1A and 1B, respectively. The Q-band region shown in panel B reveals the presence of a charge transfer band at 605 nm upon the addition of fluoride ligand to ferric DHP to make DHP-F.[64] The Soret maxima for both ferric DHP and DHP-F are both at 406 nm, which is characteristic of the mostly high spin (HS) form of the heme iron expected for both met and fluoride adducts. The addition of fluoride ligand has little effect on the Soret band maximum and intensity, but does result in a slight narrowing of the Soret band.

The absorption spectra of OH^-, N_3^- and CN^- adducts of ferric DHP are presented in Figure 2. As ligand strength in ferric adducts of DHP increases there are shifts in the Soret band maxima from 406 to 423 nm. Table 1 provides a summary of the Soret maxima for DHP, HRP and HHMb. It was difficult to detect binding of the Cl^-, Br^- and SCN^- ligands to HRP by either UV-vis or Raman spectroscopy and therefore these values are not reported. Figure 2A illustrates the shift in the Soret maxima that arises from the increasing ligation strength of the ligand, which includes both effects on spin state and the π-acid character.[65, 66] Figure 2B shows the changes in the Q-band spectral region that are consistent with the change from high to low spin. The spectra of the three adducts shown in Figure 2B all have α and β bands at 550 nm and 575 nm, respectively. DHP-OH and DHP-N_3 adducts have additional charge transfer bands at 603 and 640 nm, respectively.

The pKa for formation of the hydroxide adduct of DHP was determined from the pH dependence of Soret band. A pKa of 8.0 was determined for ferric DHP, which is in agreement with earlier pKa determination of 8.1.[6] The data are provided in the Supporting Information for comparison with Mb and HRP. In globins where water is bound to the heme iron at low pH this transition is known as the acid-alkaline transition. However, the crystal structure for DHP reveals no water bound in the ferric form of the enzyme. These data and the data presented elsewhere suggest that the low pH form may be metaquo DHP rather than five-coordinate ferric DHP. The high pH form is clearly ferric hydroxyl DHP (DHP-OH).

Resonance Raman spectra

Resonance Raman spectra were obtained for aqueous ferric DHP and ferric DHP bound to anionic ligands. The core size marker modes υ_2 and υ_3 were used for the analysis of HS and LS population since these modes are intense enough for all the ligated proteins to be measured. The υ_3 is located in the range from 1470-1510 cm^{-1} for DHP and is the most isolated core size marker mode. Based on the data obtained here, υ_3 appears to be the most reliable Raman band for the determination of the two spin state populations, LS and HS.

The resonant Raman spectra of ferric DHP, HRP and HHMb are shown in Figure 3 with the Gaussian fits to the υ_2 and υ_3 modes given in Table 5. Ferric HHMb has water bound to the iron, which is also known as metaquo, and is thus 6-coordinate. The metaquo form of HHMb has two υ_3 Raman bands at 1481 cm^{-1} and 1514 cm^{-1} whose intensities are proportional to the relative population of 67% HS and 33% LS, respectively. The 5-coordinate ferric HRP does not have the same frequency as 6-

coordinate forms and this has been ascribed to an IS or IS, HS-mixed state (*67*). Figure 3 shows that the υ_3 in DHP is observed at 1502 cm^{-1} and has strong resemblance to the HRP υ_3 mode. Keeping in mind that the crystal structure of DHP reveals a 5-coordinate heme with no water bound to the iron, we assign the υ_3 mode of ferric DHP to a mixed spin state with IS and HS population as observed in peroxidases.

The fluoride adduct has the greatest population of the high spin state of all the ligands for all three proteins. In Figure 4, the ν_3 high spin peaks are observed at 1475 cm^{-1}, 1476 cm^{-1} and 1479 cm^{-1} for DHP-F, HHMb-F and HRP-F. Low spin ν_3 peaks are observed at which 1503 cm^{-1}, 1508 cm^{-1} and 1504 cm^{-1} for DHP-F, HHMb-F and HRP-F respectively. HRP-F has more high spin character than HHMb-F and DHP-F. HRP-F has 94% HS as calculated from ν_3 where DHP-F HS is 65% and HHMb-F HS is 70%.

Cyanide is the typical ligand used to induce the LS iron for heme proteins. Tables 2-4 present the Raman data obtained for DHP-CN, HHMb-CN and HRP-CN. The low spin ν_3 is at 1504 cm^{-1}, 1506 cm^{-1} and 1506 cm^{-1} for DHP-CN, HHMb-CN and HRP-CN, respectively. DHP-CN and HHMb-CN are 100% LS and HRP-CN is 95% LS as calculated from ν_3.

The fluoride and cyanide adducts represent the two extremes of 6-coordinate HS and LS, respectively. In HHMb there is a transition as measured by υ_3 from mainly HS (Cl^-, Br^-, SCN^-, OH^-) to mostly LS (N_3^- and CN^-) as ligand strength increases. In DHP the transition to LS occurs already for the much more weakly ligating halogens. Chloride-ligated DHP is 64% LS, compared to 30% LS for HHMb-Cl. DHP-Br is 100% LS, while HHMb-Br was only 26% LS based on the analysis of υ_3. The Resonance Raman data for these ligands are presented in the Supporting Information. The core size of DHP does

appear to show a trend for the halogens in which the percentage of HS is 65%, 36% and 0% for F^-, Cl^- and Br^-, respectively. There is precedent for the chloride and bromide adducts in protohemin (*68*). The trends in the Soret band for the halide adducts of DHP shown in Table 1 do not follow the trend of spin states in Table 2, but rather are relatively constant. The DHP-SCN adduct is primarily LS, while the HHMb-SCN adduct has significant HS character, yet both show similar Soret band maxima of 412-413 nm. The azide adducts DHP-N_3 and HHMb-N_3 have similar percentages of HS character, 21% and 23%, and have Soret bands that are in the range 420-421 nm. These observations suggest that factors other than spin state are governing the position of the Soret band maximum in both HHMb and DHP.

The hydroxide adduct of DHP is representative of a mixed spin heme protein DHP-OH is 68% LS and 32% HS as measured by υ_3, data in Table 2. The hydroxide derivative of ferric Mb was previously determined to exist in thermal spin-state equilibrium at room temperature with 30% LS and 70% HS(*69, 70*). Based on υ_3, the HHMb-OH data in Table 2 indicate a 17% LS and 83% HS mixture. HRP-OH has been shown to exist in a 93% LS and 7% HS equilibrium at room temperature (*70-72*). Based on these data DHP-OH has spin population that lies almost exactly halfway between those of HHMb-OH and HRP-OH.

The axial vibrations of the ferric-hydroxyl adduct is readily observable and can be verified using deuteration as shown in Figure 5. In Figure 5A a $\nu_{(Fe\text{-}OH)}$ stretching modes has been identified for HHMb-OH at 489 cm^{-1} with a smaller Raman mode 506 cm^{-1} of unknown origin. The isotope effect and temperature dependence of SWMb-OH has been studied previously and is nearly identical the data obtained here (*70*). The corresponding

DHP-OH mode is observed at are 491 cm^{-1} with a mode of unknown origin at 513 cm^{-1} as can be seen in Figure 5B. The isotope effect is difficult to discern in a difference spectrum because for both DHP and HHMb, there is a large decrease in intensity associated with deuteration of the hydroxide adduct. Nonetheless, there are clearly two distinct bands that are evident in the DHP-OD and HHMb-OD spectra. The HRP-OH adduct has a $\nu_{(Fe\text{-}OH)}$ stretching mode at 503 cm^{-1} corresponding only to the LS species (*70, 72*). The relative population of the high-spin and low-spin hydroxy species can also be estimated from resonant Raman spectra obtained in the high frequency region as shown in Figure 6. Figure 6 shows that HHMb-OH is mainly HS, DHP-OH has significant contributions from both LS and HS, and HRP-OH is mostly LS. These observations are consistent with the above analysis of the Fe-OH stretching vibration.

The ν_4 band is also known as the electron density marker mode. It is sensitive to the oxidation state of the heme iron. It is noteworthy that in all of the adducts studied there is a trend for ν_4 to increase in frequency in the order ν_4(HRP) > ν_4(DHP) > ν_4(HHMb). This trend can be clearly seen in Figures 4, 5 and 7, for no axial ligand (or H_2O in the case of HHMb), F and OH ligands, respectively.

Density Functional Theory Calculations. Density function theory (DFT) calculations of a porphine model system shown in Figure 7 permit changes in spin state to be related to structural changes in core size. The model was geometry optimized in three spins, LS, IS and HS corresponding to S=1/2, S=3/2 and S=5/2, respectively. The core size can be defined in terms of the average Fe-Np distance and the Fe out-of-plane displacement. The Fe-Np bond distance was calculated to be 2.029 Å, 2.036 Å, and 2.080 Å, for LS, IS and HS, respectively. The Fe out-of-plane displacement is 0.194 Å, 0.206 Å, and 0.302

Å, for LS, IS and HS, respectively. The largest change occurs for the change from IS to HS. In the case of the 5-coordinate complex the highest energy d-orbital is the d_{x2-y2}, which is oriented towards along the Fe-Np bonds. Only in the S=5/2, HS, state is there significant electron density in this orbital. This leads to the large repulsion between the iron and ring and the corresponding core size expansion. The effect of the spin state populations is manifested in differences in the Fe-N_ε bond length. Here the largest change occurs between the LS and IS spin states. The calculated Fe-N_ε bond lengths are 2.034 Å, 2.199 Å, and 2.187 Å, respectively for the LS, IS and HS states. The large increase in Fe-Nε bond length occurs when the d_{z2} orbital is occupied. It is clear from the DFT calculation that the d_{z2} orbital lies below the d_{x2-y2} in energy.

Discussion

Raman scattering from the core size marker modes have been used as the basis for understanding the trends in spin states of ferric heme iron. The Soret band maxima show a less conclusive trend as indicated by comparison of the UV-vis absorption data in Table 1 with the Raman data in Tables 2-4. The resonance Raman data show that the ligands of intermediate strength are bound to the heme iron. We hypothesize that the reason for the lack of a trend in the Soret band maxima is that the effect of axial ligation on the porphyrin π-system depends more strongly on the π-acid strength of the axial ligand than on the spin state. Ligands such as CN^- and N_3^- form LS adducts with Soret bands that are shifted to the range 421 - 423 nm.[6, 7] The OH^- and SCN^-, and the halides have weaker ligation leading to varying amounts of HS and LS populations, but also with distinctly less π-character. Their Soret band maxima fall in the range 412-414 nm. In the case of SCN^- the softer sulfur atom leads to poorer overlap. The hydroxide adduct likely depends

on the hydrogen bonding. Compound II, which is a deprotonated hydroxy adduct, has a double bond and a Soret band at 419 nm in DHP.[5] The halide adducts all have Soret bands around 406 nm in DHP and 407 – 409 nm in HHMb regardless of the spin state. Thus, the Soret band alone is not a good indicator of the spin state.

The correlation of the iron spin state and core size mode frequency is based on the coupling of the vibrational modes involving the heme periphery with strain located at the pyrrole nitrogens due to metal-porphyrin interactions. High spin (S=5/2) iron has greater electron density in the d_{x2}-$_{y2}$ orbital, which is directed towards the pyrrole nitrogens. This tends to force the iron further out of the heme plane. In addition, the Fe-N_p bond lengths increase as the core size expands. However, the high-spin heme iron can only partially relieve the strain of the expanded core size by an out-of-plane displacement. The expansion of the porphyrin ring leads to ring strain on the C_α-N_p bonds and on the C_α-C_m bonds. This strain lowers the frequencies of several key vibrational modes, ν_2 (A_{1g}), ν_3 (A_{1g}), ν_{10} (B_{1g}) and ν_{11} (B_{1g}). There were early reports that ν_{19} (A_{2g}) was also affected.[50, 51] The vibronic modes (B_{1g} and A_{2g}) are easiest to observe using Q-band (α,β-band) excitation, while the A_{1g} modes are most prominent for Soret excitation. The origin of these different resonant Raman enhancements lies in the difference between a vibronic (Herzberg-Teller) mechanism for enhancement in the Q-bands and Frank-Condon enhancement in the Soret band. In spite of the fact that the Raman enhancement of the Soret band is dominated by totally symmetric modes that gain their Raman enhancement by origin displacements, there is a small degree of Herzberg-Teller enhancement in the Soret band. Weak bands such as the Q-band and charge transfer bands gain in oscillator

strength by vibronic coupling to the Soret band and this in turn means that the Soret band takes on some of the character of the forbidden transitions.[73-75]

We have used Soret band excitation to probe the change in spin state population for a series of heme iron ligands in the ferric form of DHP, HHMb and HRP. Soret band excitation was first employed to determine the core size marker band frequencies by Callahan and Babcock,[50, 51] who showed that ν_3 was more readily distinguished than ν_2 or ν_{10} because it is in a less congested region of the Raman spectrum. Callahan and Babcock[50, 51] did caution that use of ν_3 alone did not provide as good a correlation as what they called ν_{19} (but is now assigned as ν_2). However, Callahan and Babcock were measuring a number of different hemes with quite different peripheral substitution patterns.[50, 51] The present study focuses on the effects of protein structure and axial ligation on b-type hemes. There are differences in heme structure since heme doming (A_{2u}) tends to be the dominant distortion in globins, while heme saddling (B_{1u}) tends to be the dominant distortion in peroxidases.[52] The ν_3 band is adequate for our comparisons and while comparisons based on ν_2 largely agree, there are complications because of the presence of modes ν_{11} and ν_{19} in this spectral region.

The halide series shows predictable progression from HS to LS for the DHP adducts. High spin fluoride samples have 65%, 71% and 92% percentage of HS character as calculated from ν_3 for DHP, HHMb and HRP respectively. The chloride adducts DHP-Cl and HHMb-Cl have 36% and 70% HS character, respectively. Bromide adducts DHP-Br and HHMb-Br have 0% and 74% HS character, respectively, as calculated from ν_3. DHP is consistently lower spin throughout the halide series and for SCN adducts as shown in Tables 2 and 3.

The significance of the hydroxide adduct data is complicated. First, the deuterium isotope effect is unusual consisting of a Raman band shift and a decrease in Raman band intensity. Based on the isotope shift there is on band peaked at ~490 cm^{-1} that shows an isotope shift in both HHMb-OH and DHP-OH. Our data agree with other reports of a multi-component band at 490 cm^{-1}.[54, 69] The temperature dependence of the Mb-OH band reveals a 560 cm^{-1} band that shows the isotope shift at 20 K, and has been assigned as the LS component,[70] which we have not verified in DHP. Based on these data the frequency of the Fe-OH stretch is slightly higher in DHP-OH than HHMb-OH and the Fe-OH bond in DHP-OH is stronger than that in HHMb-OH in the HS form. As indicated in Scheme 1 there are two possible effects that can shift the Fe-OH frequency. For either an increase in hydrogen bond donation to the oxygen lone pair or a decrease in hydrogen bond acceptor strength with the O-H hydrogen, the interaction of OH^- with Fe(III) should weaken. In other words, the frequency of Fe-OH stretch should increase as hydrogen bond donation weakens. Since the distal histidine of DHP is shifted approximately 1.5 Å farther from the heme than in myoglobin, the weaker hydrogen bonding in DHP-OH is expected to give rise to a stronger Fe-OH bond. The pKa of 8.0 for formation of DHP-OH,[6] is significantly lower than the pKa for either HHMb-OH or HRP-OH. The pKas of HHMb-OH and HRP-OH are 9.55 and 10.3, respectively (see also Supporting Information). Given that DHP and HHMb only have the distal histidine at high pH while HRP has both His42 and Arg38, it is somewhat surprising that formation of DHP-OH has such a low pKa. It is reasonable to hypothesize that distal side hydrogen-bond acceptor interactions are stronger in DHP than in HHMb, consistent both with the higher Fe-OH frequency and the lower pKa for hydroxide adduct formation.

One of the most important states is the resting state of the enzyme (or globin). This is usually a five-coordinate adduct. The frequencies of the five-coordinate adducts of HRP and DHP are intermediate between the 6-coordinate HS and LS frequencies. This may arise from an intermediate spin state as suggested elsewhere.[65] According to DFT calculations there is a relatively small change in porphine ring structure for the LS → IS transition. There is a change in axial ligation due to electron repulsions with the electron d_{z2}. As shown in Figure 7, the out-of-plane displacement of the iron and Fe-Np bond lengths increase mainly for the IS → HS transition. These factors suggest that a quantum-mechanically mixed state proposed to explain the intermediate frequency of ν_3 in other peroxidases,[67, 76] may be general feature of 5-coordinate ferric heme iron. Whether this is the explanation for DHP remains to be seen since there is conflicting evidence concerning the axial ligation in the ferric resting state. The x-ray structure indicates that that the heme iron is five-coordinate[3, 4] while MCD,[31] UV-vis titrations[6] and the resonance Raman data (this work) are consistent with a water molecule bound in the distal axial site.

Conclusion

The hypothesis that a protein can have the dual functions of a hemoglobin and a dehaloperoxidase presents a number of mechanistic challenges. The structure of DHP is consistent with the hemoglobin function, rather than a peroxidase function. DHP lacks the most important structural features found in all other heme peroxidases on both the proximal and distal side of the heme. The Asp-His-Fe charge relay is not present in DHP and is replaced by much weaker interactions on the proximal side. However, the proximal ligation in DHP is significantly stronger that in Mb based on the data obtained in this

study, which show that the DHP spin state population is intermediate between HHMb and HRP. The measurement in this study relies on comparison of the ν_3 frequency for various ligand adducts. The combination of a distal His and Arg found in the distal pocket of peroxidases, such as HRP, is not observed in the DHP structure. The consequence of this difference can be seen in the similarity of the Fe-OH stretching mode in HHMb and DHP. Both the distal and proximal structural features are thought to be essential for rapid activation of bound H_2O_2 to form compound I. In spite of these glaring differences, DHP has an enzymatic rate for oxidation of phenols that is at least an order of magnitude higher than any other known hemoglobin. These data are in agreement with DFT calculations,[63] which indicate that a charge relay mechanism can function in DHP by means of a very strong hydrogen bond to a backbone carbonyl. These observations are consistent with a heme iron poised to act as both an oxygen-binding protein and an electron acceptor in the peroxidase reaction cycle. While there are many remaining questions regarding the nature of the DHP active site, a next step is to identify the factors that govern the switch of DHP function from an oxygen binding protein to a peroxidase.

Supporting Information Titration data for HHMb, DHP and HRP acid-alkaline transitions are available. Raman spectra for DHP-Cl, DHP-Br, DHP-SCN and DHP-N_3 are available.

Table 1. Soret maxima for Ferric HHMb, DHP and HRP ligated samples. All samples were made in 100 mM citrate buffer pH 6 with 50 mM concentration the respective anionic ligand.

Ligand	Mb Soret λ max (nm)	DHP Soret λ max (nm)	HRP Soret λ max (nm)
None	407	406	403
F^-	407	406	404
Cl^-	409	406	- - -
Br^-	409	406	- - -
SCN^-	412	413	- - -
OH^-	413	414	415
N_3^-	420	421	413
CN^-	423	423	422

Table 2. Results of Gaussian fits to Resonance Raman data collected for ferric six-coordinate DHP adducts. The parameters are ω (position), σ (Gaussian width), and % is percentage HS or LS as calculated using Eqns. 1 and 2.

	ν3 HS	ν3 LS	ν2 HS	ν2 LS
DHP-F				
ω	1475	1503	1560	1584
σ	9.68	8.84	16.6	10
%	65	35	41	59
DHP-Cl				
ω	1487	1503	1561	1584
σ	9.6	8	20.9	13.8
%	36	64	35	65
DHP-Br				
ω		1504	1557	1583
σ		7.8	10.1	13.3
%		100	27	73
DHP-SCN				
ω	1471	1502	1552	1582
σ	9.9	8.4	15.3	15.1
%	9	91	21	79
DHP-N_3				
ω	1476	1503	1560	1584
σ	11.3	8	15.5	14.2
%	21	79	40	60
DHP-OH				
ω	1476	1502	1552	1582
σ	10.2	8.4	15.7	17.3
%	32	68	31	69
DHP-CN				
ω		1502	1556	1582
σ		8.8	18.5	13.4
%		100	19	81

Table 3. Results of Gaussian fits to Resonance Raman data collected for ferric six-coordinate HHMb adducts. The parameters are ω (position), σ (Gaussian width), and % is percentage HS or LS as calculated using Eqns. 1 and 2.

	ν3 HS	ν3 LS	ν2 HS	ν2 LS
HHMb-H_2O				
ω	7	6.6	16.5	16.5
σ	1481	1516	1560	1580
%	67	33	50	50
HHMb-F				
ω	1476	1508	1557	1580
σ	6.8	5.2	12.6	8.9
%	71	29	72	28
HHMb-Cl				
ω	1476	1508	1558	1580
σ	6.6	4.9	12.6	8.5
%	70	30	72	28
HHMb-Br				
ω	1480	1512	1563	1583
σ	7.2	3.65	10.9	6.5
%	74	26	81	19
HHMb-SCN				
ω	1473	1507	1558	1580
σ	6	5.1	14.2	10.2
%	72	28	65	35
HHMb-N_3				
ω	1469	1499	1552	1579
σ	7.3	7.4	15.5	11.3
%	23	77	26	74
HHMb-OH				
ω	1486	1502	1553	1580
σ	8.6	3.8	13.7	12
%	83	17	33	67
HHMb-CN				
ω		1506		1585
σ		6.2		14
%		100		100

Table 4. Results of Gaussian fits to Resonance Raman data collected for ferric six-coordinate HRP adducts. The parameters are ω (position), σ (Gaussian width), and % is percentage HS or LS as calculated using Eqns. 1 and 2.

	ν3 HS	ν3 LS	ν2 HS	ν2 LS
HRP-F				
ω	1479	1505	1567	1582
σ	8.8	10.2	15.3	5.9
%	94	6	44	56
HRP-OH				
ω	1479	1504	1562	1585
σ	11.3	6.7	6.9	10.3
%	23	77	36	64
HRP-CN				
ω	1477	150		1585
σ	21.4	7.3		16.8
%	5	95		100

Table 5. Results of Gaussian fits to Resonance Raman data collected for ferric five-coordinate adducts. The parameters are ω (position), σ (Gaussian width) were calculated using Eqns. 1 and 2.

	ν3 IS	ν2 IS
HRP		
ω	1498	1577
σ	16	19.3
DHP		
ω	1502	1582
σ	6.5	12.5

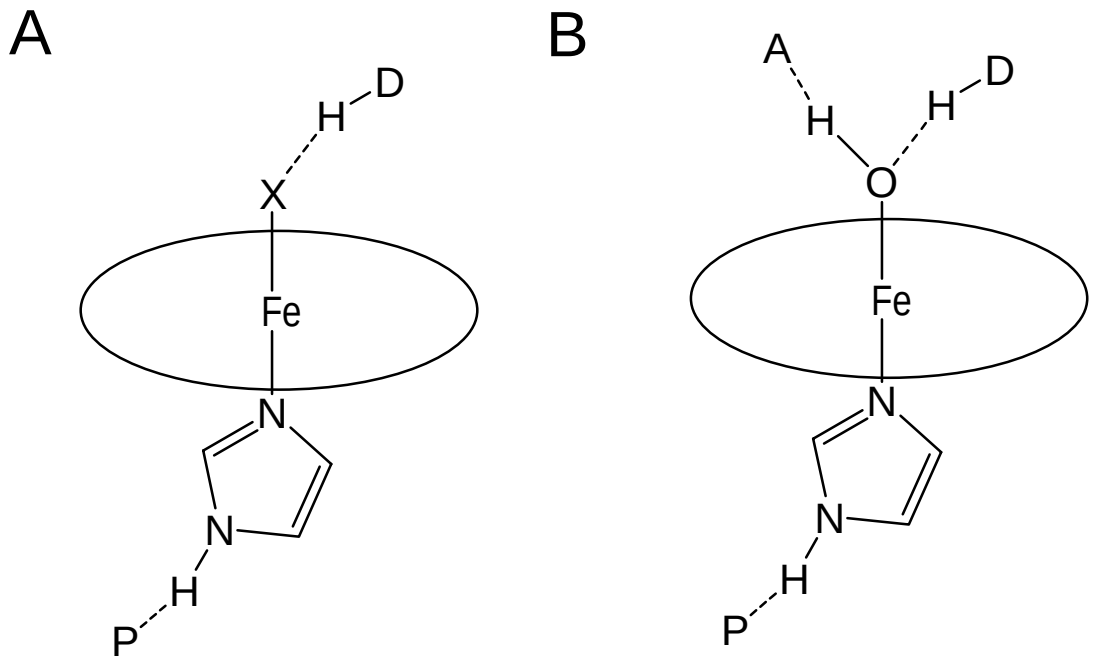

Scheme 1. Depiction of the geometry of distal and proximal side hydrogen bonding for hydrogen bond acceptor ligands X and for hydroxide. The P moiety on the proximal side is a hydrogen bond acceptor (e.g. –COO-, -O(lone pair), =C=O). The D-H moiety on the distal side is a hydrogen bond donor (e.g. N-H from histidine or arginine). The A moiety on the distal side is a hydrogen bond acceptor such as the histidine lone pair or lone pair from an oxygen on water.

.

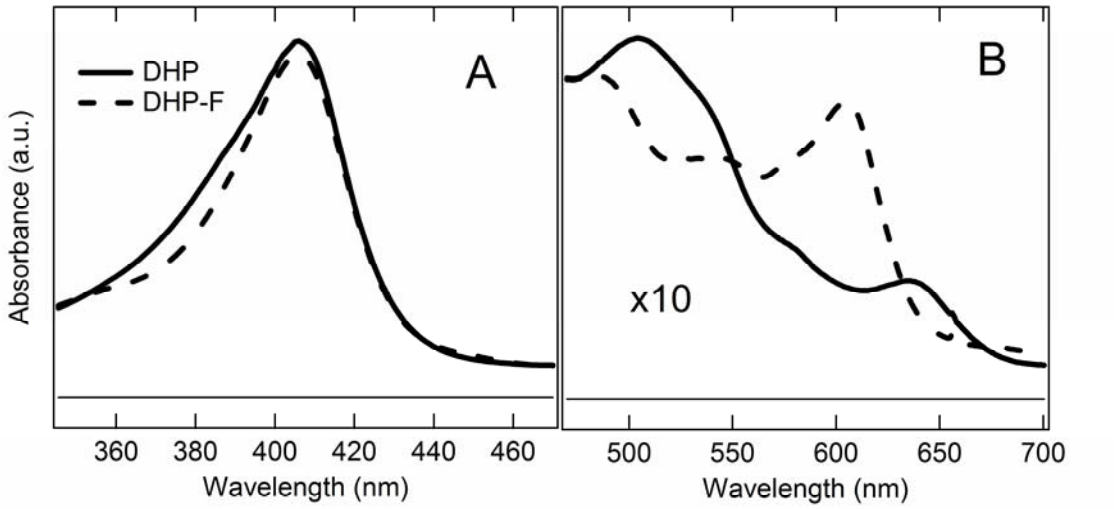

Figure 1. Absorption Soret spectra of high spin ferric DHP (solid) and ferric DHP with fluoride ligand (dash) in 100 mM phosphate buffer, pH 6.0 at room temperature. Soret maxima for both the ferric DHP and ferric DHP-F are 406 nm with small differences in the band widths. B. The Q-bands and charge transfer bands (*64*) of ferric DHP and ferric DHP-F are shown.

.

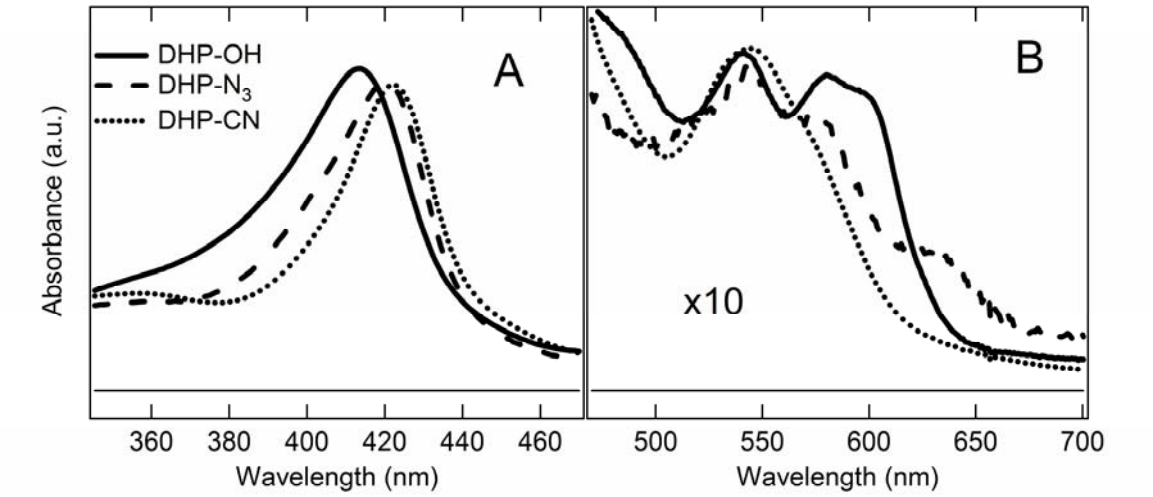

Figure 2. Absorption spectra of mixed and low spin ferric DHP samples. A. The shift in the Soret band maximum from 406nm for ferric DHP to 414, 421 and 423 nm for hydroxide (solid), azide (dash) and cyanide (dotted) ferric DHP, respectively, is characteristic of mixed to low spin form of ferric DHP. B. The Q-(α/β)-band and charge transfer band spectra[64] are shown.

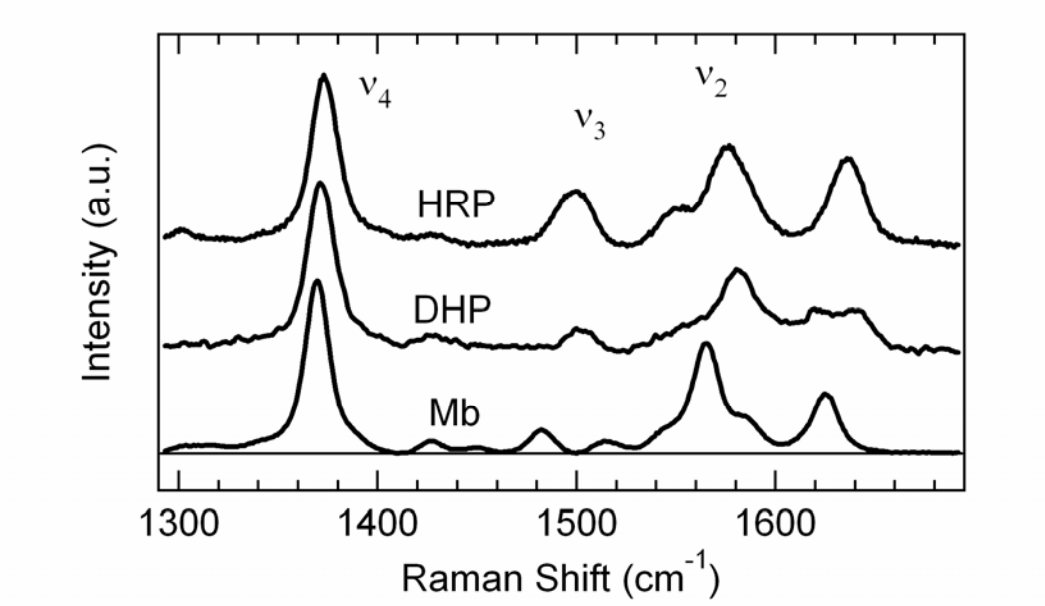

Figure 3. RR spectra are shown in the high frequency region for the ferric forms of HHMb, DHP and HRP at pH 6.0. The Raman excitation wavelength was 410 nm.

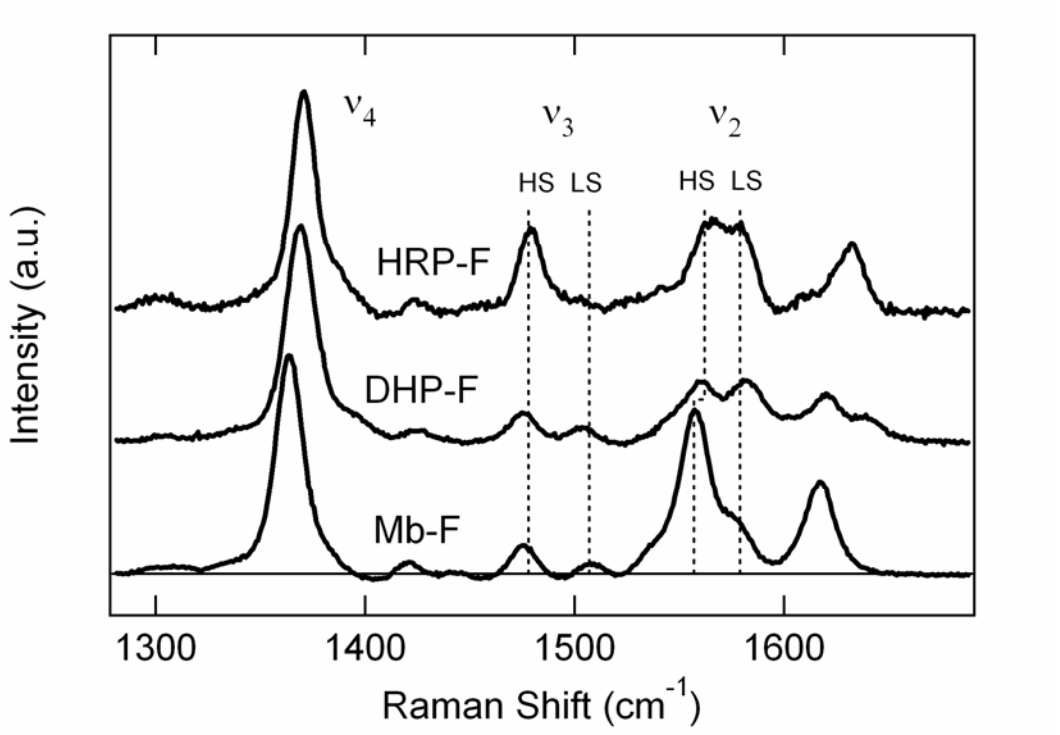

Figure 4. RR spectra are shown in the high frequency region for the fluoride adducts of HHMb, DHP and HRP. The Raman excitation wavelength was 410 nm.

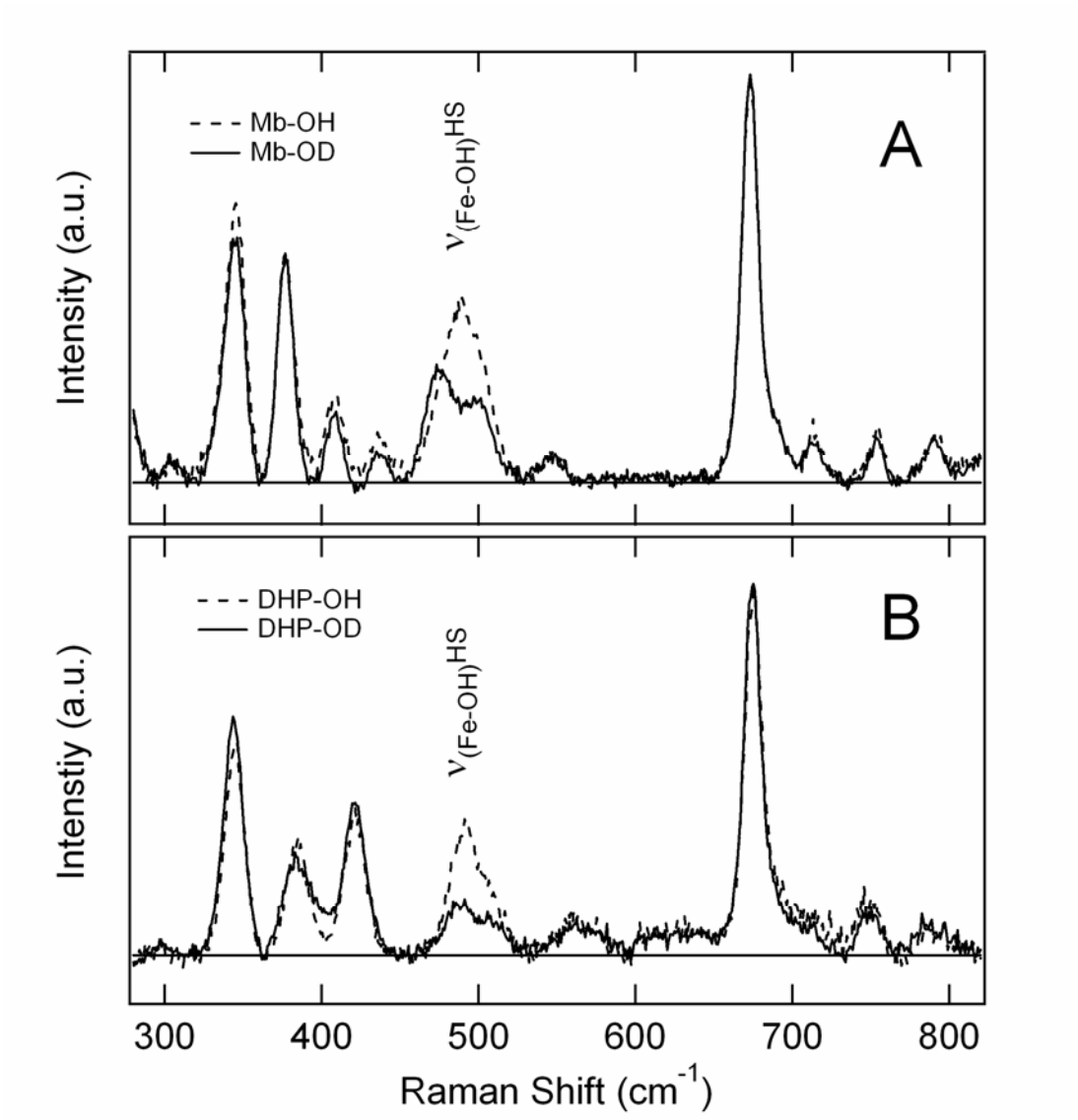

Figure 5. RR spectra collected for the lower window of the hydroxide adducts. Sample conditions are 120 μM protein dissolved in 0.025 M borate buffer, pH 10.5 or pD 10.9. The Raman excitation wavelength was 410 nm. A. The Raman data for the Mb-OH sample are shown. B. The Raman data for the DHP-OH sample are shown. For both samples the spectra are shown as OH (dashed) and OD (solid).

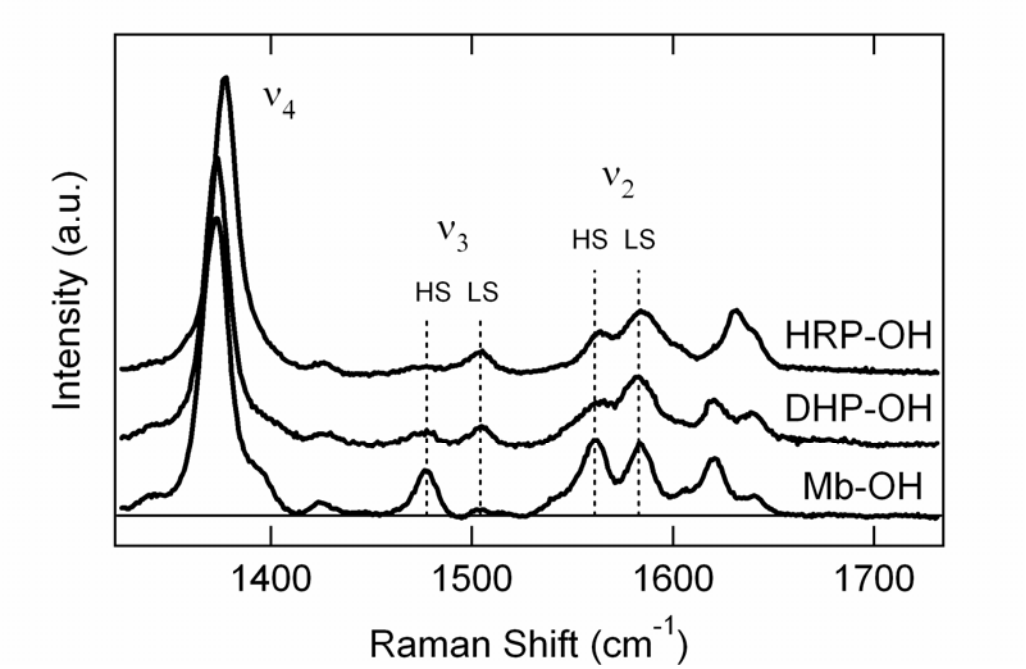

Figure 6. RR spectra are shown in the high frequency region for the hydroxy adducts HHMb-OH, DHP-OH and HRP-OH. The HRP-OH and Mb-OH samples were prepared at pH 12.0. The DHP-OH sample was prepared at pH 10.5. The Raman excitation wavelength was 410 nm.

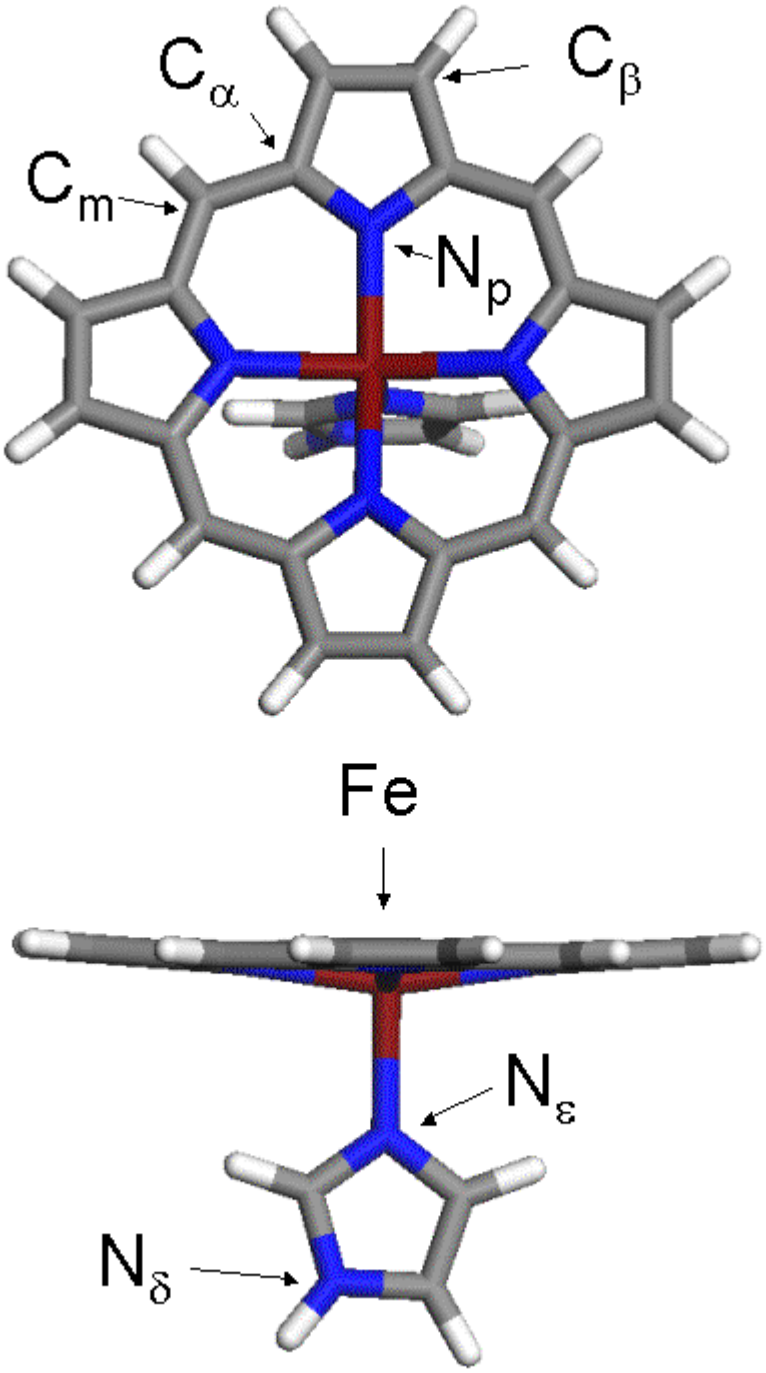

Figure 7. A representation of ferric iron porphine used for model DFT calculations. The identities of key atoms in the structure are given for reference with the text.

References

(1) Chen, Y. P.; Woodin, S. A.; Lincoln, D. E.; Lovell, C. R. **An unusual dehalogenating peroxidase from the marine terebellid polychaete *Amphitrite ornata***. J. Biol. Chem. (1996), 271(9), 4609-12.

(2) Weber, R. E.; Magnum, C. P.; Steinman, H.; Bonaventura, C.; Sullivan, B.; Bonaventura, J. **Hemoglobins of two terebellid polychaetes: *Enoplobranchus sanuigneus* and *Amphitrite ornata***. Comp. Biochem. Physiol. (1977), *56A*, 179-187.

(3) Lebioda, L.; LaCount, M. W.; Zhang, E.; Chen, Y. P.; Han, K.; WHitton, M. M.; Lincoln, D. E.; Woodin, S. A. **An enzymatic globin from a marine worm**. Nature (1999), *401*, 445.

(4) LaCount, M. W.; Zhang, E. L.; Chen, Y. P.; Han, K. P.; Whitton, M. M.; Lincoln, D. E.; Woodin, S. A.; Lebioda, L. **The crystal structure and amino acid sequence of dehaloperoxidase from *Amphitrite ornata* indicate common ancestry with globins**. J. Biol. Chem. (2000), *275*, 18712-18716.

(5) Belyea, J.; Gilvey, L. B.; Davis, M. F.; Godek, M.; Sit, T. L.; Lommel, S. A.; Franzen, S. **Enzyme function of the globin dehaloperoxidase from *Amphitrite ornata* is activated by substrate binding**. Biochemistry (2005), *44*, 15637-15644.

(6) Nienhaus, K.; Deng, P. C.; Belyea, J.; Franzen, S.; Nienhaus, G. U. **Spectroscopic study of substrate binding to the carbonmonoxy form of dehaloperoxidase from *Amphitrite ornata***. J. Phys. Chem. B (2006), *110*, 13264-13276.

(7) Franzen, S.; Jasaitis, A.; Belyea, J.; Brewer, S.; Casey, R.; MacFarlane IV, A. W.; Stanley, R.; Vos, M. H.; Martin, J.-L. **NO-heme Geminate Recombination Dynamics in Dehaloperoxidase**. J. Phys. Chem. B (2006), *110*, 14483-14493.

(8) Franzen, S.; Dyer, R. B.; Woodruff, W. H.; Roach, M. R.; Chen, Y. P.; Dawson, J. H. **The Unusual Reactivities of *Amphitrite ornata* and *Notomastus lobatus* Do Not Result from Strong Hydrogen Bonding of their Proximal Histidine Heme Iron Ligands**. J. Am. Chem. Soc. (1998), *120*, 4658-4661.

(9) Royer Jr., W. E.; Pardanani, A.; Gibson, Q. H.; Peterson, E. S.; Friedman, J. M. **Ordered water molecules as key allosteric mediators in a cooperative dimeric hemoglobin**. Proc. Natl. Acad. Sci. U. S. A. (1996), *93*, 14526-14531.

(10) Ascenzi, P.; Bocedi, A.; de Sanctis, D.; Pesce, A.; Bolognesi, M.; Marden, M. C.; Dewilde, S.; Moens, L.; Hankeln, T.; Burmester, T. **Neuroglobin and cytoglobin**

- Two new entries in the hemoglobin superfamily. Biochem. Mol. Biol. Ed. (2004), *32*, 305-313.

(11) Han, K. P.; Woodin, S. A.; Lincoln, D. E.; Fielman, K. T.; Ely, B. **Amphitrite ornata, a marine worm, contains two dehaloperoxidase genes**. Marine Biotech. (2001), *3*, 287-292.

(12) Suzuki, T.; Imai, K. **Evolution of myoglobin**. Cell. Mol. Life Sci. (1998), *54*, 979-1004.

(13) Matsui, T.; Ozaki, S.; Liong, E.; Phillips, G. N.; Watanabe, Y. **Effects of the location of distal histidine in the reaction of myoglobin with hydrogen peroxide**. J. Biol. Chem. (1999), *274*, 2838-2844.

(14) Ozaki, S.; Hara, I.; Matsui, T.; Watanabe, Y. **Molecular engineering of myoglobin: The improvement of oxidation activity by replacing Phe-43 with tryptophan**. Biochemistry (2001), *40*, 1044-1052.

(15) Roach, M. P.; Puspita, W. J.; Watanabe, Y. **Proximal ligand control of heme iron coordination structure and reactivity with hydrogen peroxide: investigations of the myoglobin cavity mutant H93G with unnatural oxygen donor proximal ligands**. J. Inorg. Biochem. (2000), *81*, 173-182.

(16) Egawa, T.; Yoshioka, S.; Takahashi, S.; Hori, H.; Nagano, S.; Shimada, H.; Ishimori, K.; Morishima, I.; Suematsu, M.; Ishimura, Y. **Kinetic and spectroscopic characterization of a hydroperoxy compound in the reaction of native myoglobin with hydrogen peroxide**. J. Biol. Chem. (2003),*278*, 41597-41606.

(17) Spiro, T. G.; Smulevich, G.; and Su, C. **Probing Protein Structure and Dynamics with Resonance Raman Spectroscopy: Cytochrome c Peroxidase and Hemoglobin**. Biochemistry (1990), *29*, 4497-4508.

(18) Gajhede, M.; Schuller, D. J.; Henriksen, A.; Smith, A. T.; Poulos, T. L. **Crystal structure of horseradish peroxidase C at 2.15 angstrom resolution.** Nature Struct. Biol. (1997), *4*, 1032-1038.

(19) Tanaka, M;, Ishimori, K.; Mukai, M.; Kitagawa, T.; Morishima, I. **Catalytic activities and structural properties of horseradish peroxidase distal His42->Glu or Gln mutant**. Biochemistry (1997), *36*, 9889-9898.

(20) Poulos, T. L.; Kraut, J. **The structure of cytochrome c peroxidase at 2.5 Å resolution**. J. Biol. Chem. (1980), *255*, 575-580.

(21) Poulos, T. L.; Edwards, S. L.; Wariishi, H.; Gold, M. H. **Crystallographic refinement of lignin peroxidase at 2 Å**. J. Biol. Chem. (1993), *268*, 4429-4440.

(22) Schuller, D. J.; Ban, N.; van Huystee, R. B.; McPherson, A.; Poulos, T. L. **The crystal structure of peanut peroxidase**. Structure (1996), *4*, 311-321.

(23) Mukai, M.; Mills, C. E.; Poole, R. K.; Yeh, S. R. **Flavohemoglobin, a globin with a peroxidase-like catalytic site**. J. Biol. Chem. (2001), *276*, 7272-7277.

(24) Goodin, D. B.; McRee, D. E. **The Asp-His-Fe Triad of cytochrome c peroxidase controls the Reduction Potential, Electronic Structure, and Coupling of the Tryptophan Free Radical to the Heme**. Biochemistry (1993), *32*, 3313-3324.

(25) Vojtechovsky, J.; Chu, K.; Berendzen, J.; Sweet, R. M.; Schlichting, I. **Crystal structures of myoglobin-ligand complexes at near-atomic resolution**. Biophys. J. (1999), *77*, 2153-2174.

(26) Parak, F.; Hartmann, H.; Aumann, K. D.; Reuscher, H.; Rennekamp, G.; Bartunik, H.; Steigemann, W. **Low-Temperature X-Ray-Investigation of Structural Distributions in Myoglobin**. Eur. Biophys. J. Biophys. Lett. (1987), *15*, 237-249.

(27) Shiro, Y.; Iizuka, T.; Marubayashi, K.; Ogura, T.; Kitagawa, T.; Balasubramanian, S.; Boxer, S. G. **Spectroscopic study of Ser92 mutants of human myoglobin - hydrogen bonding effect of Ser92 to proximal His93 on structure and property of myoglobin**. Biochemistry (1994), *33*, 14986-14992.

(28) Lloyd, E.; Burk, D. L.; Ferrer, J. C.; Maurus, R.; Doran, J.; Carey, P. R.; Brayer, G. D.; Mauk, A. G. **Electrostatic modification of the active site of myoglobin: characterization of the proximal Ser92Asp variant**. Biochemistry (1996), *35*, 11901-11912.

(29) Svistunenko, D. A. **Reaction of haem containing proteins and enzymes with hydroperoxides: the radical view**. Biochim. Biophys. Acta (2005), *1707*, 127-155.

(30) Henricksen, A.; Schuller, D. J.; Meno, K.; Welinder, K. G.; Smith, A. T.; Gajhede, M. **Structural interactions between horseradish peroxidase C and the substrate benzhydroxamic acid determined by X-ray crystallography**. Biochemistry (1998), *37*, 8054-8060.

(31) Osborne, R. L.; Sumithran, S.; Coggins, M. K.; Chen, Y. P.; Lincoln, D. E.; Dawson, J. H. **Spectroscopic characterization of the ferric states of Amphitrite ornata dehaloperoxidase and *Notomastus lobatus* chloroperoxidase: His-ligated peroxidases with globin-like proximal and distal properties**. J. Inorg. Biochem. (2006), *100*, 1100-1108.

(32) Mukai, M.; Nagano, S.; Tanaka, M.; Ishimori, K.; Morishima, I.; Ogura, T.; Watanabe, Y.; Kitagawa, T. **Effects of concerted hydrogen bonding of distal histidine on active site structures of horseradish peroxidase. Resonance Raman studies with Asn70 mutants**. J. Am. Chem. Soc. (1997), *119*, 1758-1766.

(33) Smulevich, G.; Mauro, J. M.; Fishel, L. A.; English, A. M.; Kraut, J.; Spiro, T. G. **Heme pocket interactions in cytochrome c peroxidase studied by site-directed mutagenesis and resonance Raman spectroscopy**. Biochemistry (1988), *27*, 5477-5485.

(34) Newmyer, S. L.; Sun, J.; Loehr, T. M.; deMontellano, P. R. O. **Rescue of the horseradish peroxidase His-170->Ala mutant activity by imidazole: Importance of proximal ligand tethering**. Biochemistry (1996), *35*, 12788-12795.

(35) Nissum, M.; Neri, F.; Mandelman, D.; Poulos, T. L.; Smulevich, G. **Spectroscopic characterization of recombinant pea cytosolic ascorbate peroxidase: Similarities and differences with cytochrome c peroxidase**. Biochemistry (1998), *37*, 8080-8087.

(36) Poulos, T. L.; Kraut, J. **The Stereochemistry of Peroxidase Catalysis**. J. Biol. Chem. (1980), *255*, 8199-8205.

(37) Hiner, A. N. P.; Raven, E. L.; Thorneley, R. N. F.; Garcia-Canovas, F.; Rodriguez-Lopez, J. N. **Mechanisms of compound I formation in heme peroxidases**. J. Inorg. Biochem. (2002), *91*, 27-34.

(38) Dunford, H. B. **How do enzymes work? Effect of electron circuits on transition state acid dissociation constants**. J. Biol. Inorg. Chem. (2001), *6*, 819-822.

(39) Franzen, S. **An electrostatic model for the frequency shifts in the carbonmonoxy stretching band of myoglobin: Correlation of hydrogen bonding and the Stark tuning rate**. J. Am. Chem. Soc. (2002), *124*, 13271-13281.

(40) Yamaguchi, K.; Watanabe, Y.; Morishima, I. **Push effect on the heterolytic O-O bond cleaveage of peroxoiron(II) porphyrin adducts**. Inorg. Chem. (1992), *31*, 156-157.

(41) Bizzarri, A. R.; Cannistraro, S. **Solvent Modulation of the Structural Heterogeneity in Fe(III) Myoglobin Samples - a Low-Temperature Epr Investigation**. Eur. Biophys. J. Biophys. Lett. (1993), *22*, 259-267.

(42) Kitagawa, T.; Nagai, K.; Tsubaki, M. **Assignment of the Fe-Nε (His F8) Stretching Band in the Resonance Raman Spectra of Deoxy Myoglobin**. FEBS Lett. (1979), *104*, 376-378.

(43) Bonagura, C. A.; Bhaskar, B.; Shimizu, H.; Li, H. Y.; Sundaramoorthy, M.; McRee, D. E.; Goodin, D. B.; Poulos, T. L. **High-resolution crystal structures and spectroscopy of native and compound I cytochrome c peroxidase**. Biochemistry (2003), *42*, 5600-5608.

(44) Nienhaus, K.; Olson, J. S.; Franzen, S.; Nienhaus, G. U. **The origin of stark splitting in the initial photoproduct state of MbCO**. J. Am. Chem. Soc. (2005), *127*, 40-41.

(45) Phillips, J. G. N.; Teodoro, M. L.; Li, T.; Smith, B.; Olson, J. S. **Bound CO is a molecular probe of the electrostatic potential in the distal pocket of myoglobin**. J. Phys. Chem. B (1999), *103*, 8817-8829.

(46) Morikis, D.; Champion, P. M.; Springer, B. A.; Sligar, S. G. **Resonance Raman investigations of site-directed mutants of myoglobin - Effect of distal histidine replacement**. Biochemistry (1989), *28*, 4791-4800.

(47) Yang, F.; Phillips Jr. G. N. **Crystal structures of CO-, deoxy- and met-myoglobins at various pH values**. J. Mol. Biol. (1996), *256*, 762-774.

(48) Franzen, S.; Belyea, J. L.; Gilvey, L. B. G.; Davis, M. F.; Chaudhary, C.; Sit, T. L.; Lommel, S. A. **Proximal cavity, distal histidine and substrate hydrogen-bonding mutations modulate the activity of Amphitrite ornata dehaloperoxidase**. Biochemistry (2006), *45*, 9085-9094.

(49) Neri, F.; Kok, D.; Miller, M. A.; Smulevich, G. **Fluoride binding in hemoproteins: The importance of the distal cavity structure**. Biochemistry (1997), *36*, 8947-8953.

(50) Callahan, P. M.; Babcock, G. T. **Insights into Heme Structure from Soret Excitation Raman Spectroscopy**. Biochemistry (1981), *20*, 952-958.

(51) Morikis, D.; Champion, P. M.; Springer, B. A.; Egeberg, K. D.; Sligar, S. G. **Resonance Raman Studies of Iron Spin and Axial Coordination in Distal Pocket Mutants of Ferric Myoglobin**. J. Biol. Chem. (1990), *265*, 12143-12145.

(52) Choi, S.; Spiro, T. G.; Langry, K. C.; Smith, K. M.; Budd, L. D.; LaMar, G. N. **Structural correlations and vinyl influences in resonance Raman spectra of protoheme complexes and proteins**. J. Am. Chem. Soc. (1982), *104*, 4345-4351.

(53) Jentzen, W.; Shelnutt, J. A. **The conformation of the heme is conserved in proteins of the same functional class**. Biophys. J. (1997), *72*.

(54) Desbois, A.; Lutz, M.; Banerjee, R. **Low-frequency vibrations in resonance Raman spectra of horse heart myoglobin. Iron-ligand and iron-nitrogen vibrational modes**. Biochemistry (1979), *18*, 1510-1518.

(55) Spiro, T. G.; Stong, J. D., Stein, P. **Porphyrin core expansion and doming in heme proteins. New evidence from resonance Raman spectra of six-coordinate high-spin iron(III) hemes**. J. Am. Chem. Soc. (1979), *101*, 2648-2655.

(56) Franzen, S.; Lambry, J. C.; Bohn, B.; Poyart, C.; Martin, J. L. **Direct Evidence for the Role of Heme Doming As the Primary Event in the Cooperative Transition of Hemoglobin**. Nature Struct. Biol. (1994), *1*, 230-233.

(57) Perdew, J. P.; Chevary, J. A.; Vosko, S. H.; Jackson, K. A.; Pederson, M. R.; Singh, D. J.; Fiolhais, C. **Atoms, molecules, solids and surfaces - Applications of the generalized gradient approximation for exchange and correlation**. Phys. Rev. B (1992), *46*, 6671-6687.

(58) Delley, B. J. Chem. Phys. (1990), *92*, 508-517.

(59) Delley, B. **From molecules to solids with the DMol(3) approach**. J. Chem. Phys. (2000), *113*, 7756-7764.

(60) Mermin, D. **Thermal properties of the inhomogeneous electron gas**. Phys. Rev. A (1965), *137*, 1441-1443.

(61) Franzen, S.; Fritsch, K.; Brewer, S. H. **Experimental observation of anharmonic coupling of the heme- doming and iron-ligand out-of-plane vibrational modes confirmed by density functional theory**. J. Phys. Chem. B (2002), *106*, 11641-11646.

(62) Franzen, S. **Spin-dependent mechanism for diatomic ligand binding to heme**. Proc. Nat. Acad. Sci. U.S.A. (2002), *99*, 16754-16759.

(63) Franzen, S. **Effect of a charge relay on the vibrational frequencies of carbonmonoxy iron porphine adducts: The coupling of changes in axial ligand bond strength and porphine core size**. J. Am. Chem. Soc. (2001), *123*, 12578-12589.

(64) Neri, F.; Indiani, C.; Baldi, B.; Vind, J.; Welinder, K. G.; Smulevich, G. **Role of the distal phenylalanine 54 on the structure, stability, and ligand binding of Coprinus cinereus peroxidase**. Biochemistry (1999), *38*, 7819-7827.

(65) Wang, M.-Y.; Hoffman, B. M. **Systematic trends in metalloporphyrin optical spectra** J. Am. Chem. Soc. (1994), *106*, 4235-4240.

(66) Zerner, M.; Gouterman, M.; Kobayashi, H. **Porphyrins VIII. Extended Huckel Calculations on Iron Complexes**. Theoret. Chim. Acta (1966), *6*, 363-400.

(67) Howes, B. D.; Schiodt, C. B.; Welinder, K. G.; Marzocchi, M. P.; Ma, J. G.; Zhang, J.; Shelnutt, J. A.; Smulevich, G. **The quantum mixed-spin heme state of barley peroxidase: A paradigm for class III peroxidases**. Biophys. J. (1999), *77*, 478-492.

(68) Hoard, J. L. (Smith, K. M., Ed.), Elsevier, Amsterdam (1975).

(69) Asher, S. A.; Schuster, T. M. **Resonance Raman Examination of Axial Ligand Bonding and Spin-State Equilibria in Metmyoglobin Hydroxide and Other Heme Derivatives**. Biochemistry (1979), *18*, 5377-5387.

(70) Feis, A.; Marzocchi, M. P.; Paoli, M.; Smulveich, G. **Spin state and axial ligand bonding in the hydroxide complexes of metmyoglobin, methemoglobin, and horseradish peroxidase at room and low temperatures**. Biochemistry (1994), *33*, 4577-4583.

(71) Shelnutt, J. A.; Alden, R. G.; Ondrias, M. R. **Heme-linked ionization in horseradish peroxidase detected by Raman difference spectroscopy**. J. Biol. Chem. (1986), *261*, 1720-1723.

(72) Sitter, A. J.; Shifflett, J. R.; Terner, J. **Resonance Raman spectroscopic evidence for heme iron-hydroxide ligation in peroxidase alkaline forms**. J. Biol. Chem. (1988), *263*, 13032-13038.

(73) Franzen, S.; Morre, L. J.; Woodruff, W. H.; Boxer, S. G. **Stark Effect Spectroscopy of the Heme Charge Transfer Bands of Deoxymyoglobin**. J. Am. Chem. Soc. (1999), *103*, 3070-3072.

(74) Franzen, S.; Wallace-Williams, S. E.; Shreve, A. P.; Dyer, R. B. **Heme charge-transfer band III is vibronically coupled to the soret band**. J. Am. Chem. Soc. (2002), *124*, 7146-7155.

(75) Franzen, S. **Perimeter model for the magnetic circular dichroism spectrum of deoxy ferrous heme in myoglobin**. J. Phys. Chem. B (2002), *106*, 10482-10491.

(76) Indiani, C.; Feis, A.; Howes, B. D.; Marzocchi, M. P.; Smulevich, G. **Effect of low temperature on soybean peroxidase: spectroscopic characterization of the quantum-mechanically admixed spin state**. J. Inorg. Biochem. (2000), *79*, 269-274.

Chapter 3: ESR and UV-visible characterization of the 2,4,6-trifluorophenoxyl radical produced by Dehaloperoxidase from *Amphitrite ornata*

Introduction

Dehaloperoxidase (DHP) from the marine worm *Amphitrite ornata* is a dual-function protein that switches between globin and peroxidase activity depending on the binding of substrate.[1] Consequently, substrate binding is proposed to be the trigger for the switch in function from a hemoglobin to a peroxidase. Substrate binding will be shown to effect the spin state [1,2] of the ferric iron active site and the redox potential of DHP in chapters 4 and 6, respectively.[3] The importance of substrate binding is enriched by the presence of a internal substrate binding site not found in globins.[3]

Substrate binding has been shown to result in spin state and redox potential shifts in cytochrome $P450_{cam}$.[4,5] Cytochrome $P450_{cam}$ catalyses regiospecific reaction with camphor, the regiospecific reactions have been modulated by mutagenesis of the substrate binding site. Interactions between the amino acid residues and the substrate has been shown to position the substrate in orientations that results in regiospecific reaction products.[5] The substrate binding site of cytochrome $P450_{cam}$ is a key feature that effects the regiospecific nature of products. DHP also has a substrate-binding site, which may facilitates or require two consecutive one-electron reactions with substrates. Despite the presence of the binding site, some one-electron reaction products are detected.

DHP catalyzes the oxidative dehalogenation of halogenated phenols in a hydrogen peroxide dependant reaction.[6-11] The dehalogenation of 2,4,6-trihalophenol produces 2,6-dihalo-1,4-benzoquinone via two consecutive one electron oxidation steps has been proposed in earlier DHP kinetic studies[10]. After one one-electron oxidation occurs on 2,4,6-triflorophenol a phenoxyl radical is formed as shown in scheme 1.

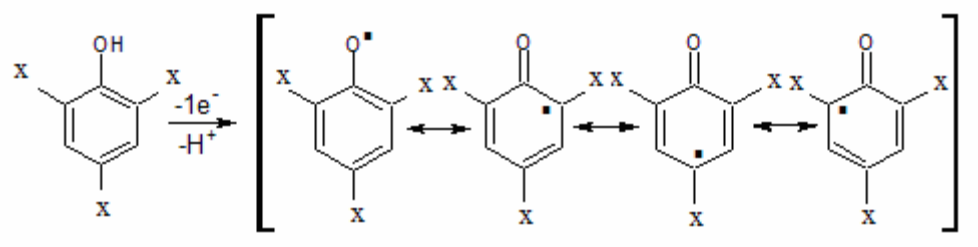

Scheme 1. 2,4,6-Trihalophenoxyl radical resonance structures.

When two consecutive oxidation steps occur on the same substrate the enzymatic cycle utilizes one equivalent of substrate per cycle and generates a quinone as shown in Scheme 2.[12] Horseradish peroxidase, HRP, reacts with substrate by a heme-edge electron transfer mechanism. HRP reacts with two one-electron oxidation steps which typically occur on two different substrate molecules thus two equivalents of substrate per cycle is typical a polymeric product results or quinone is formed.[13]

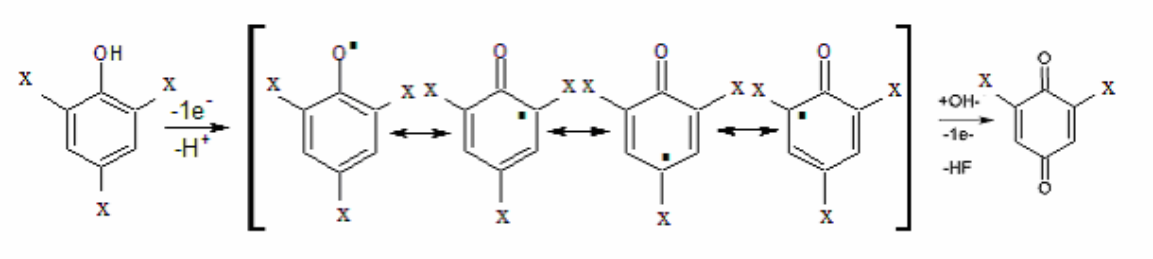

Scheme 2. 2-Electron oxidation of 2,4,6-trihalophenol

In this chapter, electron spin resonance (ESR) is utilized to detect phenoxyl radicals in order to measure the quantum yield of 1-electron reaction. UV-visible spectroscopy to quantify the amount of substrate being consumed by both one and two electron reactions. By combining ESR and UV-Visible techniques, we are able to determine the yield of the one- and two-electron reactions.

Materials and Methods.

ESR

The DHP enzyme was purified from *E. coli* following published methods.[6] DHP was immobilized on Affi-gel 10 (BioRad) according to previously published methods.[14] ESR data collection was conducted on a Bruker EMX spectrometer equipped with an SHQ resonator in the labatroy of Dr. R. P. Mason at the National Institute of Environmental Health Sciences. Data was collected using a 10 mm flatcell (Wilmad) with 10 mW microwave power, 80 G sweep with, 0.5 G_{pp} modulation amplitue (100 kHz), 164 ms time constant, 84 s scan time, and an average of 1 to 10 scans, and substrate flow rate of 1.0 ml/min.

UV-Visible Assays

A Hewlett Packard 8453 multi-wavelength spectrometer was used to obtain the relative activities of immobilized wild-type DHP. Substrate 2,4,6-tribromophenol, TBP, was obtained from Acros Organics and 2,4,6-trifluorolphenol was obtained from Fisher scientific. Samples were prepared in 100 mM potassium phosphate buffer at pH 7 and 256 μM H_2O_2 and 256 μM TBP. A Pasteure pipette was fitted with a glass wool plug, washed sea sand was added above the plug to simulate flow cell conditions and to add resistance in order to regulate flow rate. 100 μL of a 5 mg/mL immobilized DHP was placed above the sand. The top of the pipette was fitted with a rubber septum. As long as the rubber septum was in place the column did not dry out during the course of the experiment. 2 mL per minute flow rate of substrate/peroxide solution was regulated by a syringe pump equipped with a 20 mL syringe with a Vacutainer® butterfly needle. The effluent from the column of immobilized DHP was collected in fractions of 1.0 mL.

Each fraction represents 30 s of substrate/peroxide flow over the immobilized protein. Spectra were obtained for each fraction using a 1 cm cuvettee. The data were exported to Microsoft Excel and Igor Pro 5.0 for analysis. The percent consumption rate of substrate was calculated by the equation 1:

$$C = \frac{A_s - A_{f,t}}{A_s - A_{f,1}}(100\%) \qquad (1)$$

where C is the percent rate of consumption, A_s is the absorbance of the substrate at 316 nm before it has been exposed to the enzyme, $A_{f,t}$ in the absorbance at 316 nm of the fraction at time t, $A_{f,1}$ is the absorbance at 316 nm for the first fraction which represents the effluent after the enzyme has been exposed to substrate and peroxide for 1 minute. Percent consumption rate vs. time plots were made to express the rate of the consumption of the substrate by the immobilized enzyme.

Results

Figure 1 shows the phenoxyl radical signal from a one-electron oxidation of 4-hydroxyphenylacetic acid (HPA) by DHP. HPA is a classical peroxidase substrate and has been the radical signal has been identified in the literature.[15] The presence of the HPA radical indicates that DHP is capable of performing one electron oxidation chemistry. Due to the structure of HPA and the size of the substrate-binding site as determined by the crystal structure, we conclude that HPA is too large to fit within the confines of the substrate-binding pocket.

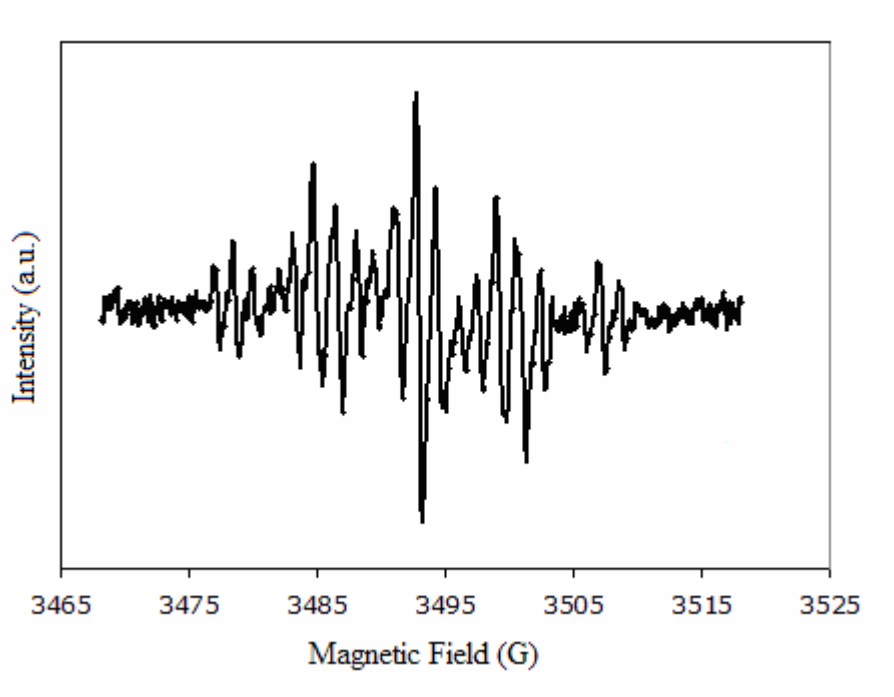

Figure 1. ESR data collected using DHP_i (4.8 mg/ml beads), HPA (2 mM), and H_2O_2 (100 uM) at pH 7.0. ESR spectra were collected using the DHP_i. and averaged for 14 minutes. ESR data was collected using the following conditions: Bruker EMX equipped with SHQ cavity, 9.78 GHz microwave frequency, 20 mW microwave power, 100 kHz modulation amplitude of 0.5 G, 82 ms conversion time, 163 ms time constant, sweep time of 84 s, and an average of 10 scans per spectrum.

Figure 2 shows the average of 4 separate data sets that demonstrate DHP is producing a phenoxyl radical of 2,4,6-triflorophenol. The insert of figure 1 shows the decay trace for the 2,4,6-triflorophenol phenoxyl radical signal as an inset. The K_{obs} for the decay trace is 7.5 ms, determined by a single exponential fit of the main SVD component. The rate constant is concentration- and flow-dependent. The decay of the 2,4,6-triflorophenol phenoxyl radical signal indicated that DHP produces fewer phenoxyl radicals with time.

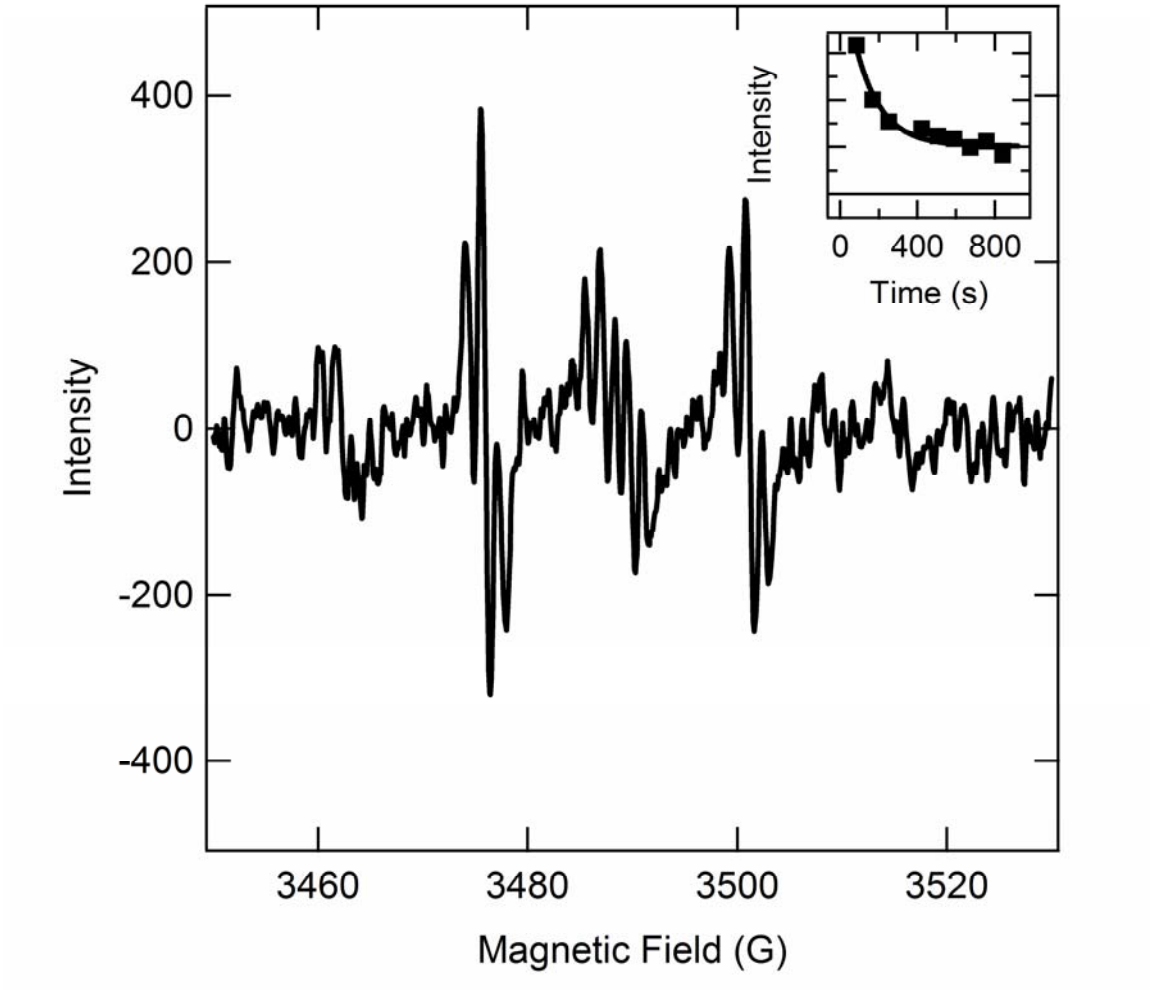

Figure 2. Average of the first 4 2,4,6-triflourophenoxyl radical signals generated by DHP. The inset shows the main component of SVD analysis of TFP phenoxyl radical signal generated by DHP and collected as a function of time.

Figure 3 shows five consecutive TFP phenoxyl radical signals generated by DHP, the same data is graphed in figure 1, that were collected 85 s apart (1 was collect from time 0-84 s, 2 was collected 85-168 s and so no). Each consecutive signal decreases in intensity, which is interpreted as a decrease in the concentration of the phenoxyl radical. DHP produces TFP phenoxyl radical for only ~ 3-5 min before the TFP phenoxyl radical signal is 50% departed. After 15 min, 90% of the TFP phenoxyl radical signal is gone.

Since DHP has demonstrated a preferential binding order to maximize activity[6] immobilized DHP, DHPi, was pre-treated with TFP by flowing TFP in buffer over the DHPi before the cosubstrate H_2O_2 was added to the flowing solution. The H_2O_2 initiates the reaction that produces the TFP phenoxyl radical. Pretreatment of DHP with TFP did not prolong the production of the TFP phenoxyl radical. The decrease in the phenoxyl radical can be interpreted as decreased reactivity between DHP/ H_2O_2/TFP or a decrease in the one-electron products, which could result in the increase of the two-electron quinone product, which is ESR silent.

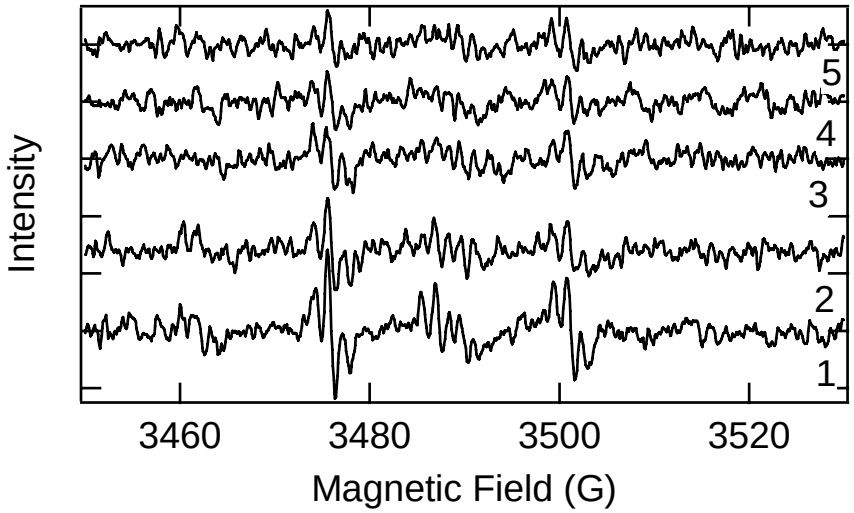

Figure 3. TFP phenoxyl radical signal generated by DHP spectra was collected in sequential order 1 to 5 at a constant flow rate, 2 mL/minute, of 1mM TFP and 1 mM H_2O_2, each sweep takes 84 s. DHP produces TFP phenoxyl radical for only ~ 3-5 min before the TFP phenoxyl radical signal is 50% departed and after 15 min, 90% of the TFP phenoxyl radical signal is gone. The numbering of spectra represents the different sweeps of the same DHPi with constant flow rate. Number 1 was completed after 84 s, number 2 was collected from 85-168 s, 3 from 169-252s, 4 from 253-420 s and 5 from 421-504 s.

Figure 4 shows the consumption of substrate as measured by UV-Vis spectroscopy. The consumption of substrate illustrates that DHPi is reacting with substrate beyond the 15 minute time limit for the TFP phenoxyl radical production. This leads to the conclusion that DHPi is participating in two consecutive 1 electron reactions on the same molecule of substrate. Thus, the TFP phenoxyl radical seems to disappear.

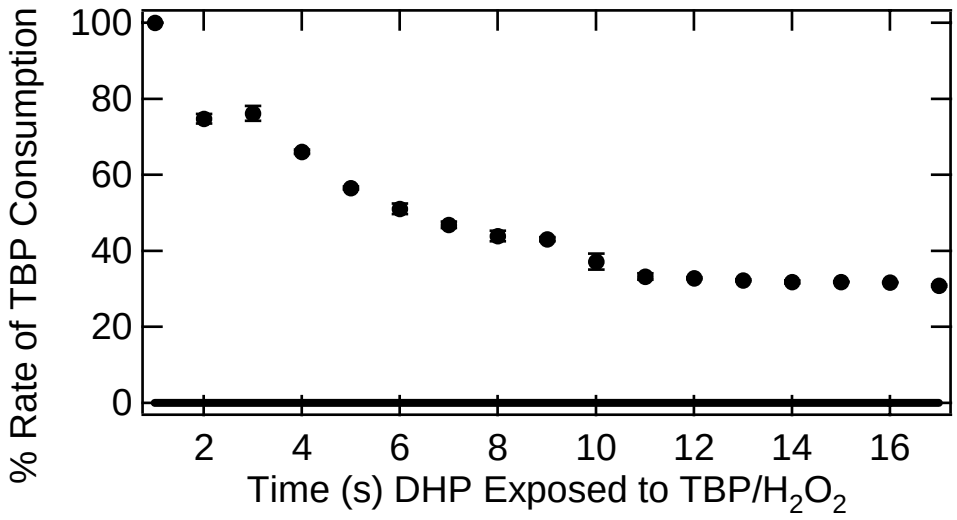

Figure 4. Rate of the TBP consumption derived by absorbance at 316 nm before and after the 2,4,6-tribromophenol/H_2O_2 flow solution has been exposed to the immobilized DHP.

As a comparison horse heart myoglobin, HHMb was used in identical ESR experiments. Figure 5 shows that HHMb continues to produce the TFP phenoxyl radical consistently for greater than 15 minutes with little change in the intensity, thus the concentration of the TFP phenoxyl radical is constant.

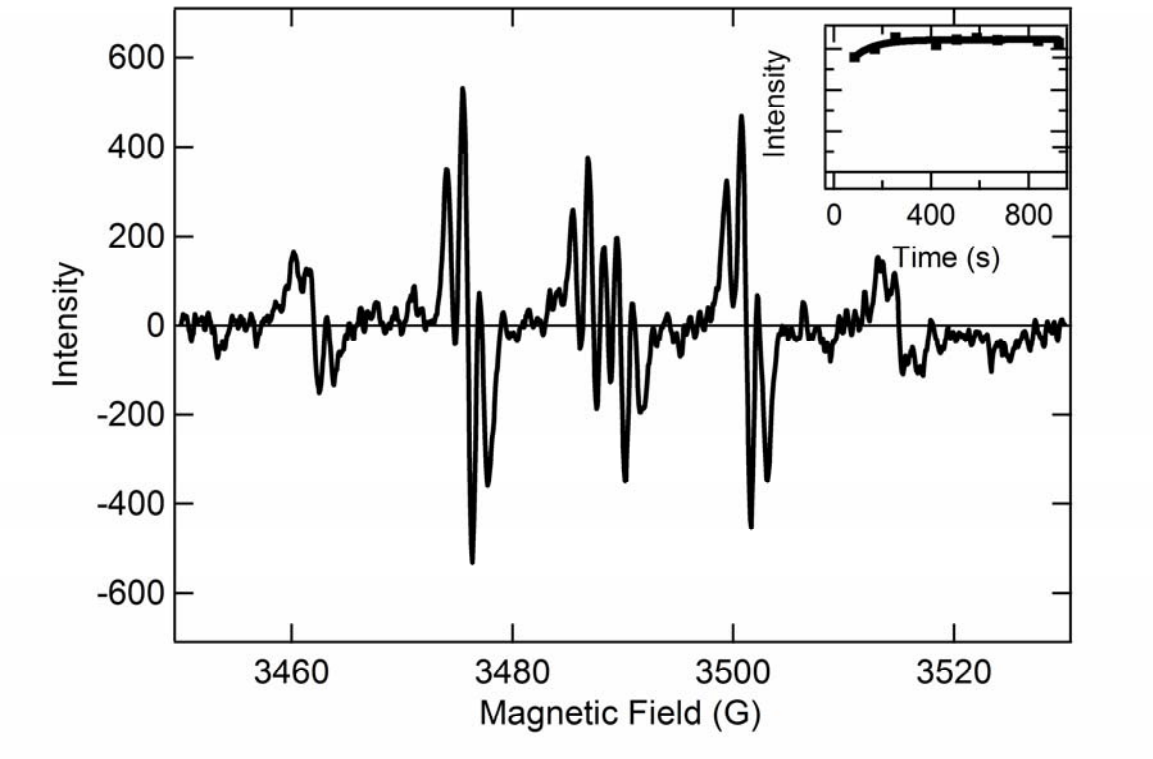

Figure 5. The TFP phenoxyl radical signal generated by Mb. The TFP phenoxyl radical signal is time stable. The inset shows the SVD analysis main component of Mb generated TFP phenoxyl radical. The SVD component is fitted to a single exponential fit resulting in a K_{obs} of 20 ms.

Figure 6 illustrates radicals generated by HRP in reactions with TFP and peroxide. The radicals generated have yet to be identified, however the species labeled as A is the TFP phenoxyl radical. Radicals B and C are unidentified.

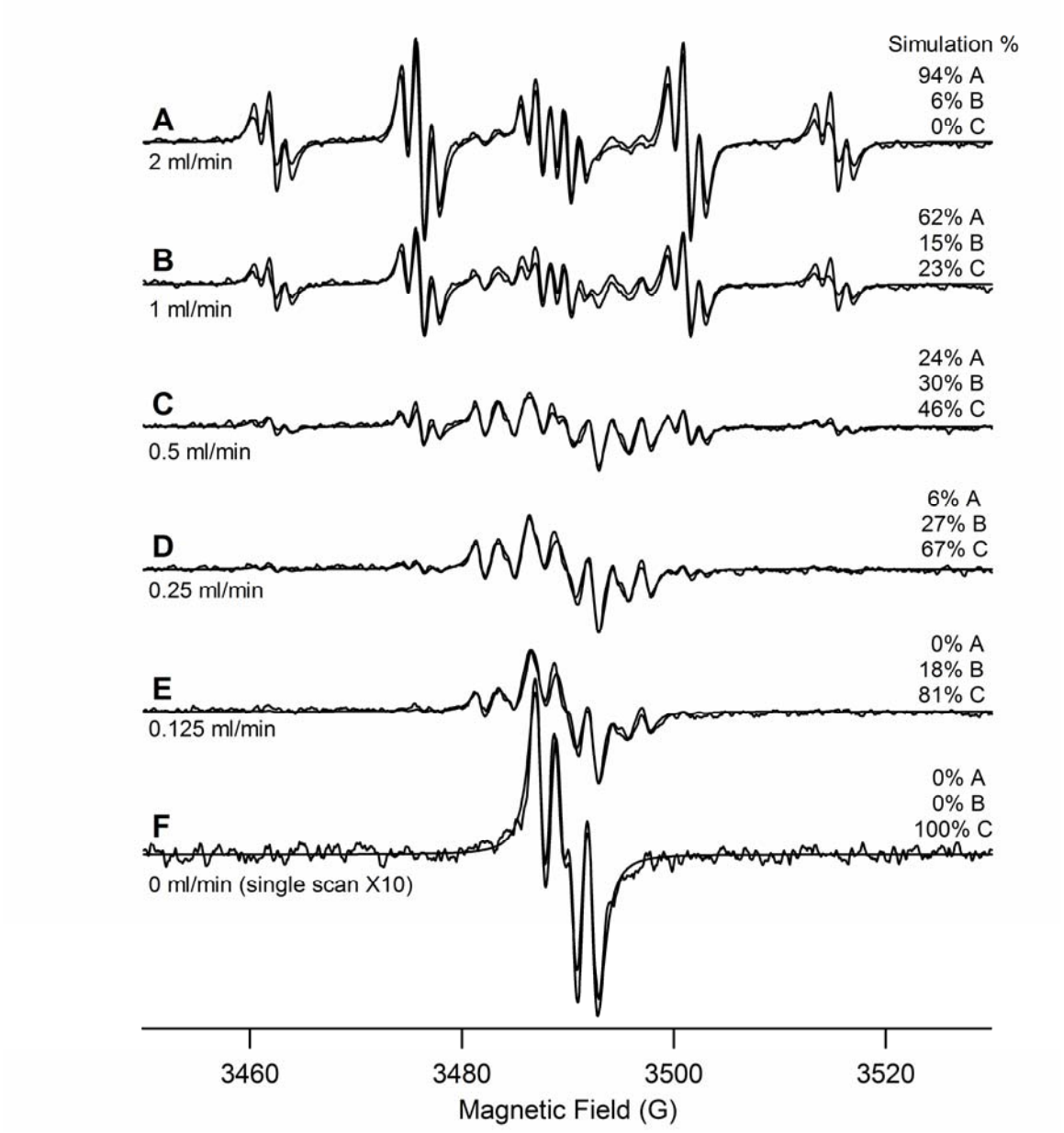

Figure 6. Radical signals generated by HRP at different flow rates. Species A is the same TFP phenoxy radical that is seen in reactions with DHP and Mb.

Discussion

The TFP phenoxyl radical production is the result of a one-electron oxidation of TFP. DHP catalyzes the same reaction, though only as a side reaction. DHP has a substrate-binding site that facilitates two consecutive one-electron reactions on the same substrate molecule. Figure 3 demonstrates that the TFP phenoxyl radical dies out. However, Figure 4 shows that the consumption of substrate does not decrease as quickly as the die out of phenoxyl radical. This does not mean that DHP has stopped reacting with TFP. However, it does mean that less TFP phenoxyl radical is being produced. The data in figure 4 leads us to believe that DHP is still reacting with the substrate since the substrate and a two-electron oxidation is occurring. Since the substrate is still being consumed, and TFP phenoxyl radical is not being produced at the initial rate, we confirmed that DHP is preferentially reacting with the same molecule of substrate twice, thus producing 2,6-dihalo-1,4-benzoquinone as determined earlier.

The complication introduce by collecting radical signal at different flow rate with immobilized HRP, as shown in figure 6, was not observed with DHP or Mb. The radical signals from DHP and Mb were lower in intensity, the decreased flow rates generated signals within the noise of the experiment thus I can not conclude that species B and or C are not being generated by Mb or DHP I simply state that species B and C are not observed.

Conclusion

DHP reacts with TFP in a 2-electron oxidation to produce quinone preferentially over 1-electron oxidation that would result in polametric products. Continued consumption of substrate tells us that DHP is still reacting with substrate. Since the radical production drops of much faster than the decrease in substrate consumption, DHP must be performing a 2-electron oxidation of a single substrate. This accounts for the decrease in radical and the continued consumption of substrate. When large substrates react with DHP 1-electron oxidation reaction is dominate. This is believed to be due to the large size of the substrate forcing the reaction to occur at the heme edge and not at the substrate binding site.

References

1. ESR X-band chapter

2. Raman chapter

3. E-Chem chapter

4. Gunsalus, I. C.; Sligar, S. G. **Redox regulation of cytochrome P450cam mixed function oxidation by putidaredoxin and camphor ligation.** Biochimie (1976), 58(1-2), 143-7.

5. Sligar, S. G.; Gunsalus, I. C.. **A thermodynamic model of regulation: Modulation of redox equilibria in camphor monoxygenase.** Proceedings of the National Academy of Sciences of the United States of America (1976), 73(4), 1078-82.

6. Belyea, J.; Gilvey, L. B.; Davis, M. F.; Godek, M.; Sit, T. L.; Lommel, S. A.; Franzen, S. **Enzyme function of the globin dehaloperoxidase from amphitrite ornata Is activated by substrate binding.** Biochemistry (2005), 44(48), 15637-15644.

7. Spiro, T. G.; Smulevich, G.; Su, C. **Probing protein structure and dynamics with resonance Raman spectroscopy: cytochrome c peroxidase and hemoglobin.** Biochemistry (1990), 29(19), 4497-508.

8. Franzen S **Effect of a charge relay on the vibrational frequencies of carbonmonoxy iron porphine adducts: the coupling of changes in axial ligand bond strength and porphine core size**. Journal of the American Chemical Society (2001), 123(50), 12578-89.

9. Poulos T L; Kraut J **The stereochemistry of peroxidase catalysis**. The Journal of biological chemistry (1980), 255(17), 8199-205.

10. Eisenmesser, E. Z.; Millet, O.; Labeikovsky, W.; Korzhnev, D. M.; Wolf-Watz, M.; Bosco, D. A.; Skalicky, J. J.; Kay, L. E.; Kern, D. **Intrinsic dynamics of an enzyme underlies catalysis.** Nature (London, United Kingdom) (2005), 438(7064), 117-121.

11. Osborne, R. L.; Taylor, L. O.; Han, K. P.; Ely, B.; Dawson, J. H. **Amphitrite ornata dehaloperoxidase: enhanced activity for the catalytically active globin using MCPBA.** Biochemical and Biophysical Research Communications (2004), 324(4), 1194-1198.

12. Wiese, F. E.; Chang, R. V.; Lloyd, J. P.; Freeman, V. M.; Samokyszyn, **Peroxidase-Catalyzed Oxidation of 2,4,6-Trichlorophenol.** *Arch. Environ. Contam. Toxicol*. (1998) ,34, 217-222 .

14. Sturgeon, B. E.; Chen, Y-R.; Mason, R. P. **Immobilized enzyme electron spin resonance: A method for detecting enzymatically generated transient radicals.** Analytical Chemistry (2003), 75(19), 5006-5011.

13. Ferrari, R. P.; Laurenti, E.; Trotta. F. **Oxidative 4-dechlorination of 2,4,6-trichlorophenol catalyzed by horseradish peroxidase**. *Journal of Biological Inorganic Chemistry* (1999), 4(2), 232-237.

15. Takahama, U.; Hirota, S.; Nishioka, T.; Oniki, T. **Human salivary peroxidase-catalyzed oxidation of nitrate and nitration of 4-hydroxyphenylacetic acid and proteins**. *Archives of Oral Biology*. (2003), 48(10), 679-690.

Chapter 4: Substrate Binding Triggers a Change in the Iron Spin State in Dehaloperoxidase from *Amphitrite ornata*

Introduction

Dehaloperoxidase (DHP) from the terebellid polychaete *Amphitrite ornata* is the first known peroxidase to bind substrate in a well-defined binding pocket. [1,2] DHP has a globin fold and an active site with a protoporphyin IX prosthetic group [3,4] consistent with the role of DHP as the hemoglobin of *A. ornata*.[5-9] Thus, DHP is dual function protein that acts as an oxygen carrier, but can also catalyze the oxidative dehalogenation of halogenated phenols in a hydrogen peroxide dependent reaction.[11-14] The requirement for a switch in function suggests that substrate binding may act as an allosteric effector that triggers the change from hemoglobin to peroxidase activity. Specifically, such a model requires an interaction between the substrate and the heme iron, which serves as the binding site for oxygen and hydrogen peroxide in the hemoglobin and peroxidase functions, respectively. Binding of substrate in DHP is shown herein to cause a shift in the population density from low to high spin of the iron in the heme active site, which provides one of the first direct measurements that substantiates the function switching hypothesis. A similar hypothesis has been demonstrated in the binding of substrate to cytochrome $P450_{cam}$, which results in a shift from a low to high spin state of the heme iron. This change in the spin state is correlated with a shift in the redox potential of the heme iron.[17,18]

Materials and Methods.

Preparation of Protein Samples for EPR experiments

The DHP protein was expressed and purified as described previously.[11] The substrate, 2,4,6-trifluorophenol (TFP), was purchased from Acros and buffer salts were purchased from Fisher Scientific. All chemicals were used without further purification.

Lyophilized protein was dissolved in 100 mM citrate pH 6.0. Excess potassium ferricyanide was added to the protein solution to oxidized the iron heme to the ferric state. Excess oxidant was removed by size exclusion chromatography using a Sephadex G-25 column (Sigma-Aldrich G2580-10G). Protein was collected and concentrated using Millipore Amicon Ultra-4 MWCO 10,000 concentrators (Fisher Scientific UFC8 010 24). Concentrated protein was diluted with ligand solution to result in final concentrations of 4 mM protein and 0.5 M ligand. A volume of 20μL of ferric DHP and ferric DHP with bound TFP was placed into separate 20 cm lengths of Teflon tubing. Protein filled tubing was folded several times and placed in the bottom of a 5 mm quartz EPR tube. The tube was sealed with rubber septa to prevent condensation of paramagnetic solid oxygen. Samples were stored on ice until used and flash frozen in liquid nitrogen prior to being placed in the cavity.

Samples containing 2,4,6-triflorophenol were made dissolving lyophilized protein in 100 mM citrate pH 6.0. Excess potassium ferricyanide was then removed by size exclusion chromatography using a Sephadex G-25 column (Sigma-Aldrich G2580-10G). Protein was collected and concentrated in Millipore Amicon Ultra-4 MWCO 10,000 (Fisher Scientific UFC8 010 24). Substrate was added to the samples by dialyzing the protein with 100 mM citrate pH 6.0 buffer containing 1 mM 2,4,6-triflourophenol. The

protein samples were concentrated to 4mM by using Millipore Amicon Ultra-4 centrifugal filters, WMCO 10,000

All protein samples were concentrated in Millipore Amicon Ultra-4 MWCO 10,000 and the pH of the effluent was measured to ensure the protein substrate solution was pH 6.0. Protein samples were concentrated to 4mM and diluted with glycerol to a final concentration of 2 mM protein in 50% buffer-glycerol mixture. Concentration of protein was checked by absorption spectroscopy, using a Hewlett Packard 8453 multi-wavelength spectrometer before and after data collection. The ferric DHP in 100 mM citrate buffer pH 6.0 had a Soret band maximum at 406 nm and a broad Q band from 550-575 nm (Figure 1). The addition of substrate did not affect the absorption spectra of DHP.

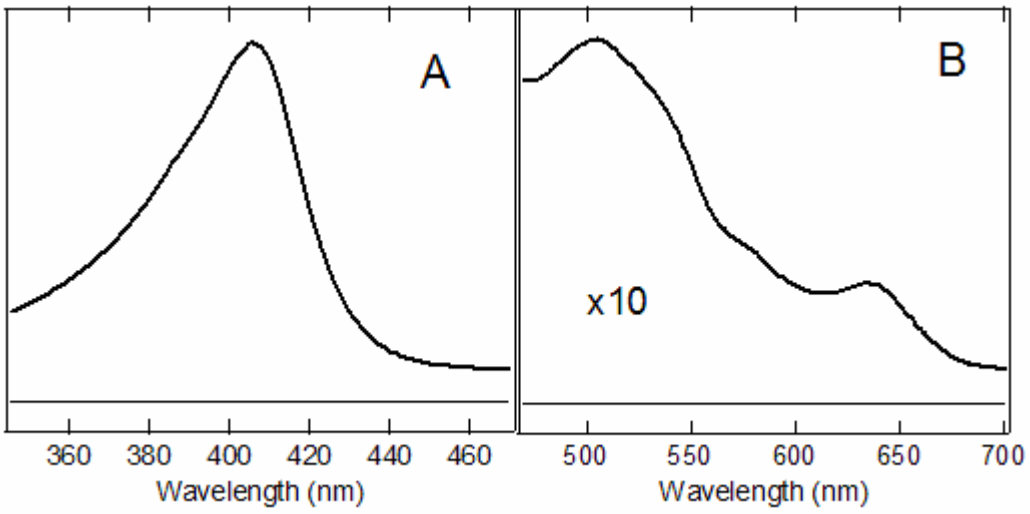

Figure 1. A: Absorption Soret spectra of high spin ferric DHP in 100 mM phosphate buffer, pH 6.0 at room temperature. Soret maximum for the ferric DHP is 406 nm showed no changes upon addition of 2,4,6-triflorophenol. B: The Q-bands and charge transfer bands of ferric DHP. No changes were observed in this region of the spectra upon the binding of TFP.

EPR spectra were recorded on Bruker (model EN503 NRSRG208)X-band spectrometer equipped with an Oxford cryostat and temperature controller. Spectral intensity of g=6

transition was estimated by measuring a double integral of the spectral feature in g=6 region. The variable temperature spectra were amplitude-normalized by using the EPR signal from the quartz tube as an internal standard.

Results and Discussion

The protein environment can control the spin state by imposing bond length restrictions between the iron and its ligands[15]. The iron in DHP is coordinated equatorially to heme and axially to the proximal histidine and distal ligands. According to the X-ray crystal structure ferric DHP has a 5-coordinate heme iron with an axial histidine.[4, 10] However solution studies have indicated that DHP is hexacoordinate in the ferric form with a water molecule as the sixth ligand.[1,16] The different geometries of the ferric protoporphyrin IX in DHP with and without the substrate 2,4,6-triflorophenol bound were studied by X-band EPR in order to measure the equilibrium between the S=1/2 and S=5/2 spin state populations of the iron heme.[19-22] While the substrate does not interact directly with the heme iron, Figure 2 shows that the EPR absorption corresponding to g ≅ 6 (6.06 ferric DHP and 6.20 substrate bound ferric DHP) is more intense when substrate is added to the protein compared to the substrate-free form of the protein. Transitions from the ground state to the lowest Kramers doublets results in absorption signals at g ≅ 6 and g ≅ 2 intensities, which are proportional to the S=5/2 (HS) and S=1/2 (LS) populations of the heme iron.[18]

The zero field splitting parameters D and E, are defined by the spin Hamiltonian equation 1 .[23] The spin system can be described by Hamiltonian equation 1

$$\mathcal{H} = \beta B \cdot g \cdot S + D[\hat{\mathbf{S}}_z^2 - S(\hat{\mathbf{S}} + 1)/3] + E(\hat{\mathbf{S}}_x^2 - \hat{\mathbf{S}}_y^2) \qquad (1)$$

where E and D are the second rank rhombic and axial zero field splitting parameters, [19] , $\hat{\mathbf{S}}_x$, $\hat{\mathbf{S}}_y$ and $\hat{\mathbf{S}}_z$ are spin angular momentum operator and its components the molecular z-axis is taken to be perpendicular to the average porphine plane, B is the magnetic field, **g** is the electronic g-tensor and β is the Bohr magneton. D and E characterize the magnitude of the tetragonal and rhombic symmetry lowering, respectively. The axial zero-field splitting parameter D for the heme in DHP and DHP-TBP were determined by measuring the integrated intensity of the heme iron g=6 EPR transition as a function of temperature. The intensity was measured by calculating the signal amplitude calculated by double integration of the data. Figure 3 shows the integrated intensity of the g=6 heme iron in DHP and DHP-TBP transition as a function of temperature. The solid squares are data points from DHP-TBP, open squares are data points from the substrate-free DHP sample, and the solid line through the data points is a fit to equation 2. [24]

$$I(T) = \frac{N(1 - e^{-\theta/T})}{1 + e^{-\theta/T} + e^{-(2D-\theta)/T} + e^{-2(D+\theta)/T} + e^{-2(3D-\theta)/T} + e^{-3(2D+\theta)/T}} \qquad (2)$$

Where I(T) is the integrated EPR signal intensity, θ is the Zeeman splitting expressed as $h\upsilon/k_B$ = 0.44 K , D is the zero-field splitting parameter, and N is an overall scale factor. When D is positive, the doublets $|5/2, \pm 3/2\rangle$ and $|5/2, \pm 5/2\rangle$ lie 2D and 6D above the ground state doublet, respectively. [24] Thermal population of these levels leads to a reduction in the signal intensity observed in Figure 3. The fit of data in Figure 3 to eq. 2 results in D values of 1.3 cm^{-1} and 2.1 cm^{-1} for ferric DHP and its substrate-bound form, respectively.

The ratio of E/D is related to rhombic distortion of the heme and is given by $\lambda = \Delta g/48$ where Δg is the absolute difference in g factors between the two components of the $g \cong 6$ band, which is estimated by the difference in g-factors corresponding to the

positions of the peak (positive and negative). . The data in Figure 1 correspond to λ = 0.0163 and λ = 0.0123 for ferric DHP with substrate and without substrate, respectively. The ratio E/D has a maximum value of 1/3. The percent rhombicity R, can be calculated as a percentage of the total difference between a completely tetragonal and a completely rhombic field, equation 3.[21]

$$R = (\Delta g/16) \times 100\% \qquad (3)$$

The percent rhombicity of substrate bound ferric DHP is ~ 2.4% and the percent rhombicity of ferric DHP is ~ 1.8%. Thus, we conclude that the binding of TBP results in protein conformational changes that increase the population of the HS state of the heme with an increase in the zero-field splitting and a reduction in rhombicity. These observed changes in spectroscopic EPR parameters at g=6 reflect changes in the iron spin state. It is still not resolved whether the coordination sphere is altered by this change. The observed changes may arise from expulsion of water from the sixth coordination binding site. On the other hand, changes in hydrogen bonding of ligated water could also be responsible for the change in spin on the heme iron. It is also possible that changes in proximal ligation are communicated to the heme iron through the protein by the constraint of the bound substrate. These changes may be associated with a change in the redox potential of the iron or of the coordination sphere that permit the rapid binding of H_2O_2, both of which may be important for the change in function from a globin with a ferrous resting state to a peroxidase with a ferric resting state.[11]

Conclusion

The results observed for substrate binding in DHP have surprising similarity to the effect of substrate binding in cytochrome $P450_{cam}$[25]. In both cases the iron is largely LS prior to substrate binding. It is known that cytochrome P450 has a water in the sixth coordination position and that this water is displaced when the substrate binds resulting a change in the spin state of the heme iron. In Cyt P450 the HS population increases significantly, but without complete conversion to the HS state. These features are also observed in DHP, but we cannot state definitively that the mechanism is the same. The X-ray crystal structure of DHP does not show a H_2O bound to the heme iron, despite spectroscopic evidence to suggest that the water is present in solution. Based on these spectroscopic data we hypothesize that DHP has a similar triggering mechanism to that observed in the monooxygenase Cyt P450. This observation places DHP in a unique intersection of the heme protein structures. DHP is the first globin that functions as a true peroxidase and also the first enzyme outside the Cyt P450 superfamily to exhibit a substrate triggered change in heme protein coordination. These features raise the question: why does DHP have a triggered change that is so similar to Cyt P450? Is it simply a trigger that permits a change in structure from globin to peroxidase structure or does DHP share other features of typical monooxygenases? Based on the similarity of DHP with chloroperoxidase and flavohemoglobins, we believe that the results presented here suggest that DHP may also be activated for electron transfer by substrate binding. The existence of associated flavoprotein and associated change in redox potential are being actively investigated to substantiate this hypothesis.

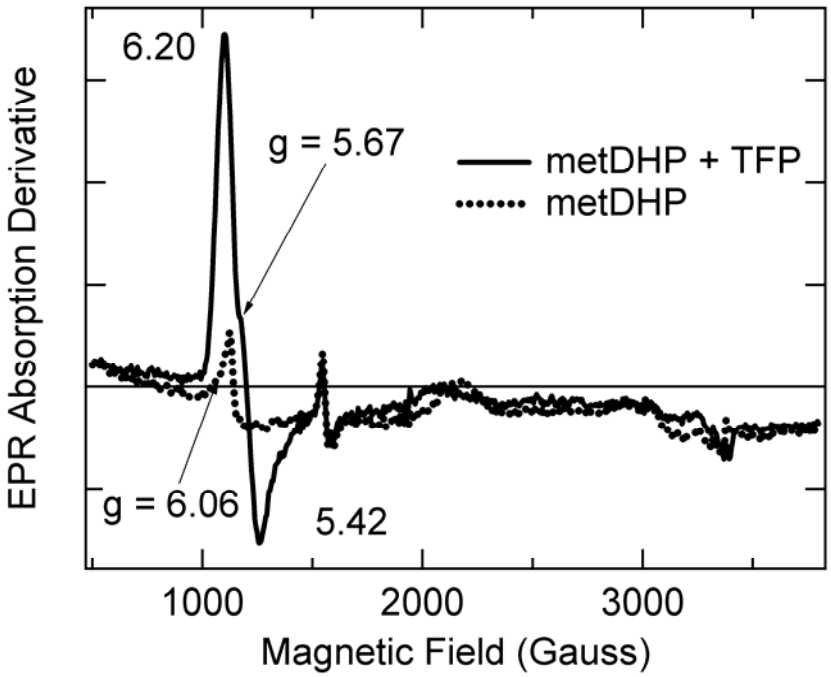

Figure 2. 9.5 GHz field-swept EPR spectra from ferric DHP with 2,4,6-tribromophenol bound (solid line and ferric DHP (dotted line). Conditions: temperature 4.5 K; 2 mW microwave observed power, frequency, 9.44955GHz, modulation amplitude 10 G. Samples were prepared in 100 mM citrate buffer pH 6.0.

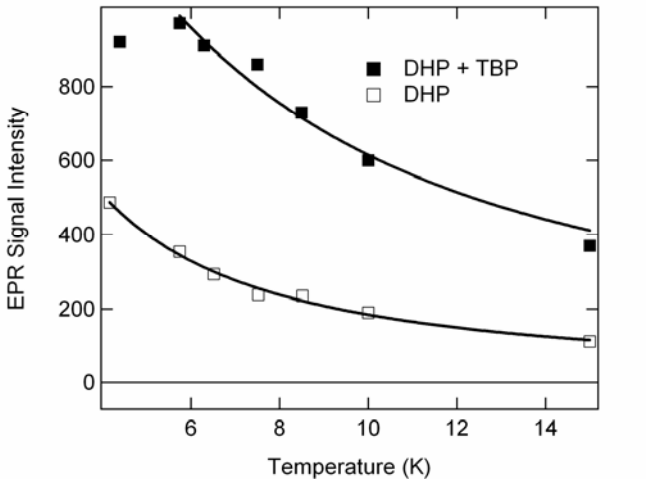

Figure 3. Determination of the heme iron zero-field splitting in ferric DHP and ferric DHP with 2,4,6-tribromophenol bound. The open squares show a temperature dependence of the integrated signal intensities of the heme iron g=6, transition in ferric DHP the solid squares are for the TBP bound ferric DHP. Solid lines show the best fit to Eqn. 2

References

1. Nienhaus, K.; Deng, P.; Belyea, J.; Franzen, S.; Nienhaus, G. U. **Spectroscopic Study of Substrate Binding to the Carbonmonoxy Form of Dehaloperoxidase from Amphitrite ornata.** Journal of Physical Chemistry B (2006), 110(26), 13264-13276.

2. Franzen, S.; Belyea, J.; Gilvey, L. B.; Davis, M. F.; Chaudhary, C. E.; Sit, T. L.; Lommel, S. A. **Proximal Cavity, Distal Histidine, and Substrate Hydrogen-Bonding Mutations Modulate the Activity of Amphitrite ornata Dehaloperoxidase.** Biochemistry ACS ASAP. Available on-line

3. Franzen, S.; Jasaitis, A.; Belyea, J.; Brewer, S. H.; Casey, R.; MacFarlane, A. W., IV; Stanley, R. J.; Vos, M. H.; Martin, J-L. **Hydrophobic Distal Pocket Affects NO-Heme Geminate Recombination Dynamics in Dehaloperoxidase and H64V Myoglobin.** Journal of Physical Chemistry B (2006), 110(29), 14483-14493.

4. Zhang, E.; Chen, Y-P.; Roach, M. P.; Lincoln, D. E.; Lovell, C. R.; Woodin, S. A.; Dawson, J. H.; Lebioda, L. **Crystallization and initial spectroscopic characterization of the heme-containing dehaloperoxidase from the marine polychaete Amphitrite ornata.** Acta Crystallographica, Section D: Biological Crystallography (1996), D52(6), 1191-1193.

5. Fushitani, K.; Bonaventura, J.; Bonaventura, C. **Isolation of polypeptide chains with heme from the extracellular hemoglobin of Amphitrite ornata (Polychaeta, Annelida).** Comparative Biochemistry and Physiology, Part B: Biochemistry & Molecular Biology (1986), 84B(1), 137-41.

6. Chiancone, E.; Ferruzzi, G.; Bonaventura, C.; Bonaventura, J. **Amphitrite ornata erythrocruorin. II. Molecular controls of function.** Biochimica et Biophysica Acta, Protein Structure (1981), 670(1), 84-92.

7. Chiancone, E.; Brenowitz, M.; Ascoli, F.; Bonaventura, Celia; Bonaventura, J. **Amphitrite ornata erythrocruorin. I. Structural properties and characterization of subunit interactions.** Biochimica et Biophysica Acta, Protein Structure (1980), 623(1), 146-62.

8. Weber, R. E.; Magnum, C.; Steinman, H.; Bonaventura, C.; Sullivan, B.; Bonaventura, J. **Hemoglobins of two terebellid polychetes: Enoplobranchus sanguineus and Amphitrite ornata.** Comparative Biochemistry and Physiology, Part A: Molecular & Integrative Physiology (1977), 56(2A), 179-87.

9. Mangum, C. P.; Woodin, B. R.; Bonaventura, C.; Sullivan, B.; Bonaventura, J. **Celomic and vascular hemoglobin in the annelid family Terebellidae.**

Comparative Biochemistry and Physiology, Part A: Molecular & Integrative Physiology (1975), 51(2A), 281-94.

10. LaCount, M. W.; Zhang, E.; Chen, Y-P.; Han, K.; Whitton, M. M.; Lincoln, D. E.; Woodin, S. A.; Lebioda, L. **The crystal structure and amino acid sequence of dehaloperoxidase from Amphitrite ornata indicate common ancestry with globins.** Journal of Biological Chemistry (2000), 275(25), 18712-18716.

11. Belyea, J.; Gilvey, L. B.; Davis, M. F.; Godek, M.; Sit, T. L.; Lommel, S. A.; Franzen, S. **Enzyme function of the globin dehaloperoxidase from amphitrite ornata Is activated by substrate binding.** Biochemistry (2005), 44(48), 15637-15644.

12. Spiro, T. G.; Smulevich, G.; Su, C. **Probing protein structure and dynamics with resonance Raman spectroscopy: cytochrome c peroxidase and hemoglobin.** Biochemistry (1990), 29(19), 4497-508.

13. Franzen, S. **Effect of a Charge Relay on the Vibrational Frequencies of Carbonmonoxy Iron Porphine Adducts: The Coupling of Changes in Axial Ligand Bond Strength and Porphine Core Size.** Journal of the American Chemical Society (2001), 123(50), 12578-12589.

14. Poulos, T. L.; Kraut, J. **The stereochemistry of peroxidase catalysis.** Journal of Biological Chemistry (1980), 255(17), 8199-205.

15. Loew, G.; Dupuis, M. **Characterization of a Resting State Model of Peroxidases by ab Initio Methods: Optimized Geometries, Electronic Structures, and Relative Energies of the Sextet, Quartet, and Doublet Spin States.** Journal of the American Chemical Society (1997), 119(41), 9848-9851.

16. Osborne, R. L.; Sumithran, S.; Coggins, M. K.; Chen, Y-P.; Lincoln, D. E.; Dawson, J. H. **Spectroscopic characterization of the ferric states of Amphitrite ornata dehaloperoxidase and Notomastus lobatus chloroperoxidase: His-ligated peroxidases with globin-like proximal and distal properties.** Journal of Inorganic Biochemistry (2006), 100(5-6), 1100-1108.

17. Gunsalus, I. C.; Sligar, S. G.. **Redox regulation of cytochrome P450cam mixed function oxidation by putidaredoxin and camphor ligation.** Biochimie (1976), 58(1-2), 143-7.

18. Sligar, S. G.; Gunsalus, I. C. **A thermodynamic model of regulation: Modulation of redox equilibria in camphor monoxygenase.** Proceedings of

the National Academy of Sciences of the United States of America (1976), 73(4), 1078-82.

19. Peisach, J.; Blumberg, W. E.; Ogawa, S.; Rachmilewitz, E. A.; Oltzik, R.. **Effects of protein conformation on the heme symmetry in high spin ferric heme proteins as studied by electron paramagnetic resonance.** Journal of Biological Chemistry (1971), 246(10), 3342-55.

20. Yonetani, T.; Drott, H. R.; Leigh, J. S., Jr.; Reed, G. H.; Waterman, M. R.; Asakura, T. **Electromagnetic properties of hemoproteins. III. Electron paramagnetic resonance characteristics of iron(III) and manganese(II) protoporphyrins IX and their apohemoprotein complexes in high spin states.** Journal of Biological Chemistry (1970), 245(11), 2998-3003.

21. Blumberg, W. E.; Peisach, J.; Wittenberg, B. A.; Wittenberg, J. B. **Electronic structure of protoheme proteins. I. Electron paramagnetic resonance and optical study of horseradish peroxidase and its derivatives.** Journal of Biological Chemistry (1968), 243(8), 1854-62.

22. Wittenberg, B. A.; Kampa, L.; Wittenberg, J. B.; Blumberg, W. E.; Peisach, J. **Electronic structure of protoheme proteins. II. Electron paramagnetic resonance and optical study of cyctochrome c peroxidase and its derivatives.** Journal of Biological Chemistry (1968), 243(8), 1863-70.

23. Bleaney, B.; Stevens, K. W. H.. **Paramagnetic Resonace.** Reports on progeress in physics (1953), 16(1), 108-159.

24. Galli, C.; MacArthur, R.; Abu-Soud, H. M.; Clark, P.; Stuehr, D. J.; Brudvig, G. W. **EPR Spectroscopic Characterization of Neuronal NO Synthase.** Biochemistry (1996), 35(8), 2804-2810.

25. Tsai, R.; Yu, C. A.; Gunsalus, I. C.; Peisach, J.; Blumberg, W.; Orme-Johnson, W. H.; Beinert, H. **Spin-state changes in cytochrome P-450cam on binding of specific substrates**. Proceedings of the National Academy of Sciences of the United States of America (1970), 66(4), 1157-63.

26. Sage, J. T.; Morikis, D.; Champion, P. M. **Spectroscopic studies of myoglobin at low pH: heme structure and ligation.** Biochemistry (1991), 30(5), 1227-37.

27. Lebioda, L.; LaCount, M. W.; Zhang, E.; Chen, Y-P.; Han, K.; Whitton, M. M.; Lincoln, D. E.; Woodin, S. A. **An enzymatic globin from a marine worm.** Nature (London) (1999), 401(6752), 445.

Chapter 5 Effect of Substrate binding on fluoride and cyanide binding to Dehaloperoxidase from *Amphitrite ornata*

Introduction

It is of great interest to determine conditions of substrate binding to DHP at room temperature and in solution. We have observed that substrate binding can be detected using EPR spectroscopy at ~4 K in Chapter 4. It can also be observed using Fourier-transform infrared spectroscopy [1] and 1H NMR spectroscopy.[2]. However, neither of these is a routine measurement that can be carried out in solution. We have attempted to observe substrate binding by UV-vis spectroscopy (Figure 1). However, the effect of substrate (2,4,6-tribromophenol) binding on the Soret band and Q band was too small to be detected. For this reason we explored the combined binding of ligands fluoride and cyanide with substrate.

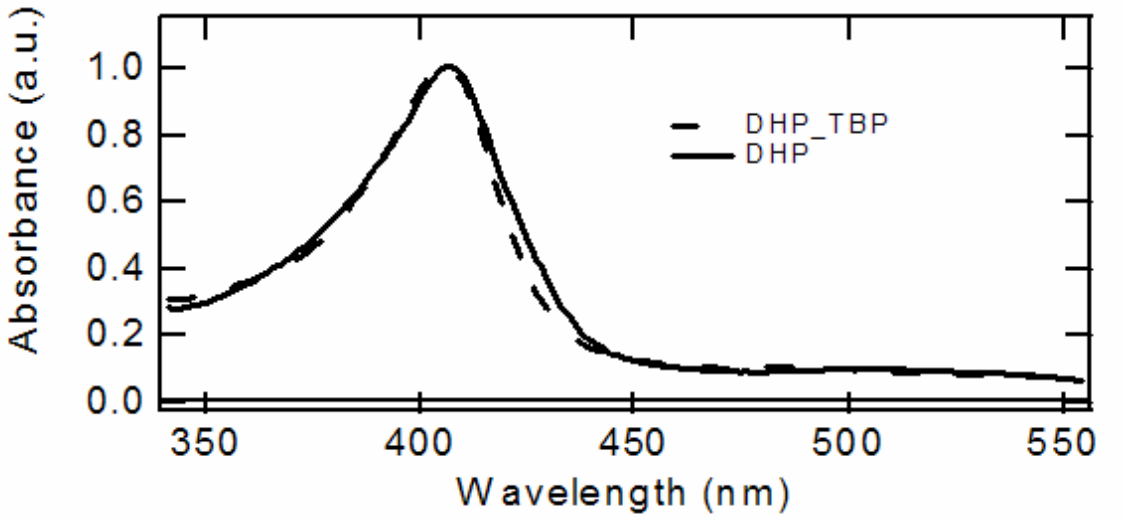

Figure 1. Soret spectra of DHP and DHP with TBP. Notice there is no change in the position of the Soret Band.

The function of a globin is to reversibly bind oxygen in the ferrous form. However, both myoglobin and hemoglobin can bind a variety of other ligands such as NO, CO in the ferrous form and CN-, N_3-, Br-, Cl-, F- etc. in the ferric form. For the general case we write the following equation:

$$P + L \leftrightarrow PL \qquad (1)$$

where P represents protein, L is a ligand and PL is the ligand bound protein complex. An association constant of K_a can be expressed as:

$$K_a = [PL]/[P][L] \qquad (2).$$

Equation 2 can be rearranged to indicate that the ratio bound to free protein should be directly proportional to the concentration of free ligand:

$$K_a[L] = [PL]/[P] \qquad (3).$$

Binding equilibria are simplified when the concentration of the ligand is much greater than the concentration of ligand-binding sites, because the binding of the ligand by the protein does not appreciably change the concentration of free ligand.

Experimental data are often plotted as the fraction bound θ as shown in equation 4.

$$\theta = [PL] / [PL] + [P] \qquad (4)$$

Substituting from equation 3 into equation 4 generates equation 5.

$$\theta = K_a[L]/(K_a[L] +1) \qquad (5)$$

K_a can be determined form a plot of θ vs. the concentration of free ligand. In the case of Mb, the graph is a hyperbola and $1/K_a$ (or the dissociation coefficient K_d) is found a θ = 0.5.

For proteins with more than one binding site, we must start with the following equation 6:

$$P + nL \leftrightarrow PL_n \qquad (6)$$

where *n* is the number of binding sites. The expression for θ is:

$$\theta = [L]^n / [L]^n + K_d \qquad (7)$$

now rearrange to:

$$\theta / (1 - \theta) = [L]^n / (K_d) \qquad (8)$$

Take the log of both sides yields the Hill equation:

$$\log (\theta / (1 - \theta)) = n \log [L] - \log K_d. \qquad (9)$$

The plot of log (θ / (1 - θ)) versus log [L] is called a Hill plot. The slope from a Hill plot is called the Hill coefficient, n_H. The degree of cooperativity can be determined from the Hill coefficient. When n_H is greater than 1 there is positive cooperatively in ligand binding. Positive cooperativity means that the binding of one ligand molecule facilitates the binding of additional ligand molecules. When $n = n_H$ the theoretical limit has been met, thus binding would be completely cooperative thus all binding sites on the protein are occupied simultaneously. When n_H is less than 1, there is negative cooperatively thus, the binding of one ligand inhibits additional binding other ligands.[3]

Cooperative binding models.

The first model proposed to explain cooperative binding was the symmetry model. The symmetry model assumes that the subunits of an allosteric protein are functionally identical and each can exist in the bound and unbound states. The two conformations are in equilibrium.[4] The second model is the sequential model. The sequential model assumes that ligand binding can induce a change of conformation in an

individual subunit.[5] The conformational change in one subunit makes a similar change in another subunit more likely, thus binding of one ligand lowers the energy barrier for the binding of a second ligand. The symmetry model is viewed as the lower and upper limit of the sequential model.[5]

Allosteric binding models

Allosteric effects occur when the binding properties of a protein change as a consequence of a second ligand binding to the protein and altering its affinity towards the first, ligand. Direct interaction between the two ligands is not necessary, and in fact the two ligands may bind on different subunits. Homotropic allosteric effects occur when the two ligands are identical and heterotropic allosteric effects are observed when the two ligands are different.

Allosteric effects require the presence of two forms of the protein, generally referred to as the tense (T) and relaxed (R) states. In the case of hemoglobin the T state has low oxygen affinity and the R state has high oxygen affinity. Positive cooperativity implies that each ligand binding event increases the binding constant for the successive ligand. Negative cooperativity results in a decreasing binding constant resulting from each ligand binding event. When R state is dominant the initial binding affinity is high. However, the binding of ligand increases the amount of T state, thus reducing the binding affinity.

The mechanism of positive cooperativity in hemoglobin of diatomic oxygen involves spatial rearrangement around the heme active site. The binding of oxygen to the iron causes the proximal His residue to move. Since the proximal His is part of the F helix the F helix moves to adjust for the new conformation by movement of $\alpha\beta$ subunits.

This movement is referred to as a hinge and helix ratchet.[4, 5] All of this movement alters the conformation of the iron at the unliganded sites.

Allosteric binding is modeled by the concerted[4] or sequential models[5]. Both models assume that the protein subunits exist in T and R states and that the R state binds ligands with a higher affinity. The two models differ in assumptions about subunit interaction and the existence of both T and R states.

The concerted model suggests that enzyme subunits are all in the same conformation and that a change in state of one subunit directly causes the change in state for all other subunits. The binding of substrate to any one subunit forces the remaining subunits to assume the R state thus increasing their affinity for substrate.[4] The sequential model assumes that the subunits are not linked thus the change of state for one subunit does not directly force the change of state in the remaining subunits. However, when one subunit binds a ligand slight changes in structure of the remaining subunits occurs. When one ligand binds facilitates the binding of additional ligands.[5]

Materials and Methods

Dehaloperoxidase samples were purified from *E. coli* according to published methods.[6] Protein was dialyzed against water to remove all salts and concentrated using Millipore Ultra-4 centrifugal filters, WMCO 10,000 (catalog # UFC801024). Concentrated samples were flash frozen using liquid nitrogen or dry ice then lyophilized using a Labconco Freezer Dryer 4.5 (catalog # 7750000). DHP samples were prepared by dissolving lyophilized DHP in water at a final concentration of 6 mM. Excess potassium ferricyanide was added to the protein solution to reduce the iron heme to the ferric state. Excess oxidant was removed by size exclusion chromotragrapy using a

Sephadex G-25 column (Sigma-Aldrich G2580-10G). Protein was collected and concentrated in Millipore Amircon Ultra-4 MWCO 10,000 (catalog # UFC801096). A buffer exchange was performed in the Amircon Ultra-4 so the resulting proteins solutions were buffered in 100 mM citrate pH 5.0 and 6.0 or 100 mM phosphate pH 7.0 and 8.0. Lyophilized horseradish peroxidase was purchased from Fluka (EC. 1.11.1.7 catalog # 77334), and lyophilized horse heart myoglobin was purchased from Sigma (cas # m1882, catalog number 100684-32-0). Both horseradish peroxidase and horse heart myoglobin were used without further purification. Lyophilized Mb and HRP proteins were dissolved in 100 mM citrate buffer pH 5.0 and 6.0 and 100 mM phosphate pH 7.0.

Absorption spectra were recorded using a Hewlett Packard 8453 multi-wavelength spectrometer. Addition of fluoride ligand was done quantitatively and spectroscopic changes were observed. Ligand affinity measurements were made using a Hewlett Packard 8453 multi-wavelength spectrometer. Addition of 2 - 5 μl of 0.5 M fluoride ligand in buffers were added to 60 μM ferric DHP in 100 mM citrate pH 6.0 in a 1 cm path length cuvette. Data were processed in Igor Pro 5.0 using equation 1 to determine the determine the fractional binding as a function of the ligand concentration [L], where A is an arbitrary scaling factor and K is the binding constant.

$$\theta = A\frac{K[L]}{1 + K[L]} \qquad \text{eq. 1}$$

Results

Addition of substrate (TBP) to a solution of ferric DHP did not alter the Soret band of DHP(see Figure 1). Earlier work (Chapter 4) showed that the iron heme undergoes a spin state change upon the binding of the substrate. Typically, a change in the spin state of a iron would result in a shift in the Soret peak. However, this was not observed for the binding of TBP by DHP.

The successive addition of fluoride ligand resulted in increased population of fluoride bound heme, which was monitored by the increase in absorbance in a charge transfer band at the wavelengths 605, nm for DHP as shown in Figure 2. The metaquo spectrum shown in Chapter 4 Figure 1 lacks the charge transfer band so that the binding of fluoride can be monitored by observation of the change in absorbance at the wavelengths of the charge transfer associated with the fluoride adduct. No shift in the Soret band is observed.

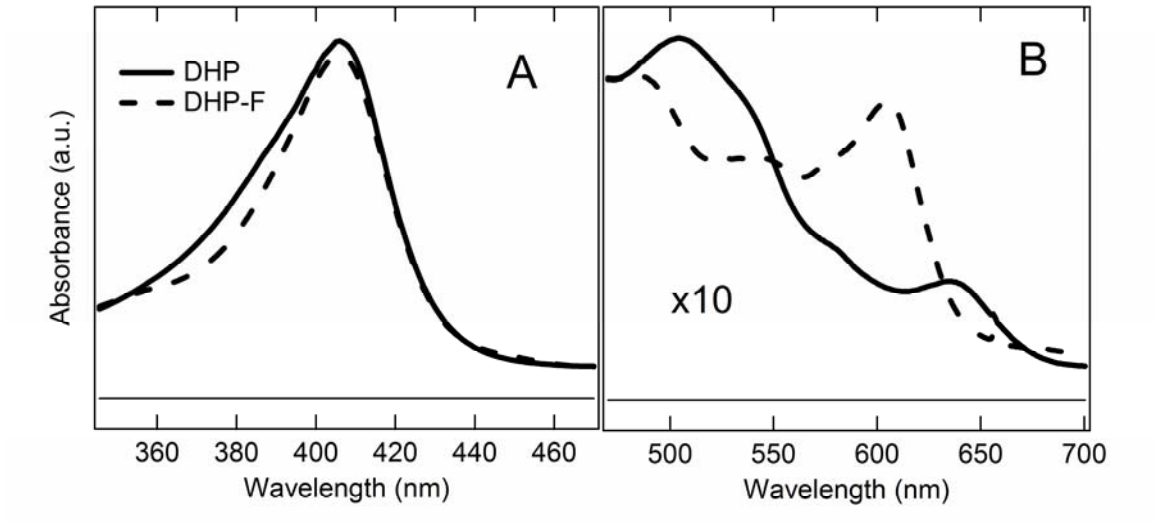

Figure 2. Absorption Soret spectra of high spin ferric DHP (solid) and ferric DHP with fluoride ligand (dash) in 100 mM phosphate buffer, pH 6.0 at room temperature. Soret maxima for both the ferric DHP and ferric DHP-F are 406 nm with small differences in the bandwidths. B. The Q-bands and charge transfer bands of ferric DHP and ferric DHP-F are shown.

The binding of F- at a pH 5.0, 6.0, 7.0 and 8.0 to ferric DHP was done to establish binding constants for fluoride without substrate interaction. The binding of F^- is pH dependent as shown in Figure 3. Binding constants for DHP are 167, 172, 110 and 96 μM^{-1} for pH 5.0, 6.0, 7.0 and 8.0. A decrease binding affinity for the F- is observed at pH 7.0 and 8.0 and is attributed to competitive binding of hydroxide from solution that forms the ferric hydroxide adduct of the protein.

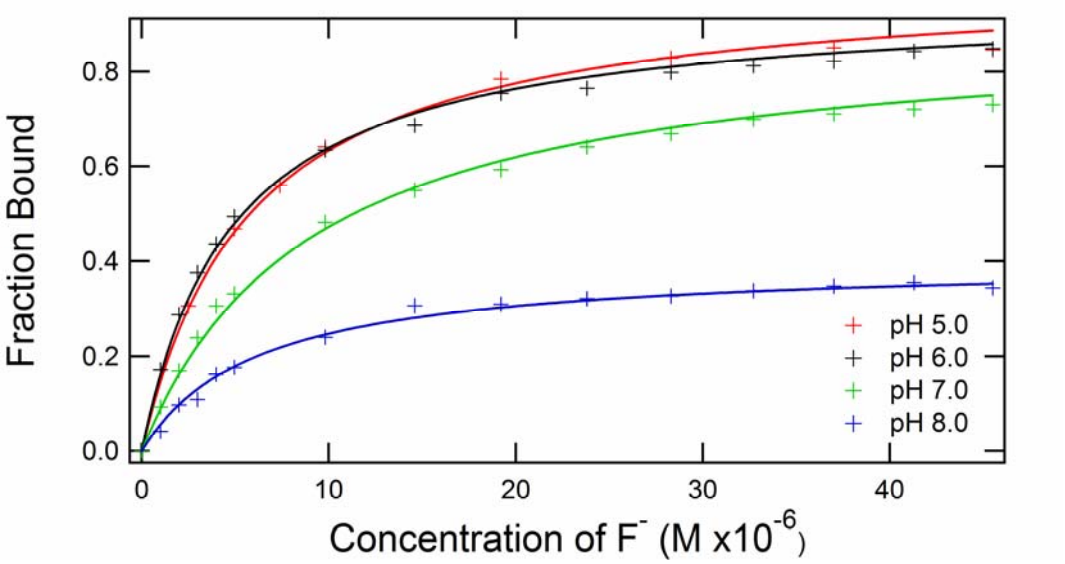

Figure 3. The pH dependence of F^- binding. Each assay was preformed in 100mM buffer, citrate pH's 5.0 and 6.0 or phosphate pHs 7.0 and 8.0. Binding constants for DHP are 167, 172, 110 and 96 μM^{-1} for pH 5.0, 6.0, 7.0 and 8.0.

Various substrates were tested for their effect on fluoride binding. The substrates used in these assays were 2,4,6-tribromophenol (TBP), 2,4,6-trichlorophenol (TCP), 2,4,6-trifluorophenol (TFP), 4-hydroxyphenyl acetic acid (HPA) and n-acetyl-L-tyrosine (NAY) at a concentration of 530 μM and for the pH range from 5.0 to 8.0. The substrate 2,4,6-tribromophenol (TBP) has been shown, in Chapter 4, to bind to ferric DHP. Thus we chose to investigate the effects of F- binding in the presence of TBP. Figure 4 shows the binding curves of F^- binding when TBP is present. The binding constants show that TBP inhibits the binding of F^- at pH 6.0. Similar substrates, TCP and TFP, only vary in halogen to TCP and both inhibit the binding of F^- at pH's 5.0 and 6.0. Fluoride binding curves to TCP and TFP bound DHP are shown in Figures 5 and 6, respectively.

The larger substrates, HPA and NAY, did not inhibit the binding of fluoride to ferric DHP at any pH studied. HPA and NAY facilitated the binding of fluoride at all

pH's studied. The fluoride binding curves for HPA and NAY are shown in Figures 7 and 8, respectively Fluoride binding constants for ferric DHP and ferric DHP with TBP, TCP, TFP, HPA and NAY are reported in Table 1.

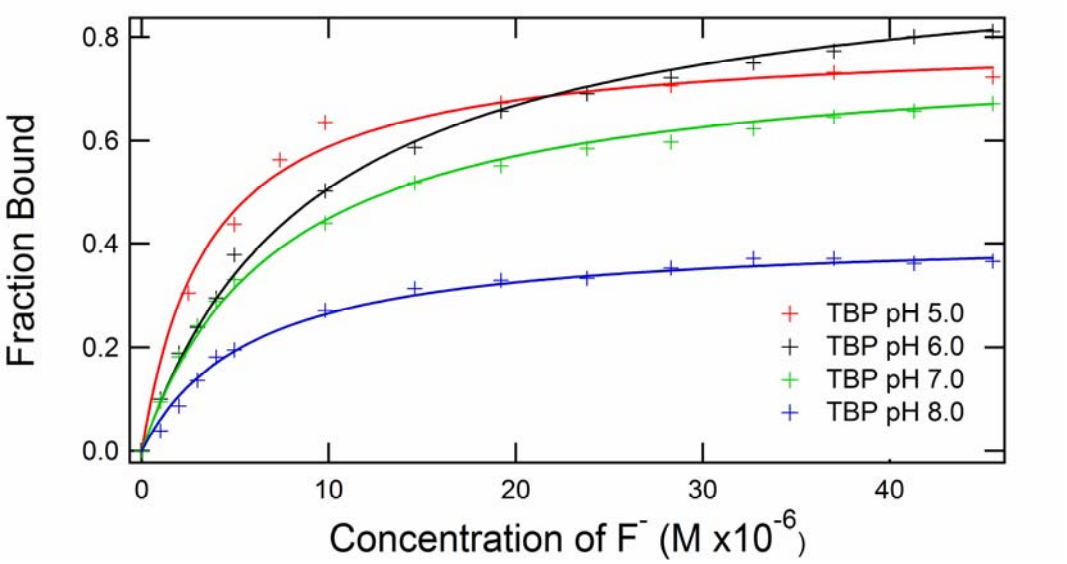

Figure 4. Binding of F^- to DHP at pH 5.0, 6.0, 7.0 and 8.0 in the presence of 530 μM 2,4,6-tribromophenol. Binding constants of 278, 107, 136 and 171 μM^{-1} were obtained for pH 5.0, 6.0, 7.0 and 8.0, respectively.

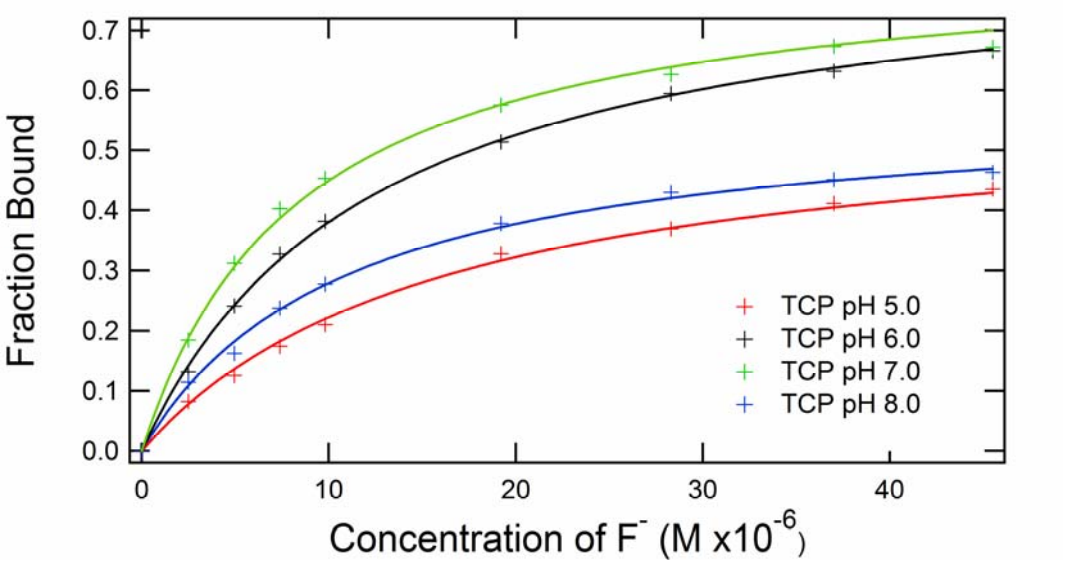

Figure 5. Binding of F^- to DHP at pH 5.0, 6.0, 7.0 and 8.0 in the presence of 530 μM 2,4,6-trichlorophenol. Binding constants of 62, 81, 118 and 93 μM^{-1} were obtained for pH 5.0, 6.0, 7.0 and 8.0, respectively.

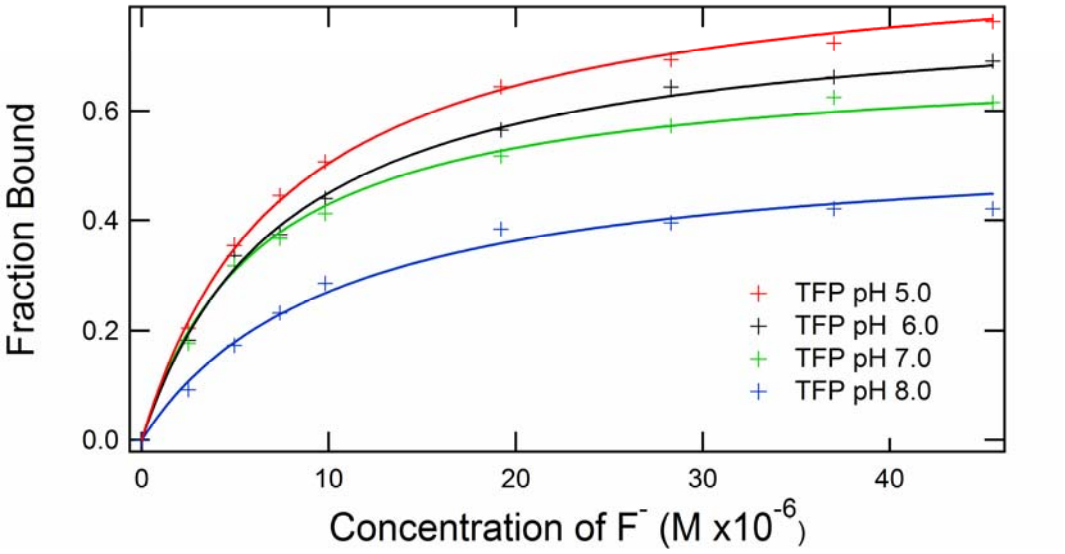

Figure 6. Binding of F^- to DHP at pH 5.0, 6.0, 7.0 and 8.0 in the presence of 530 μM 2,4,6-trifluorophenol. Binding constants of 127, 129, 159 and 97 μM^{-1} were obtained for pH 5.0, 6.0, 7.0 and 8.0, respectively.

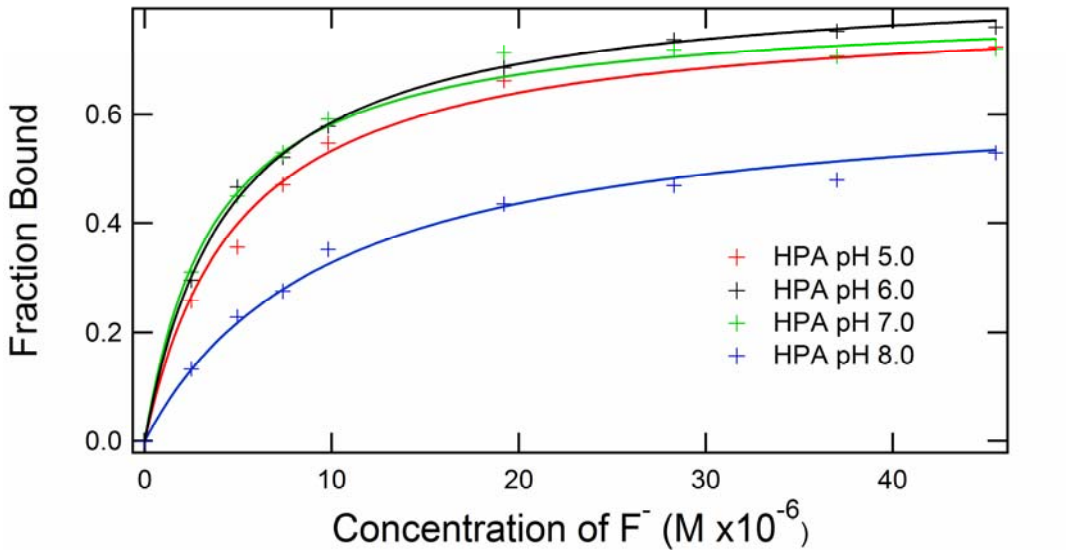

Figure 7. Binding of F^- to DHP at pH 5.0, 6.0, 7.0 and 8.0 in the presence of 530 μM 4-hydroxyphenyl acetic acid. Binding constants of 200, 222, 267 and 102 μM^{-1} were obtained for pH 5.0, 6.0, 7.0 and 8.0, respectively.

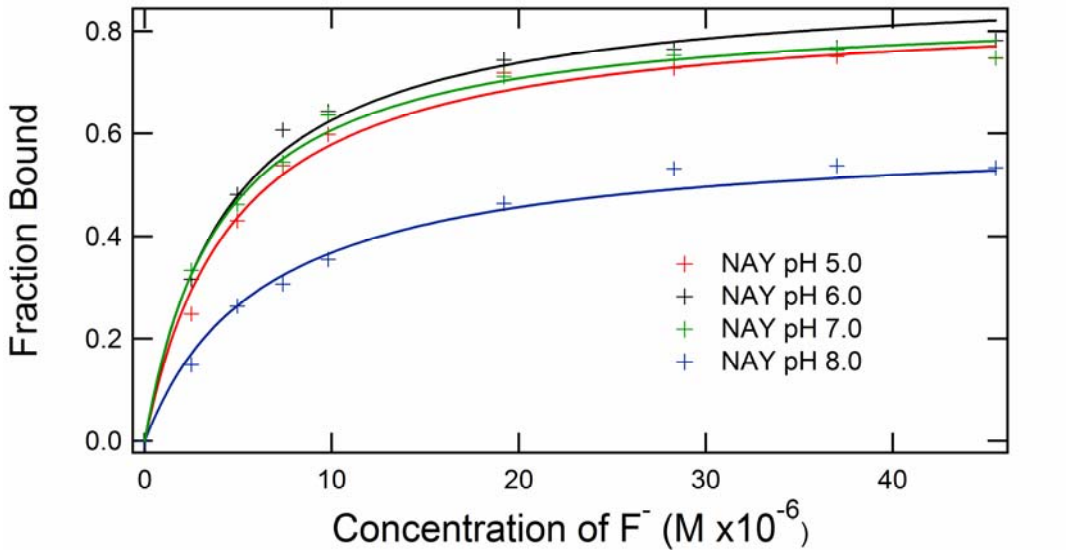

Figure 8. Binding of F^- to DHP at pH 5.0, 6.0, 7.0 and 8.0 in the presence of 530 μM n-acetyl-L-tyrosine. Binding constants of 213, 269, 249 and 159 μM^{-1} were obtained for pH 5.0, 6.0, 7.0 and 8.0, respectively.

Table 1. Binding constants and scaling factor for F- binding to DHP and in the presence of 530 μM substrate at pH 5.0, 6.0, 7.0 and 8.0.

Substrate	pH	K	A	Substrate	pH	K	A
none	5.0	167	1.0	TFP	5.0	128	0.9
	6.0	172	1.0		6.0	129	0.8
	7.0	110	0.9		7.0	159	0.7
	8.0	96	0.4		8.0	97	0.55
TBP	5.0	278	0.8	HPA	5.0	200	0.8
	6.0	107	0.98		6.0	222	0.85
	7.0	136	0.78		7.0	267	0.8
	8.0	171	0.42		8.0	102	0.65
TCP	5.0	62	0.58	NAY	5.0	213	0.85
	6.0	81	0.85		6.0	229	0.9
	7.0	118	0.83		7.0	249	0.85
	8.0	93	0.58		8.0	159	0.6

Cyanide binding to ferric DHP displaces a weak ligand, water, thus giving rise to an obvious shift in the Soret band form 406 nm to 423 nm as seen in Figure 9. The shift in the Soret band is typical for a transition from high spin to low spin state of the iron heme. Figure 10 shows the binding of cyanide appears sigmoidal, which is indicative of cooperativity.

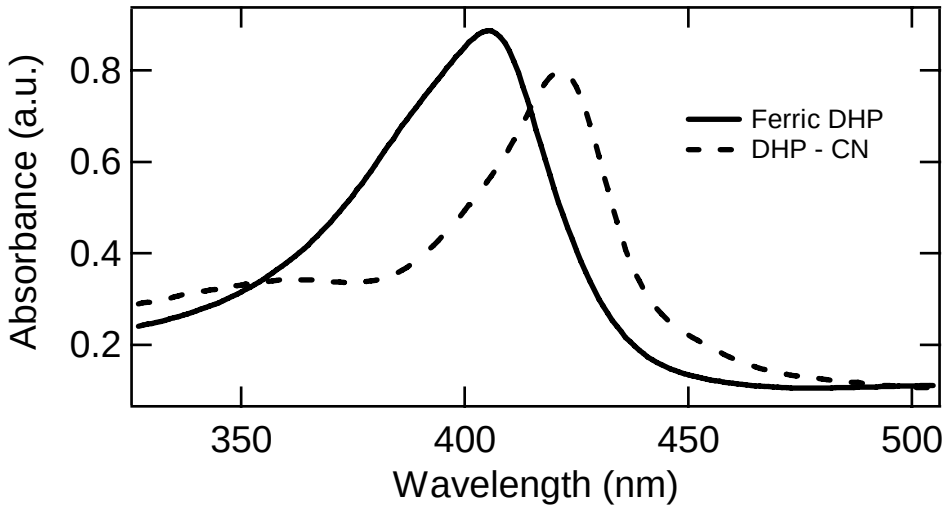

Figure 9. The Soret band shifts from 406 nm to 423 nm when cyanide binds to ferric DHP.

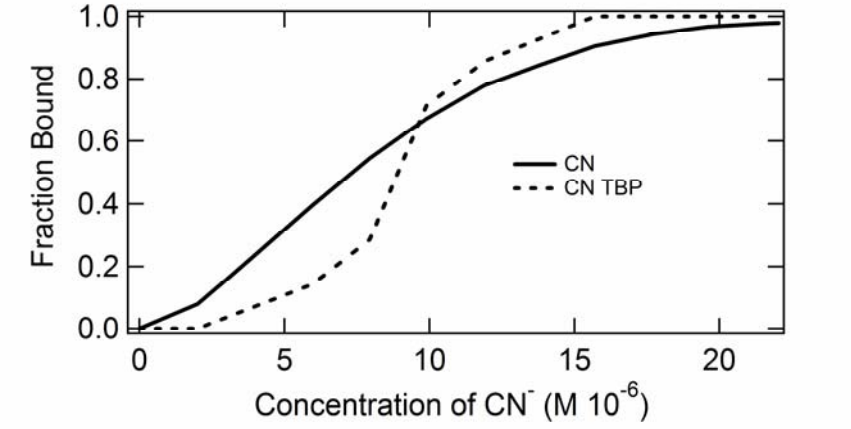

Figure 10. The binding of cyanide to ferric DHP with (dashed) and without (solid) TBP present.

Figures 11-37 are the hill plots used to determine the Hill coefficients, n_H, for all combinations of the substrate and pH that were studied. The effect of substrate concentration on the binding of ligand was studied of TBP at pH 6.0 and 8.0. All Hill coefficients are summarized in Table 2.

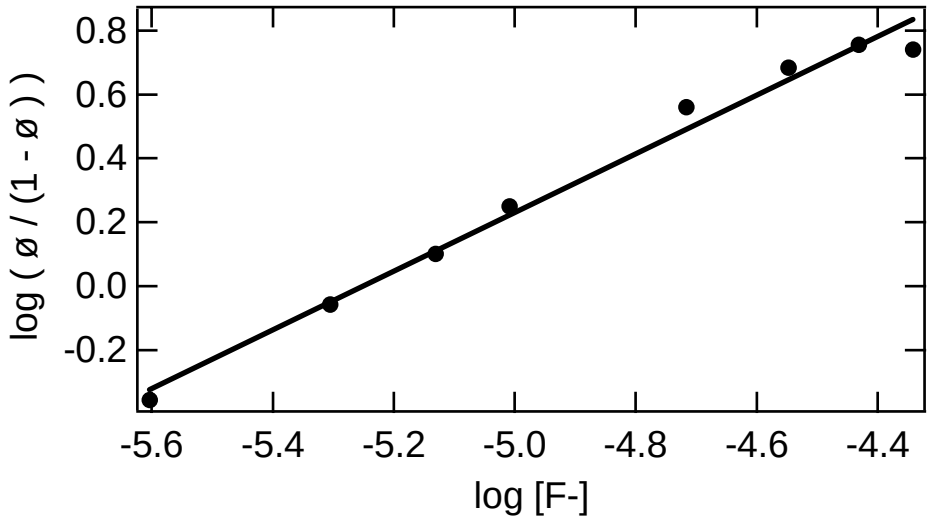

Figure 11. Hill plot for the binding of fluoride to ferric DHP at pH 5.0. The Hill coefficient was determined from the slope to be 0.92.

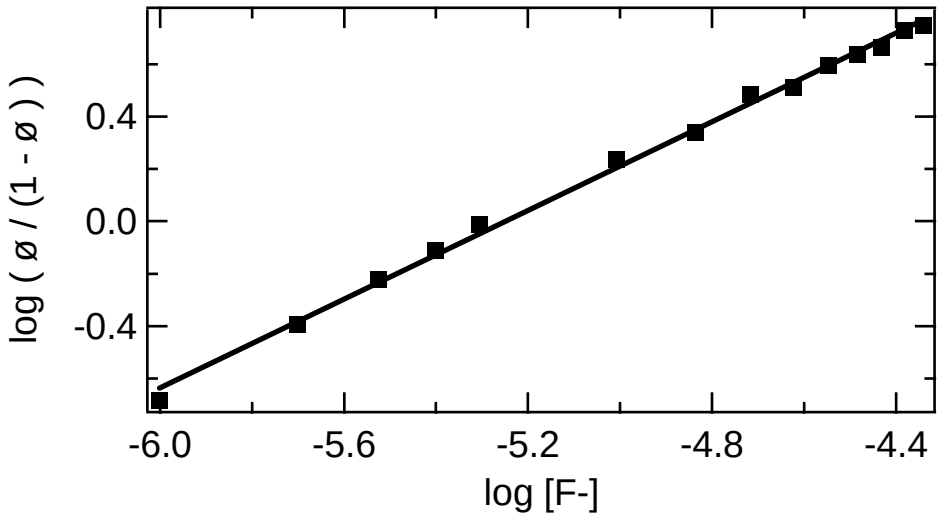

Figure 12. Hill plot for the binding of fluoride to ferric DHP at pH 6.0. The Hill coefficient was determined from the slope to be 0.85.

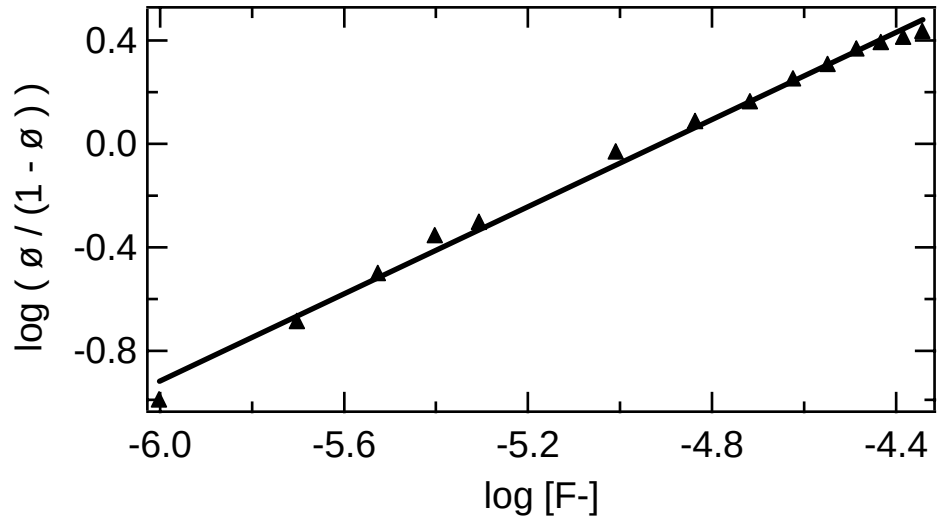

Figure 13. Hill plot for the binding of fluoride to ferric DHP at pH 7.0. The Hill coefficient was determined from the slope to be 0.84.

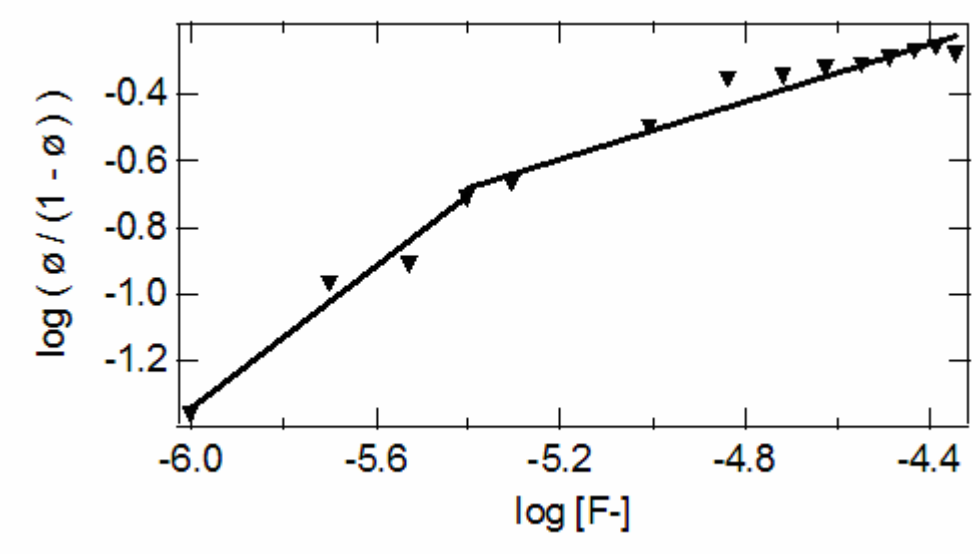

Figure 14. Hill plot for the binding of fluoride to ferric DHP at pH 8.0. The Hill coefficient was determined from the slope to be 1.03 and 0.43.

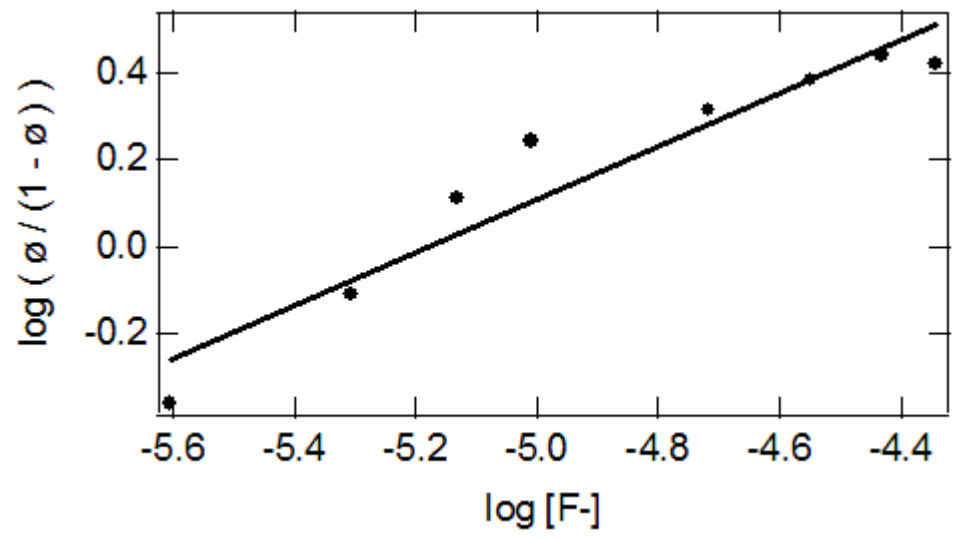

Figure 15. Hill plot for the binding of fluoride to ferric DHP in the presence of 100 molar excess TBP at pH 5.0. The Hill coefficient was determined from the slope to be 0.61.

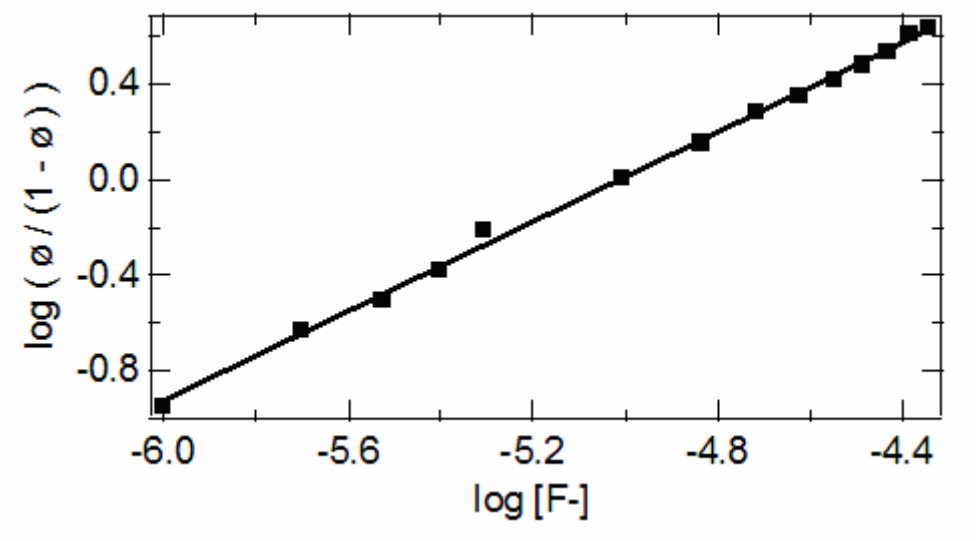

Figure 16. Hill plot for the binding of fluoride to ferric DHP in the presence of 100 molar excess TBP at pH 6.0. The Hill coefficient was determined from the slope to be 0.94.

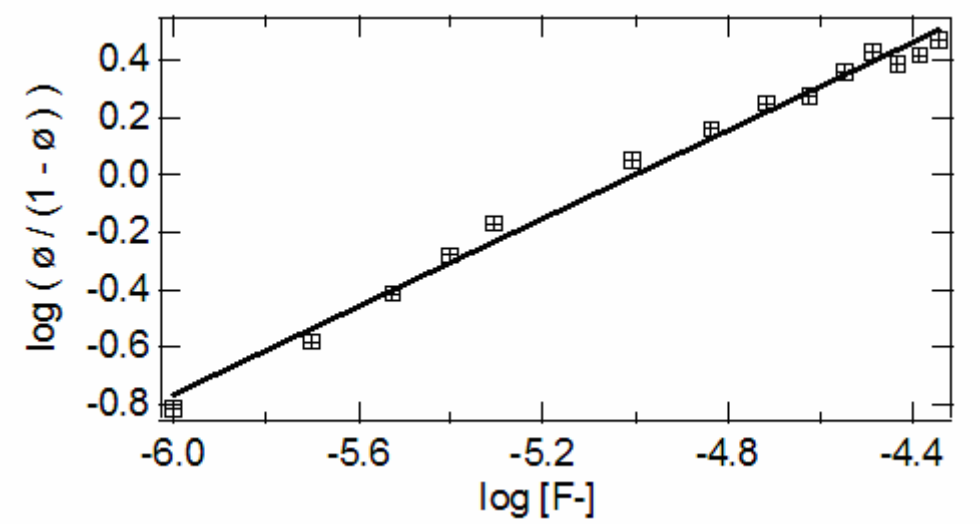

Figure 17. Hill plot for the binding of fluoride to ferric DHP in the presence of 10 molar excess TBP at pH 6.0. The Hill coefficient was determined from the slope to be 0.77.

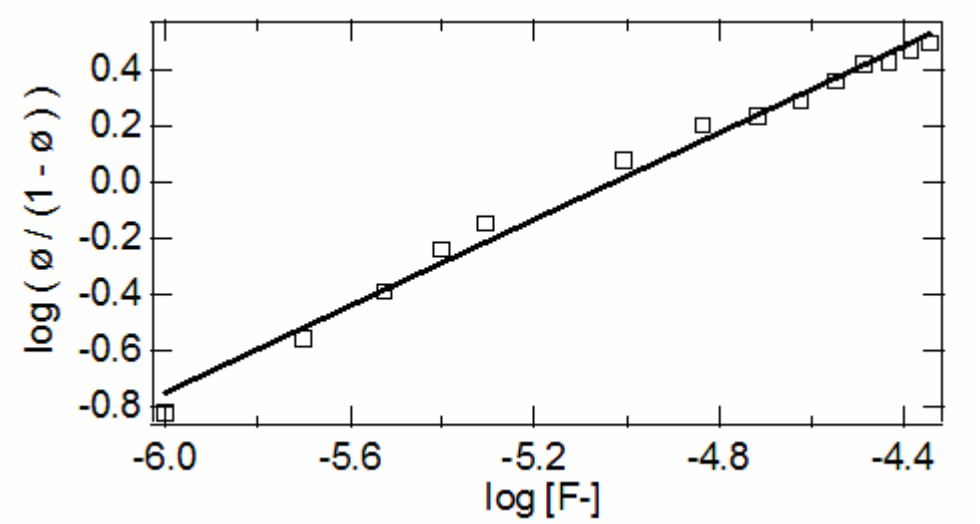

Figure 18. Hill plot for the binding of fluoride to ferric DHP in the presence of equal molar TBP at pH 6.0. The Hill coefficient was determined from the slope to be 0.77.

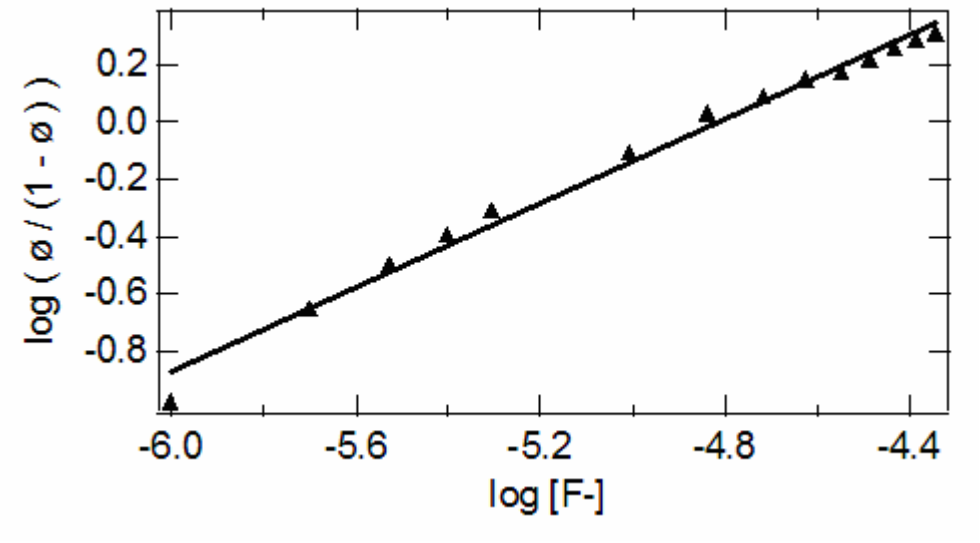

Figure 19. Hill plot for the binding of fluoride to ferric DHP in the presence of 100 molar excess TBP at pH 7.0. The Hill coefficient was determined from the slope to be 0.73.

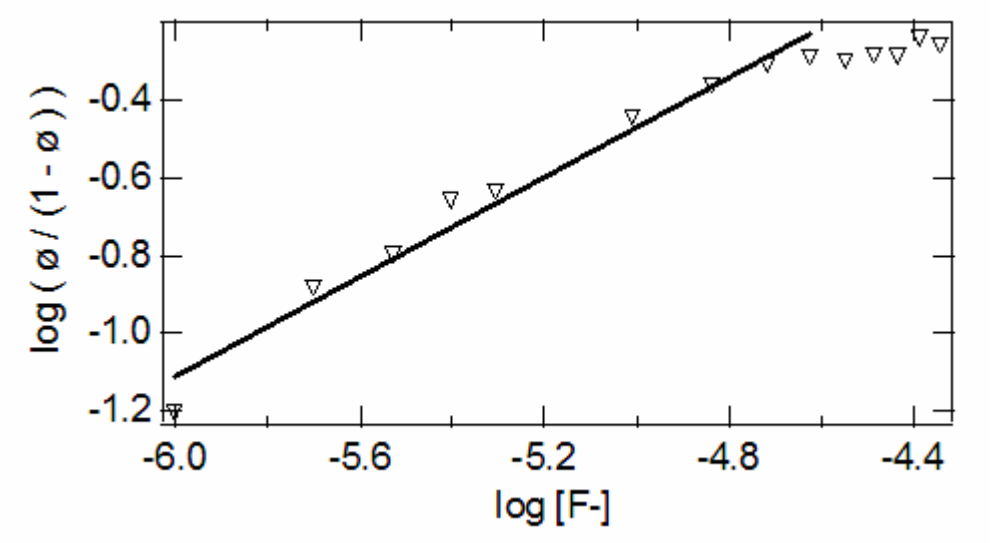

Figure 20. Hill plot for the binding of fluoride to ferric DHP in the presence of equal molar TBP at pH 7.0. The Hill coefficient was determined from the slope to be 0.64.

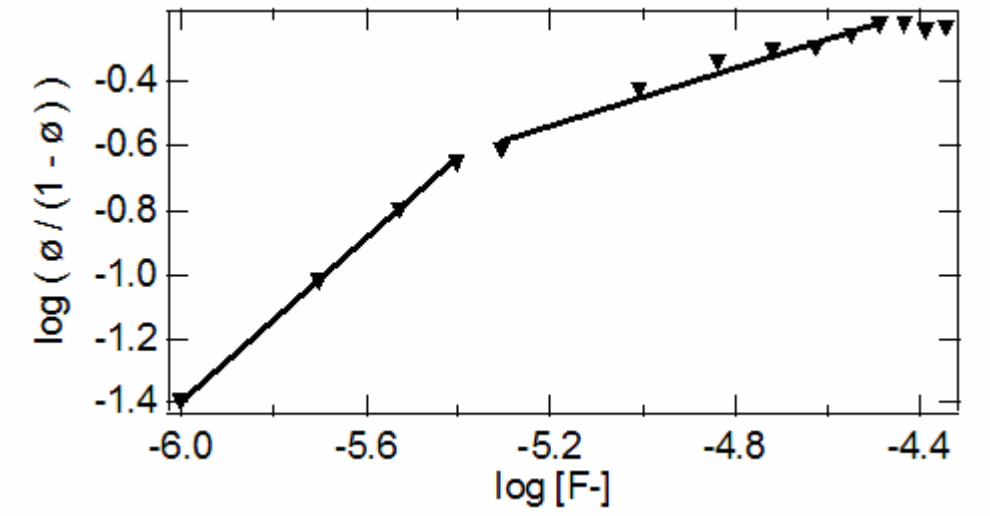

Figure 21. Hill plot for the binding of fluoride to ferric DHP in the presence of 100 molar excess TBP at pH 8.0. The Hill coefficient was determined from the slope to be 1.16 and 0.47.

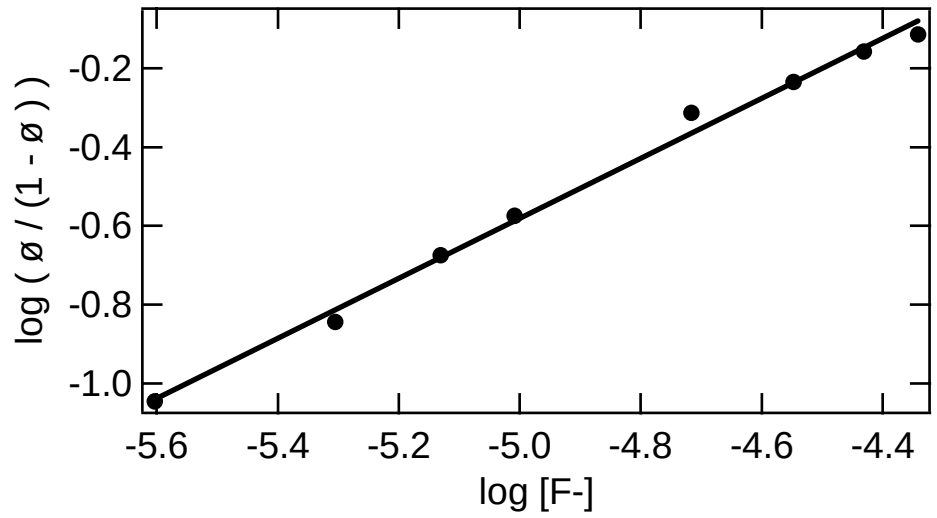

Figure 22. Hill plot for the binding of fluoride to ferric DHP in the presence of 100 molar excess TCP at pH 5.0. The Hill coefficient was determined from the slope to be 0.76.

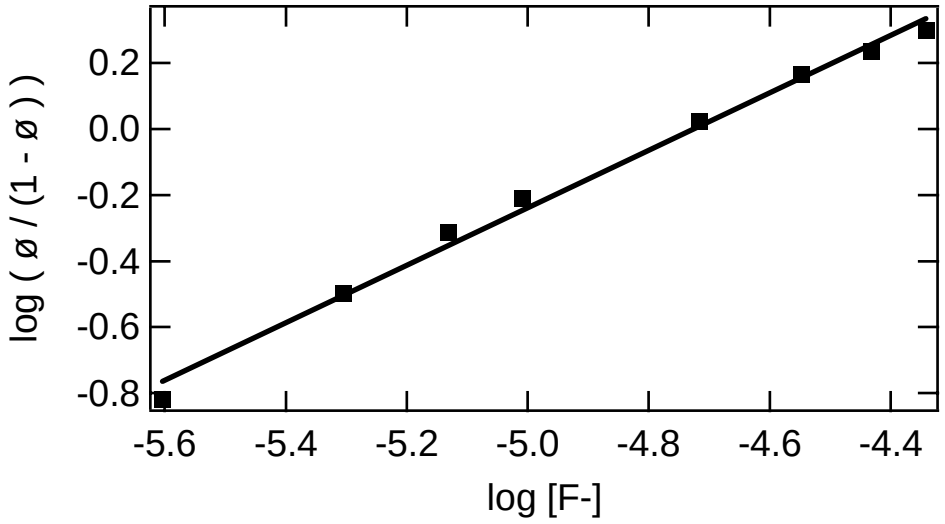

Figure 23. Hill plot for the binding of fluoride to ferric DHP in the presence of 100 molar excess TCP at pH 6.0. The Hill coefficient was determined from the slope to be 0.87.

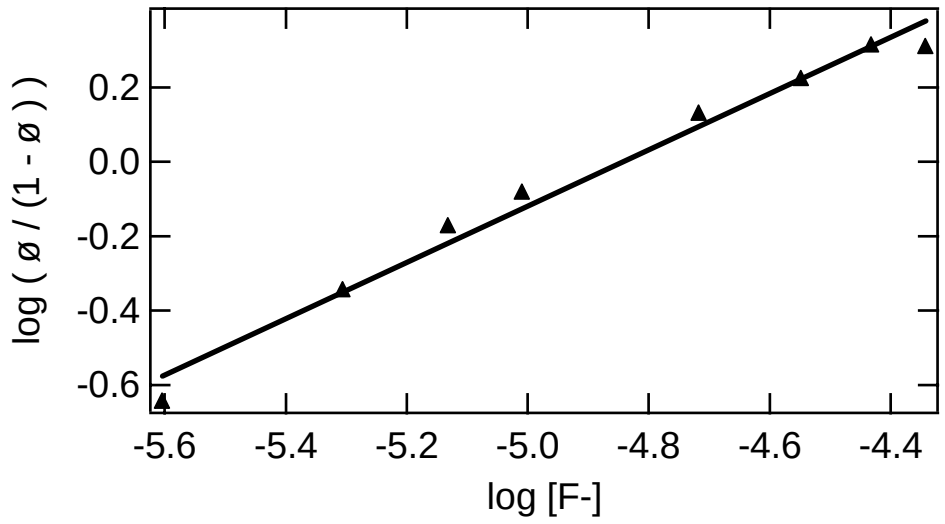

Figure 24. Hill plot for the binding of fluoride to ferric DHP in the presence of 100 molar excess TCP at pH 7.0. The Hill coefficient was determined from the slope to be 0.76.

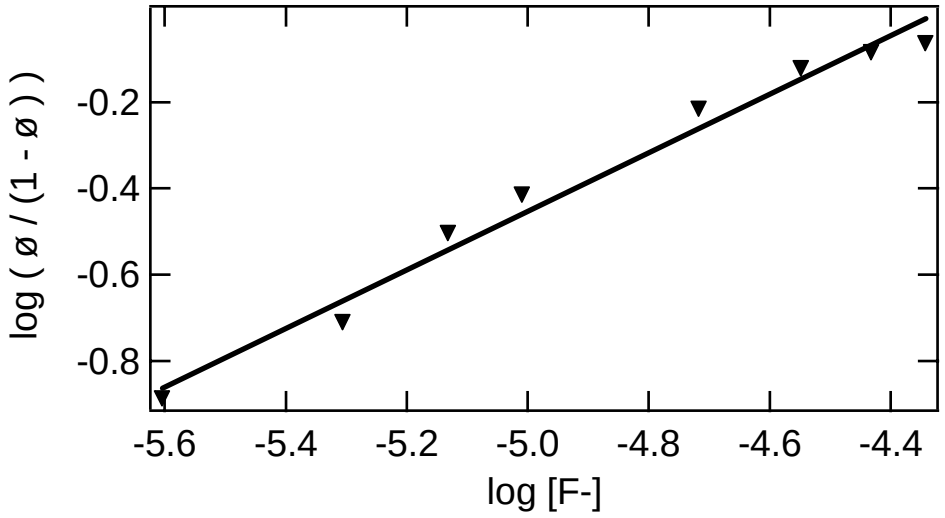

Figure 25. Hill plot for the binding of fluoride to ferric DHP in the presence of 100 molar excess TCP at pH 8.0. The Hill coefficient was determined from the slope to be 0.87.

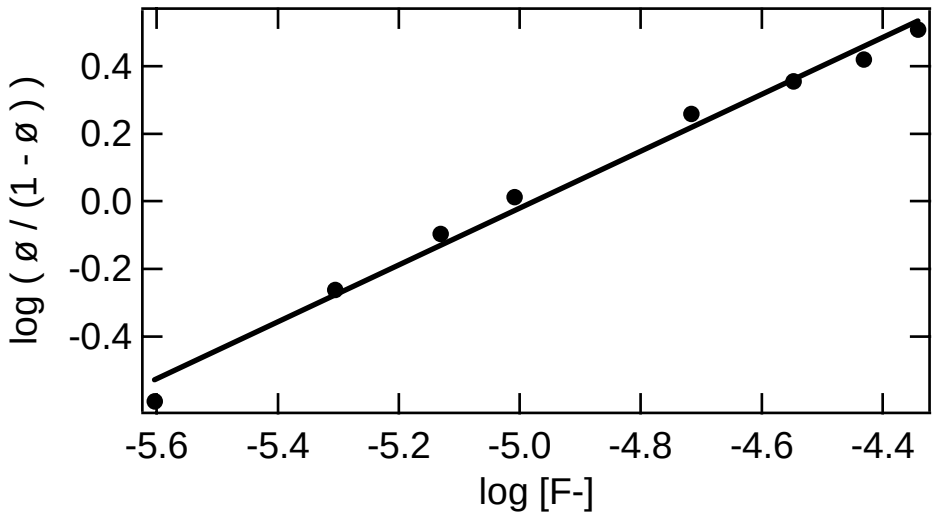

Figure 26. Hill plot for the binding of fluoride to ferric DHP in the presence of 100 molar excess TFP at pH 5.0. The Hill coefficient was determined from the slope to be 0.84.

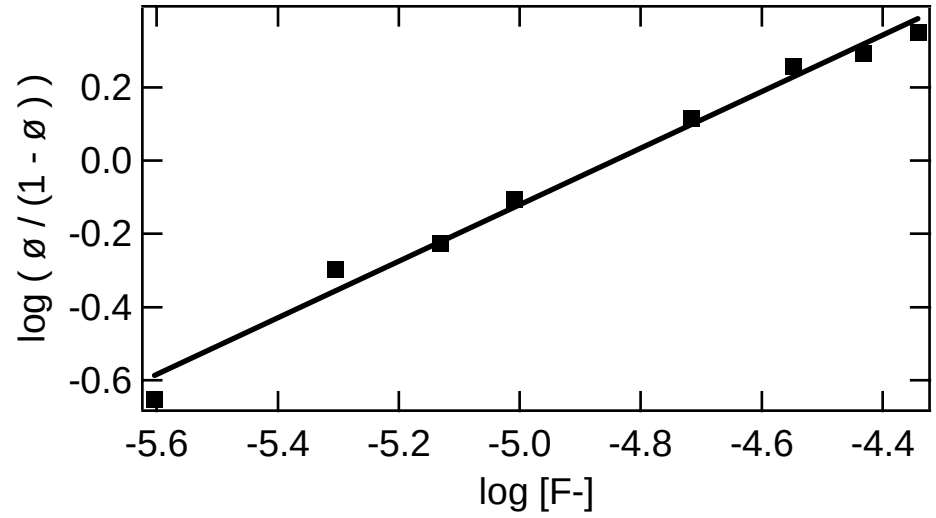

Figure 27. Hill plot for the binding of fluoride to ferric DHP in the presence of 100 molar excess TFP at pH 6.0. The Hill coefficient was determined from the slope to be 0.77.

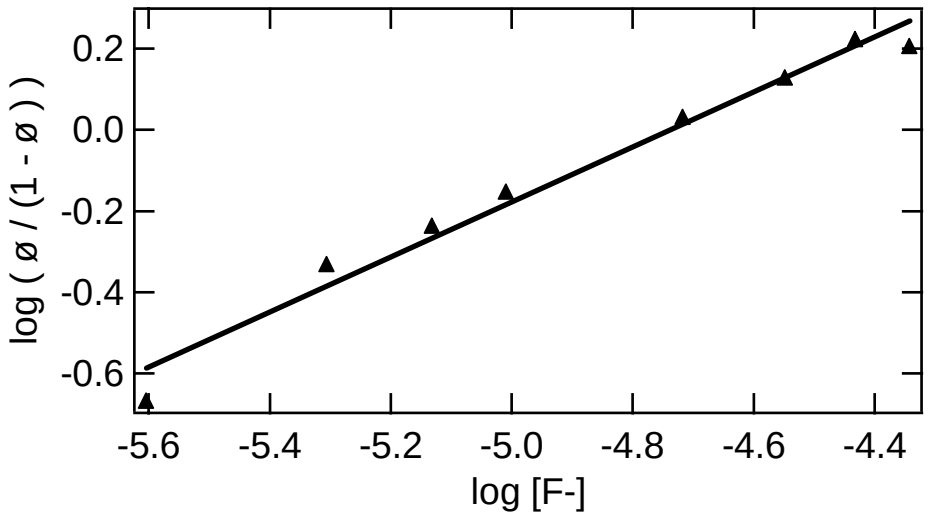

Figure 28. Hill plot for the binding of fluoride to ferric DHP in the presence of 100 molar excess TFP at pH 7.0. The Hill coefficient was determined from the slope to be 0.68.

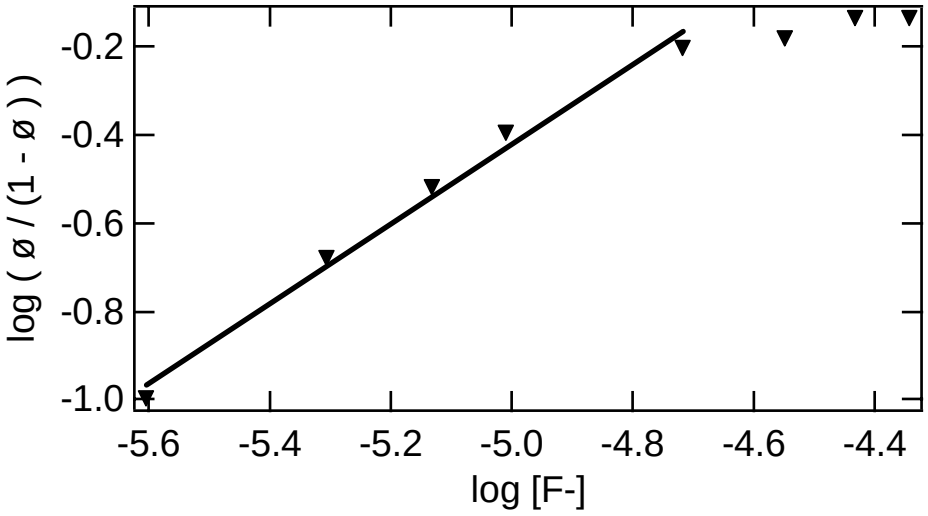

Figure 29. Hill plot for the binding of fluoride to ferric DHP in the presence of 100 molar excess TFP at pH 8.0. The Hill coefficient was determined from the slope to be 0.90.

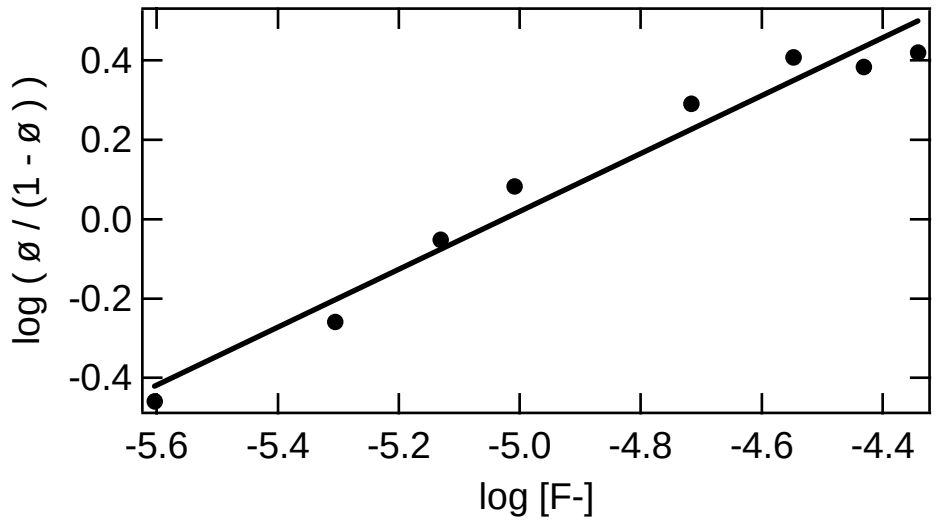

Figure 30. Hill plot for the binding of fluoride to ferric DHP in the presence of 100 molar excess HPA at pH 5.0. The Hill coefficient was determined from the slope to be 0.73.

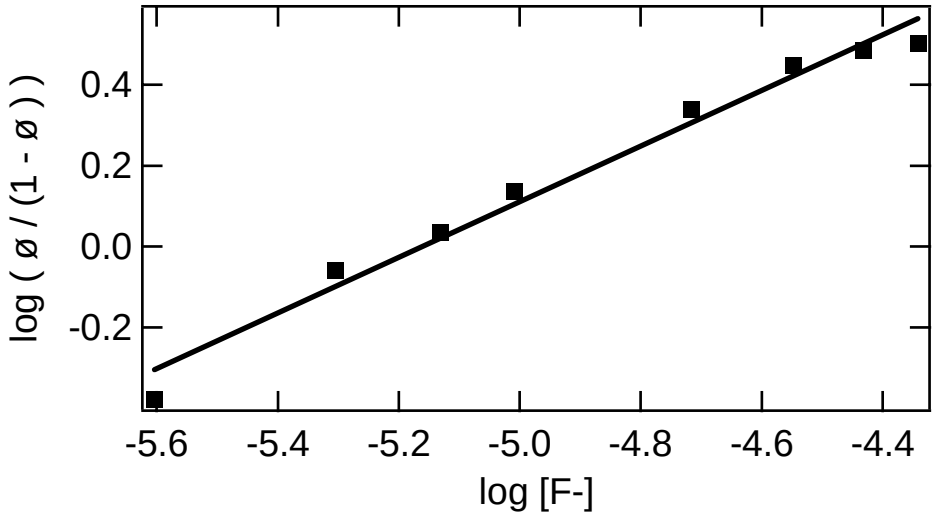

Figure 31. Hill plot for the binding of fluoride to ferric DHP in the presence of 100 molar excess HPA at pH 6.0. The Hill coefficient was determined from the slope to be 0.69.

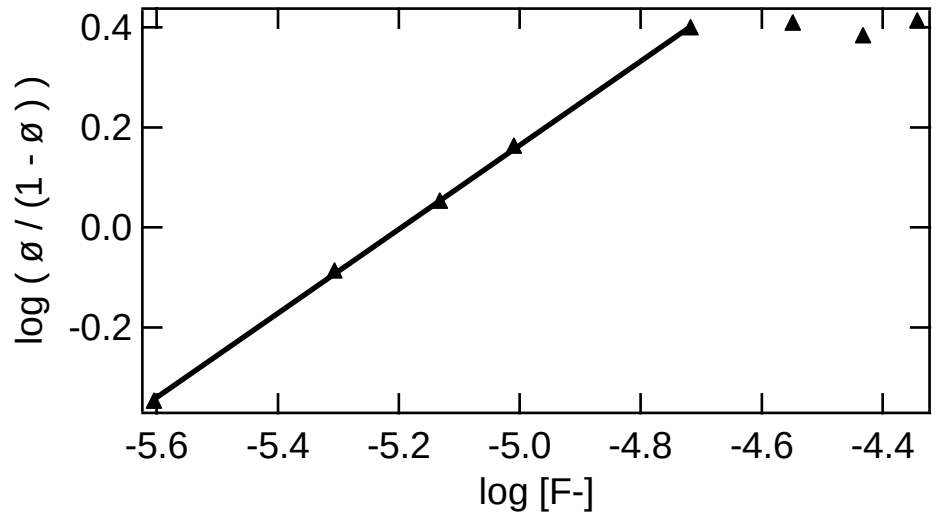

Figure 32. Hill plot for the binding of fluoride to ferric DHP in the presence of 100 molar excess HPA at pH 7.0. The Hill coefficient was determined from the slope to be 0.84.

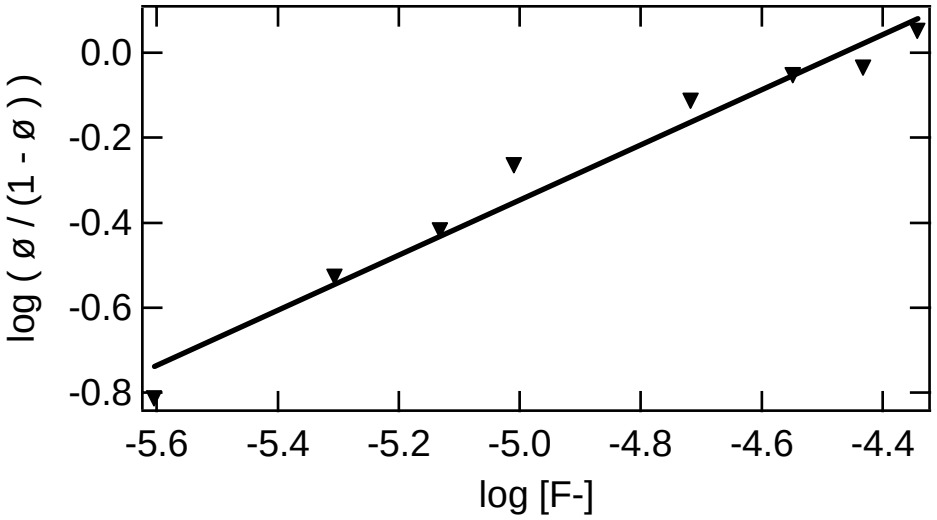

Figure 33. Hill plot for the binding of fluoride to ferric DHP in the presence of 100 molar excess HPA at pH 8.0. The Hill coefficient was determined from the slope to be 0.65.

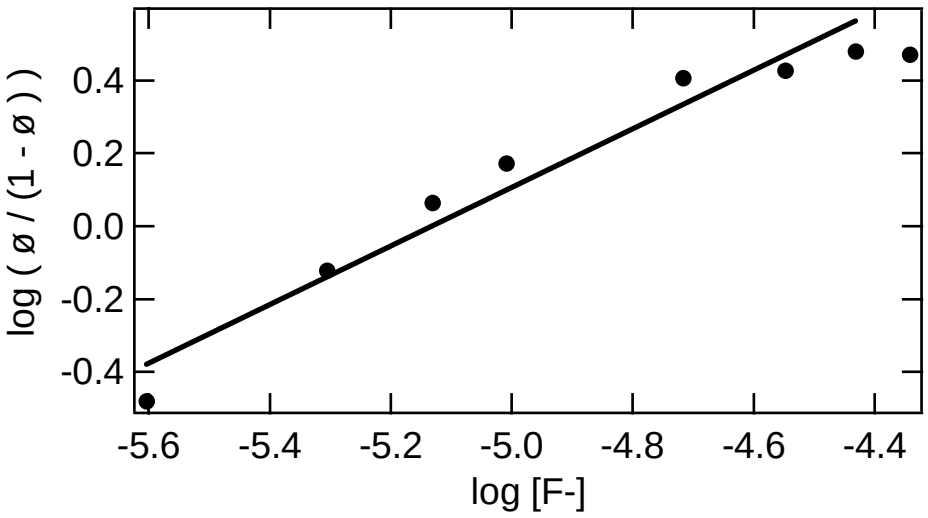

Figure 34. Hill plot for the binding of fluoride to ferric DHP in the presence of 100 molar excess NAY at pH 5.0. The Hill coefficient was determined from the slope to be 0.80.

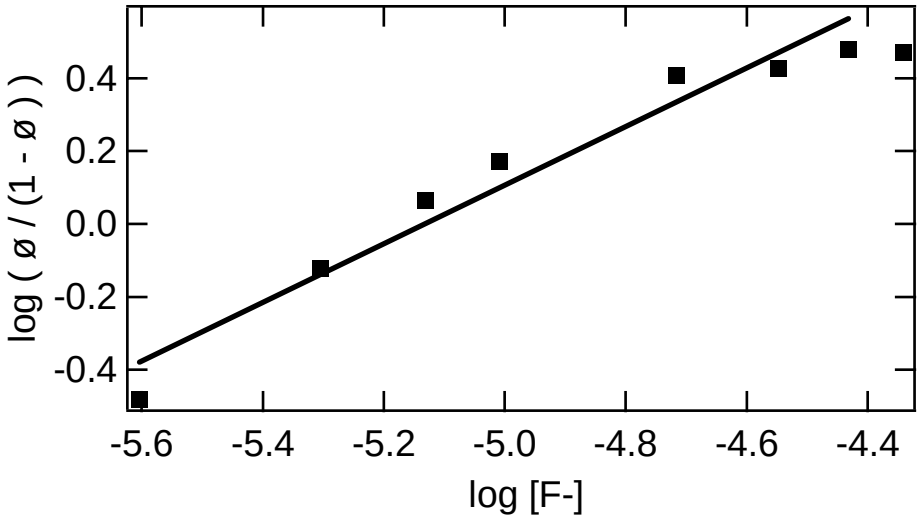

Figure 35. Hill plot for the binding of fluoride to ferric DHP in the presence of 100 molar excess NAY at pH 6.0. The Hill coefficient was determined from the slope to be 0.80.

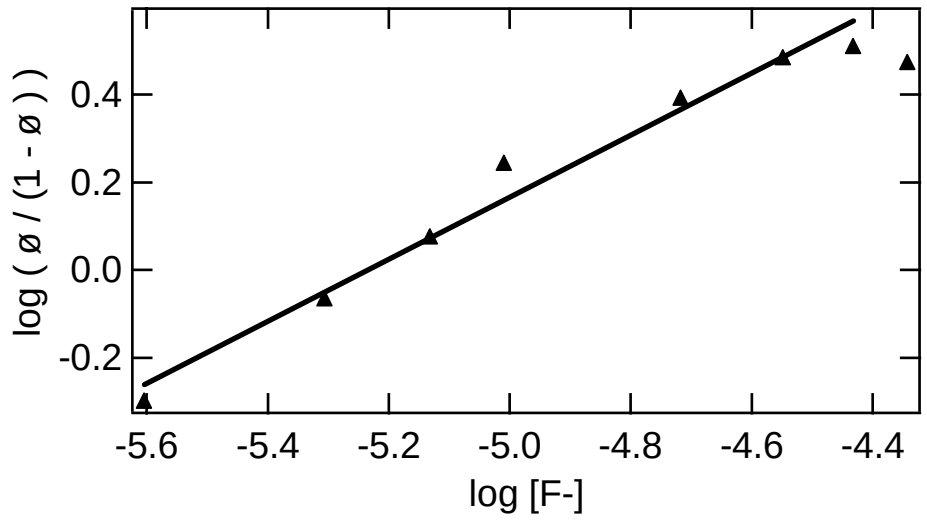

Figure 36. Hill plot for the binding of fluoride to ferric DHP in the presence of 100 molar excess NAY at pH 7.0. The Hill coefficient was determined from the slope to be 0.71.

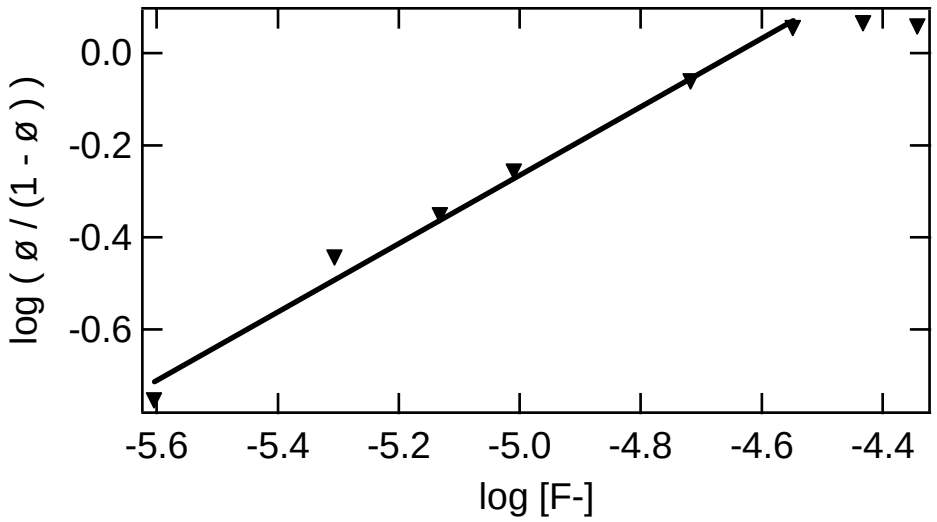

Figure 37. Hill plot for the binding of fluoride to ferric DHP in the presence of 100 molar excess NAY at pH 8.0. The Hill coefficient was determined from the slope to be 0.75.

Table 2. Hill coefficients determined for fluoride binding to ferric DHP at pH 5.0, 6.0, 7.0, 8.0 with a variety of substrates at 1, 10 and 100 molar ratio to DHP.

Substrate/ excess	pH 5.0	pH 6.0	pH 7.0	pH 8.0
None	0.92	0.85	0.76	0.68
TBP/100	0.61	0.94	0.73	1.16, 0.47
TBP/10		0.77		
TBP/1		0.77		0.64
TCP/100	0.76	0.87	0.76	0.68
TFP/100	0.84	0.77	0.68	0.9
HPA/100	0.73	0.69	0.84	0.65
NAY/100	0.80	0.80	0.71	0.75

Fluoride binding to Mb and HRP was done at pH 6.0 with and without 100 molar excess TBP was done in order to determine if the presence of TBP affected the binding of fluoride. Little to no effect on fluoride binding is observed for Mb and HRP in the presence of excess TBP as shown in Figure 37. The presence of TBP does affect the binding of fluoride for DHP.

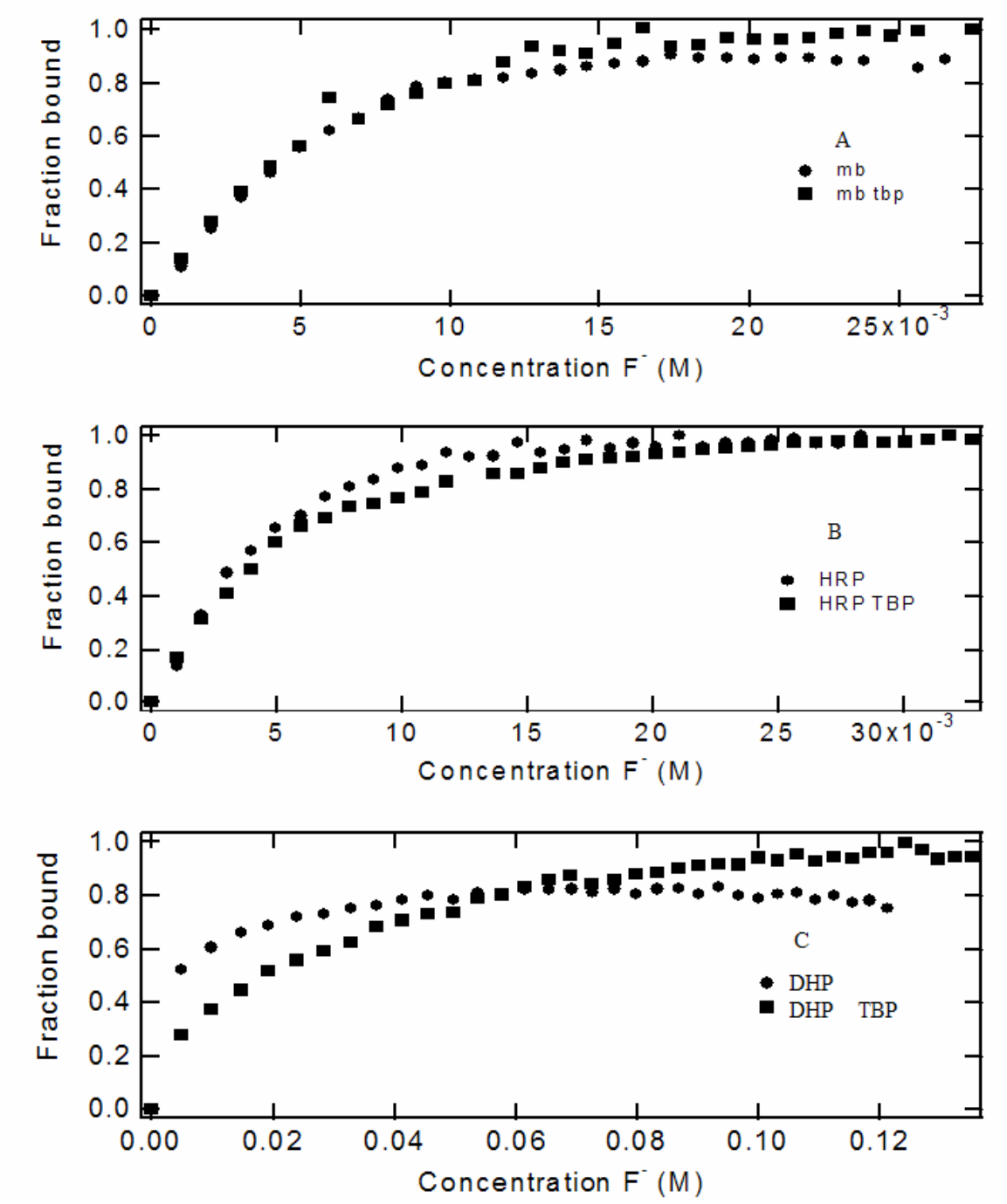

Figure 38. Results from binding assays of fluoride to Mb (A), HRP (B), and DHP (C) with and without TBP. Reaction conditions are 100 mM citrate pH 6.0 and 100 molar excess TBP or 0 TBP at 20^{o}C.

Figure 39 and 40 are Hill plots for the binding of cyanide at pH 6.0 without and with 100 molar excess TBP. The binding of cyanide is cooperative and multiple binding sites exist since the hill coefficients are greater than 1.

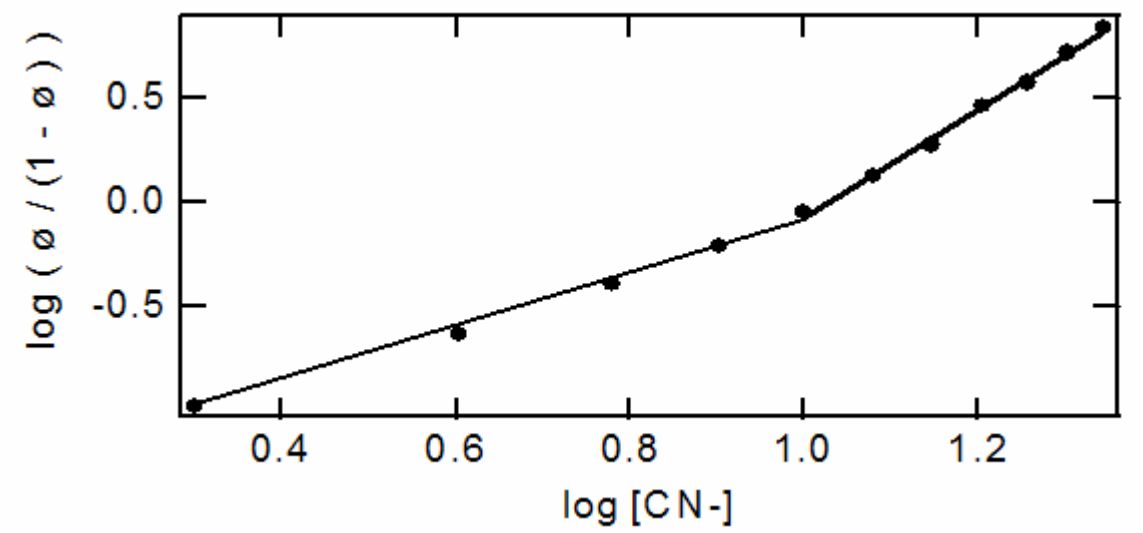

Figure 39. Hill plot for the binding of cyanide to ferric at pH 6.0. The Hill coefficient was determined from the slope to be 2.6069 and 1.3189.

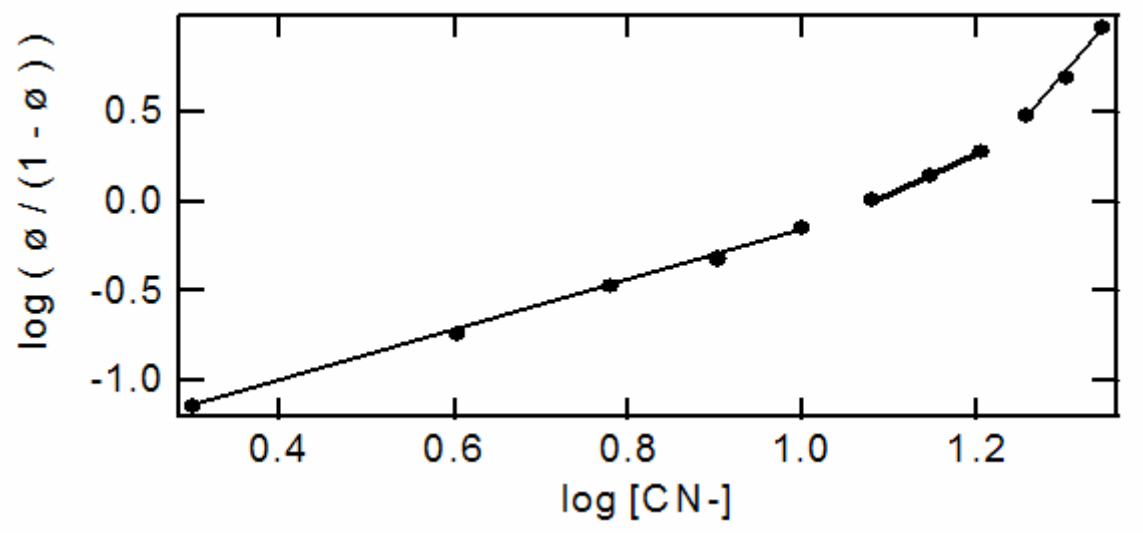

Figure 40. Hill plot for the binding of cyanide to ferric DHP in the presence of 100 molar excess TBP at pH 6.0. The Hill coefficient was determined from the slope to be 1.4492, 2.2188 and 5.6848.

Conclusion

Trihalogenated phenols inhibit the binding of fluoride at acidic pHs below the pKa of the substrate. This leads us to conclude that the substrate must bind in the anionic form. Hill coefficients for fluoride binding are less then one which means that fluoride binding is negatively cooperative or that more than one binding site exist and the different binding sites have different affinities. The cooperative nature of cyanide binding to the ferric DHP is occurring due to the high to low spin transition of the iron. Cyanide is a strong ligand that forces the ferric ligand to go low spin thus the binding of cyanide is similar to the binding of oxygen in myoglobin. The Hill coefficients for cyanide binding to DHP is greater than two, thus it is believed that cyanide can occupy cavities within the protein. In Mb such sites are called Xe binding sites and have been shown to be occupied by CO upon photolysis.[7]

References

1. Nienhaus, K.; Deng, P.; Belyea, J.; Franzen, S.; Nienhaus, G. U. **Spectroscopic Study of Substrate Binding to the Carbonmonoxy Form of Dehaloperoxidase from Amphitrite ornata.** Journal of Physical Chemistry B (2006), 110(26), 13264- 13276.

2. Unpublished work by Mike Davis.

3. Di Prisco, G., Condo, S.G., Tamburrini, M., Giardina, B. **Oxygen transport in extreme environments**. Trends Biochem. Sci. 1991 16, 471-474.

4. Mondo, J., Wyman, J., Changeux, J.P. **On the nature of allosteric transitions: a plausible model**. *J. Mol. Biol*. 1965 12, 88-118.

5. Koshland, D.E., Jr., Nemethy, G., Filmer, D. **Comparison of experimental binding data and theoretical models in proteins containing subunits**. *Biochemistry* 1966 5, 365-385.

6. Belyea, J.; Gilvey, L. B.; Davis, M. F.; Godek, M.; Sit, T. L.; Lommel, S. A.; Franzen, S. **Enzyme function of the globin dehaloperoxidase from *amphitrite ornata* Is activated by substrate binding.** Biochemistry 2005, 44(48), 15637-15644.

7. Schotte, F.; Lim, M.; Jackson, T. A.; Smirnov, A. V.; Soman, J.; Olson, J. S.; Phillips, G. N. Jr.; Wulff, M.; Anfinrud, P. A. **Watching a protein as it functions with 150-ps time-resolved X-ray crystallography**. *Science*. 2003 300, 1944-1947.

Chapter 6 Electrochemical Characterization of Dehaloperoxidase from *Amphitrite ornata*

Introduction

The redox potential of the heme iron is a key determinant of the reactivity of a heme enzyme. DHP is an enzyme, but it is also a globin. We measured the redox potential of the oxy/deoxy couple of DHP and attempted to measure the redox potential of the ferric/ferrous couple form. The difficulty of measuring the redox potential of the ferric/ferrous couple of DHP is puzzling. Reports of the Fe(II)/Fe(III) redox couple are available for myoglobin (50 mV)[1], horseradish peroxidase (-270 mV)[1], cytochrome $P450_{cam}$ (-170 mV and -270 mV for the high and low spin forms, respectively).[2]

Although DHP is a peroxidase and a globin, it binds the substrate in an internal binding pocket. This aspect of DHP structure most closely resembles the monooxygenase, cytochrome P450 $_{cam}$. The mechanism of substrate oxidation involves direct transfer of oxygen to a substrate bound in an internal binding pocket. A dramatic change in the Soret region is observed through the binding of camphor and cytochrome P450 $_{cam}$. The change in the Soret is explained by the change in spin states of the heme iron center after binding camphor[3]. The low-spin state of $P450_{cam}$ is observed in the absence of substrate, while the high-spin state is observed in the presence of substrate. The redox potential of $P450_{cam}$ increases 100 mV when substrate is bound[3]. The increase in the redox potential results in easier reduction of bound diatomic oxygen to form the oxoferryl compound I that is catalytically active.[3]

The binding of several substrates to $P450_{cam}$ has been analyzed in various studies that determined the dissociation constant (K_d) and spin-state equilibrium constant (K_{spin}). Thus, the binding selectivity of substrates were determined. [4] Typically, factors controlling redox potential are thought to be due to local dielectric constant, and pH.[5]

Through the analysis of P450 $_{cam}$ a linear relationship between reduction potential and free energy of ferric spin equilibrium is observed. This suggests that ligand field stabilization energy of the heme center of $P450_{cam}$ regulates the oxidation-reduction potential as a response to substrate binding.

In this chapter we discuss substrate-binding effects on the redox potential of dehaloperoxidase, DHP. Based on the results in Chapter 4 we have determined by EPR that the binding of substrate affects the spin state of the iron in DHP. In this chapter we explore whether the change in the spin state results in the change in the redox potential upon the binding of substrate.

Materials and Methods

Gold electrode surfaces were prepared by cleaning with (UVO-CLEANER Model No. 42 Jelight Company Inc.) plasma cleaner for 7.5 minutes. The gold electrode was placed in 1% vol/vol liquinox/distilled deionized 18 MΩ pure water (DI H_2O) from (Barnstead E-pure), sonicated using (Fisher Scientific FS20) for 10 minutes, and then washed with 18 MΩ DI H_2O. The process was repeated in triplicate. An electrochemical cell was then assembled using the gold slide and filled with 1 mL 18 MΩ DI H_2O. The sealed cell is rinsed three times with 18 MΩ DI H_2O, and then 0.1 M H_2SO_4 / 0.01 M KCl cleaning solution is added. The cell is cleaned electrochemically by scanning from 0 to 1.5 V using (EG&G PAR Potentiostat/Galvanostat Model 275A). This was done 10 times at a scan rate of 100 mV/s. A mixed SAM was prepared by addition of a 5 mM 11-undecanocanoic (MUA) acid and 2.5 mM 6-mercatohexanol (MH) solution to the cell so that the gold slide surface was covered. The cell was covered with a rubber septum or parafilm and allowed to set for 6 hours at 4^{o}C. After 6 hours the cell was rinsed with

water and 100 mM potassium phosphate pH 5.0. Cyclic Voltammograms were collected by scanning from -200 mV to +600 mV. An initial equilibration time of 15-30 s at -200 mV was used. Background CV's were collected using buffer solution only. Platinum wire was used as the counter electrode and a Ag/AgCl electrode was used as the reference electrode for all measurements. The above experimental conditions were modified from work done by KeAndra Robinson.[6]

Protein samples

DHP protein was purified from *E.coli* according to previously published methods.[7] Protein samples were 60 μM DHP with varying amounts of 2,4,6-tribromophenol. Samples containing 2,4,6-tribromophenol, TBP, were made by dialyzing the protein with the desired concentration of TBP in 100 mM phosphate pH 5.0. The protein samples were concentrated to 60 μM by Millipore Amicon Ultra-4 MWCO 10,000 (Fisher Scientific UFC8 010 24). The pH of the effluent was measured to ensure the protein substrate solution was pH 5.0. Concentration of protein and TBP was checked by absorption spectroscopy, using a Hewlett Packard 8453 multi-wavelength spectrometer before and after data collection. The Soret band of the DHP protein sample was 416nm, indicative of oxy-DHP. Spectroelectrochemical data were collected at Los Alamos National Laboratory by Dr. Rocha and Dr. Rein. Experimental conditions for the SEC are as follows, potential was held at -200 mV, UV-Visible spectrum was collected every 10 minutes, path length was 100 microns, 100 mM citrate pH 6.0.

Results

Figure 1 shows the CVs from one cell with varying scan rate using oxy-DHP obtained. The scan rate of 100 mV/s was selected as the best scan rate to use so all data collected herein were collected at 100 mV/s. The scan rate did not affect the redox potential and the faster scan rate was more time efficient and resulted in a larger current. The x-axis of Figure 1 is graphed verses Ag/AgCl thus the redox potential of DHP is 220 mV (vs. Ag/AgCl) or 440 mV (vs. NHE).

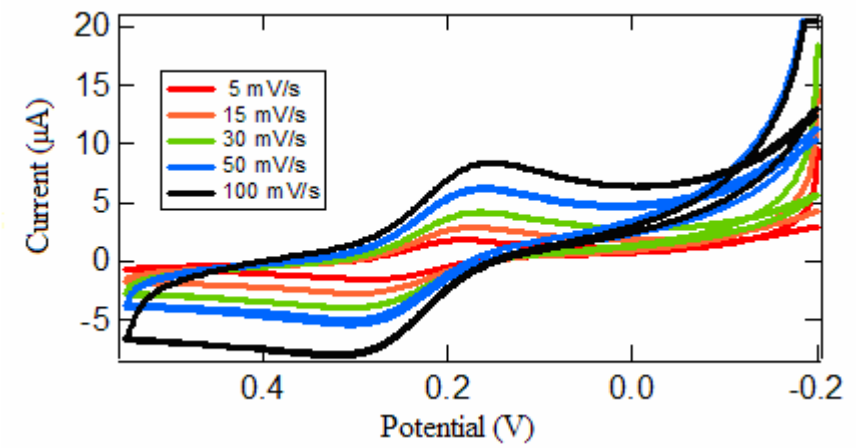

Figure 1 Varied scan rates for DHP oxygen present sample using a gold electrode with a mixed SAM (67% MUA/33% MH termination) with an initial potential of -200 mV. The redox potential of DHP is +220 mV vs. Ag/AgCl reference electrode or +440 mV vs. NHE.

Following precedent in other heme proteins we attempted to prepare a sample under anaerobic conditions to determine the Fe^{2+}/Fe^{3+} redox potential. Oxygen in the protein solution had to be removed to prevent the formation of DHP-O_2 species in the reduced (Fe^{2+}) state of the heme. However, as oxygen was removed from the protein solution, the current measured in the CV decreased. Figure 2 shows the decrease in the measured current as oxygen was removed. Spectroelectrochemical experiments in which the Soret and Q-bands could be observed were conducted in order to identify the protein

species involved in the CV experiments in Figure 1 and 2. Figure 3 illustrates the conversion of oxy-DHP to deoxy-DHP as determined by the spectroelectrochemistry.

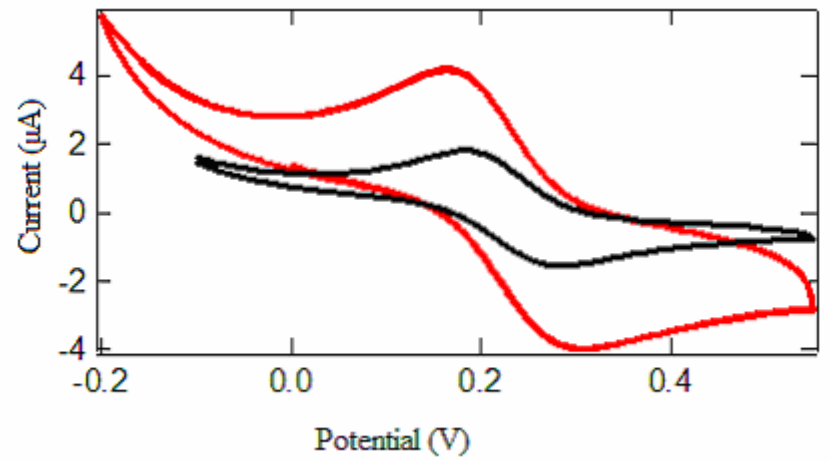

Figure 2 shows the decrease in the current caused by deoxygenation of the DHP protein solution. The red CV was collected before the argon flow was started and the black CV was collected after the argon had been exposed to the cell for 10 minutes. The redox potential of DHP is 220 mV vs. Ag/AgCl.

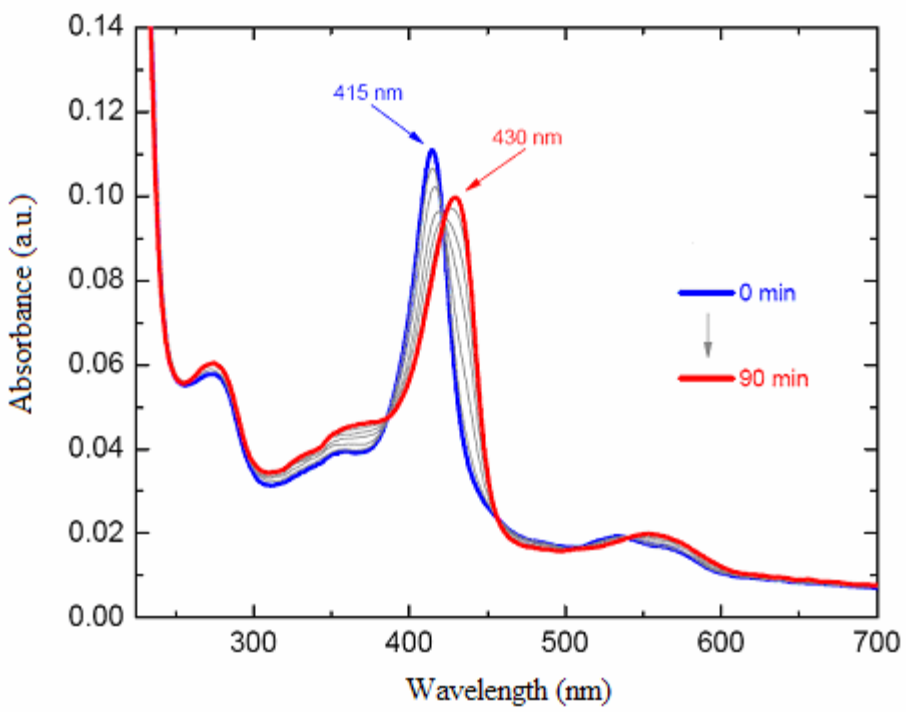

Figure 3 Data obtained from a spectroelectrochemical (SEC) experiment using gold minigrid as the working electrode. The initial spectra, thick line blue, is of oxyDHP. The red spectra is deoxyDHP. SEC was preformed by Dr. Rocha and Dr. Rein at Los Alamos National Laboratory by holding the potential at -200 mV and collecting UV-Visible spectra every 10 minutes.

Figure 4 shows the redox potential titration of the DHP as a function of the substrate concentration. The redox potential of DHP was determined to be 440 mV vs. SHE in the presence of oxygen. The addition of the TBP caused a negative shift in the redox potential. A shift in this direction implies that DHP is more readily oxidized when substrate is bound. Data were collected for molar ratios of 0:1 to 3:1 TBP:DHP. Due to the low solubility of TBP higher ratios were not used. In Figure 5 the blue CV is of DHP at pH 5.0 and results in the redox potential of 220 mV vs. SHE. The red CV is of DHP with a 1:1 ratio of TBP and results in a CV of 312 mV vs. SHE.

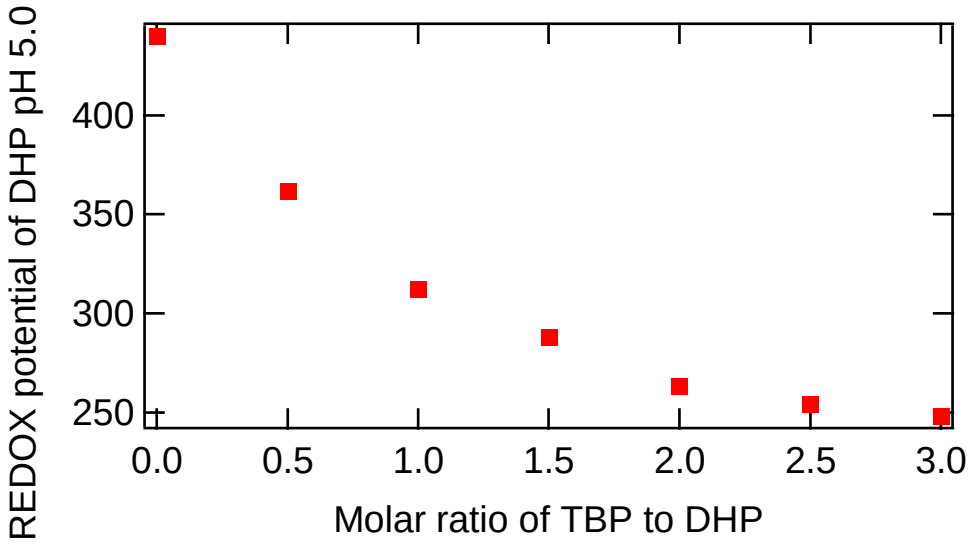

Figure 4 shows the redox potential of DHP as a function of TBP concentration. All data were collected in the presence of oxygen.

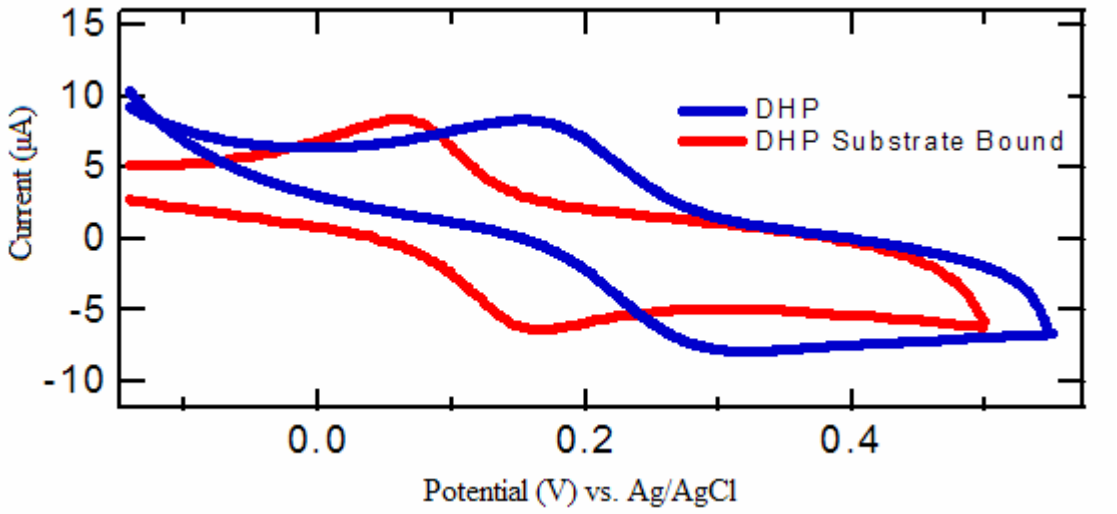

Figure 5 Cyclic voltammetry of DHP and DHP with 2,4,6-tribromophenol bound in a 1:1 molar ratio. The redox potential of DHP at pH 5.0 was determined to be +220 mV and +312 mV for the substrate bound form both vs. SHE.

Conclusions

According to the cyclic voltammetry and spectroelectrochemistry, the binding of substrate causes the redox potential to of oxy/deoxy couple to shift a more negative values as a function of substrate concentration. In other words, substrate binding makes it easier to oxidize the heme. Many questions remain unanswered and additional work is necessary to understand all of the observation presented here.

References

1. Chattopadhayay, K.; Mazumdar, S. **Direct electrochemistry of heme protein: Effects of electrode surface modification by neutra surfactant**. *Bioelectrochemistry* (2000), 52, 17-24.

2. Goodin, D. B.; McRee, D. E. **The Asp-His-Iron triad of cytochrome c peroxidase controls the reduction potential electronic structure and coupling of the tryptophan free radical to the heme**. *Biochemistry* (1993), 32, 3313-3324.

3. Sligar, Stephen G. **Coupling of spin, substrate, and redox equilibriums in cytochrome P450.** *Biochemistry* (1976), 15(24), 5399-406.

4. Gunsalus, I. C.; Sligar, S. G. **Equilibrium states and dynamic reactions of iron in the camphor monoxygenase system.** *Advances in Experimental Medicine and Biology* (1976), 74(Iron Copper Proteins), 254-62.

5. Gunsalus, I. C.; Sligar, S. G. **Redox regulation of cytochrome P450cam mixed function oxidation by putidaredoxin and camphor ligation.** *Biochimie* (1976), 58(1-2), 143-7.

6. Robinson, K. R. **Interfacial electrochemical investigation of Dehaloperoxidase**. Masters thesis (2003)

7. Belyea, J.; Gilvey, L. B.; Davis, M. F.; Godek, M.; Sit, T. L.; Lommel, S. A.; Franzen, S. **Enzyme function of the globin dehaloperoxidase from *amphitrite ornata* Is activated by substrate binding.** *Biochemistry* (2005), 44(48), 15637-15644.

Appendix

Supporting Information For Chapter 2

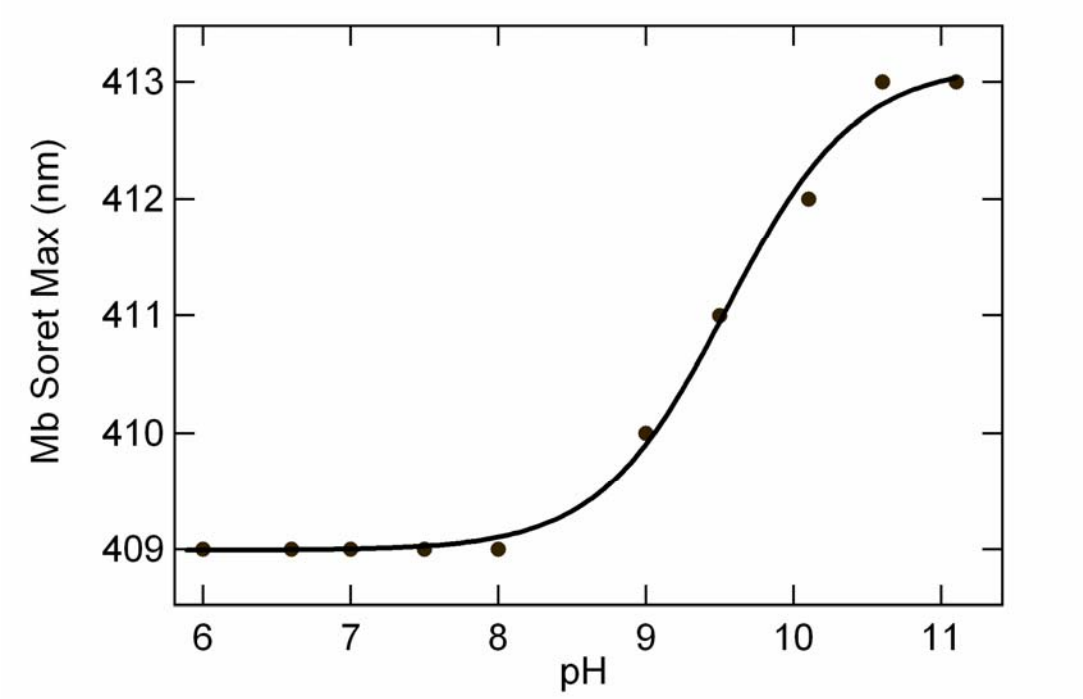

Figure S1. Myoglobin titration to determine the pKa of the acid-alkaline transition. The pKa from the fit to the data is 9.55.

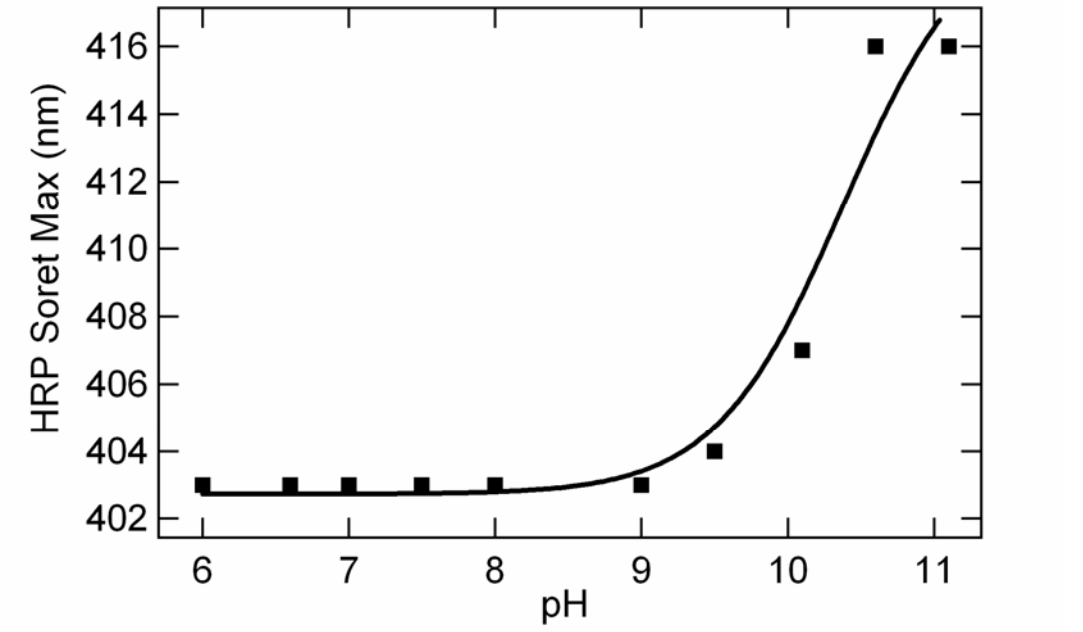

Figure S2. Horseradish peroxidase titration to determine the pKa of the acid-alkaline transition. The pKa from the fit to the data is 10.3.